A CLIMATOLOGICAL STUDY OF THE RELATIONSHIP BETWEEN ALPINE TREELINE AND THERMALLY-DRIVEN UPSLOPE WINDS ON NIWOT RIDGE, COLORADO

by

BRIAN J. BUTTERWORTH

B.S., University of Delaware, 2007

A thesis submitted to the

Faculty of the Graduate School of the

University of Colorado in partial fulfillment

of the requirement for the degree of

Master of Arts

Department of Geography

2011

This thesis entitled:
A Climatological Study of the Relationship between Alpine Treeline and Thermally-driven Upslope Winds on Niwot Ridge, Colorado

Written by Brian Jeffrey Butterworth
has been approved for the Department of Geography
by

_____
Peter Blanken

_____
Daniel Wolfe

_____
Mark Serreze

Date_____

The final copy of this thesis has been examined by the signatories, and we
Find that both the content and the form meet acceptable presentation standards
Of scholarly work in the above mentioned discipline.

Butterworth, Brian Jeffrey (M.A., Geography)

A Climatological Study of the Relationship between Alpine Treeline and Thermally-driven Upslope Winds on Niwot Ridge, Colorado

Thesis directed by Professor Peter D. Blanken

Abstract

Thermally-driven upslope winds are one of the many different wind patterns unique to mountainous terrain. While the general mechanics of these winds have been widely studied, there is a lack of information on how transitions in land cover influence these wind systems. Questions also remain about how these wind systems affect the biological functioning of mountain ecosystems.

This two year measurement program indentified the upslope flow regimes common to the southeast face of Niwot Ridge, an east-west running ridge directly east of the Continental Divide in the Colorado Front Range. The study focused on the role that alpine treeline played in the generation of upslope winds, as well as whether the airmass composition of upslope versus downslope winds influenced the spatial distribution of alpine vegetation.

Observations showed that thermally-driven upslope winds were most common in summer daytime hours. Differentiation between two different types of thermally-driven upslope winds, land cover-induced flow and anabatic flow, was done through an investigation of surface pressure and sensible heat flux at sites in the subalpine forest and alpine tundra. It was found

that anabatic forces, not transitions in land cover from forest to tundra, were responsible for the generation of upslope winds on Niwot Ridge.

Analyses on the composition of airmasses showed that upslope winds were generally cooler, more humid, and weaker in strength than downslope, westerly winds. These characteristics, combined with the higher frequency of upslope winds in the subalpine forest compared to the alpine tundra, suggested that upslope winds played an important role in the spatial distribution of vegetation in the alpine treeline ecotone.

Acknowledgements

There are a number of people who helped in the completion of this thesis that deserve recognition. First I would like to thank my advisor, Dr. Peter Blanken, for his help in guiding me through this process. Your help in the research design, obtainment of equipment, and editing were all crucial to the completion of this study. You have been a very stable force throughout this process. Thank you. I would also like to thank my committee members, Daniel Wolfe and Dr. Mark Serreze, for their help and insight. In addition, I would like to thank Dan for taking his time to help with field experiements. It was very much appreciated.

I also would like to thank all those who helped along the way. To all those at the Mountain Research Station – Sean Burns, Kurt Chowanski, Casey Flynn, and John Knowles, thank you for being there to answer questions and help me in obtaining data. In addition, I would like to thank all those who have helped in the collection of the datasets that I used for this work, especially those associated with the Ameriflux Tower and the Tvan eddy covariance towers.

Lastly I would like to thank my family for all the support. I would also like to thank my colleagues in Geography - Cole, Galen, Mou, Bock, and the rest, who have been great at helping keep things in perspective. And finally to Kendle Wade, your support and patience throughout this process were most appreciated. Thank you.

Table of Contents

List of Tables

Table

List of Figures

Figure

List of Variables

ABL	Atmospheric boundary layer	T_d	Dewpoint temperature
c_p	Specific heat capacity	T_s	Surface temperature
f	Turbulent friction	T_{soil}	Soil temperature (10 cm depth)
g	Gravity	TKE	Turbulent kinetic energy
h	Relative humidity	T_v	Virtual (sonic) air temperature
H	Sensible heat flux	U	Horizontal wind speed
L	Atmospheric lapse rate	w	Vertical wind speeds
p	Pressure	WD	Wind direction
p_o	Surface pressure	z	Height above ground level
PGF	Pressure gradient force	β	Bowen ratio; $\beta = H/\lambda E$
R	Gas constant	ε	Emissivity
$\boldsymbol{R}$	Spectral radiance	θ	Potential temperature
R_n	Net radiation	λ	Wavelength
t	Time	λE	Latent heat flux
T_a	Air temperature	ρ	Density
T_b	Brightness temperature	τ	Momentum flux

Chapter 1

Introduction

Mountain environments are places which experience a wide variety of unique meteorological phenomena. The wind patterns that affect these alpine regions are complex and numerous, with many scales of climatic processes combining to determine local meteorology. Locations in the same mountain region may experience different meteorological conditions even between short distances. Since wind has been known to transport many different atmospheric compounds, such as water and organic & inorganic aerosols (Parrish *et al.* 1990), differences in local climatologies can have important implications for these sensitive ecosystems. Transport of natural compounds is often inextricably linked to vegetation patterns on a mountain (Duane *et al.* 2008). However transport of atmospheric pollutants by mountain weather systems often causes alpine regions to take a greater burden of certain environmental problems (Lu and Turco 1994, Kossman *et al.* 1998).

One type of mountain wind that may be responsible for such transport is upslope, thermally-driven flows. Thermally-driven flows (or mountain-valley breezes) are phenomena that have been well documented. The basic mechanics of these winds is the development of upslope winds during the day as incoming radiation increases the sensible heat flux on the face of a mountain. A horizontal pressure gradient forms between the slope surface and the adjacent above-valley air. This force, when combined with a buoyancy force due to surface heating, causes winds to blow uphill (Orville 1964). Strong sensible heat flux promotes the existence of

upslope flows more than high latent heat flux and for this reason such thermally-driven flows are more common of mountains in the semi-arid western United States (Whiteman and Doran 1993).

This research focuses on the local meteorology of Niwot Ridge, an east-west running ridge located directly east of the Continental Divide in the Colorado Front Range (Figure 1.1). This site is an area of extensive ecological research and currently is designated as a Long-Term Ecological Research site. Due to its mid-latitude location, Niwot Ridge most often experiences synoptic-scale westerly winds (Barry 1973). However this region also experiences upslope winds. Upslope winds, while often the result of thermal forcings, can also be caused by a variety of other factors. It has been found that synoptic-scale storms, passing to the south of Niwot Ridge, are capable of generating upslope winds in the winter months (Turnipseed *et al.* 2002, Blanken *et al.* 2009). The existence of upslope winds has also been attributed to mechanical forcing by mountain gravity waves (Turnipseed *et al.* 2004). These waves can cause rotors to form on the lee side of a mountain ridge, which can effectively recirculate air upslope. Such local upslope events have been found to be common in nighttime conditions, when synoptic-scale wind speeds are high.

While there are different forms of upslope winds, it has been found that summer daytime conditions give rise to thermally-driven, upslope winds. These thermally-driven flows occur 25% to 40% of the time during summer days over subalpine forest on Niwot Ridge (Baumann *et al.* 1993, Turnipseed *et al.* 2002, Blanken *et al.* 2009). While these upslope flows are common in the summer months they do not affect all of Niwot Ridge uniformly. A recent two year study, the impetus for this research, by Blanken *et al.* (2009) that found that on Niwot Ridge upslope flows occurred more often over a subalpine forest site than over an alpine tundra site 4 km

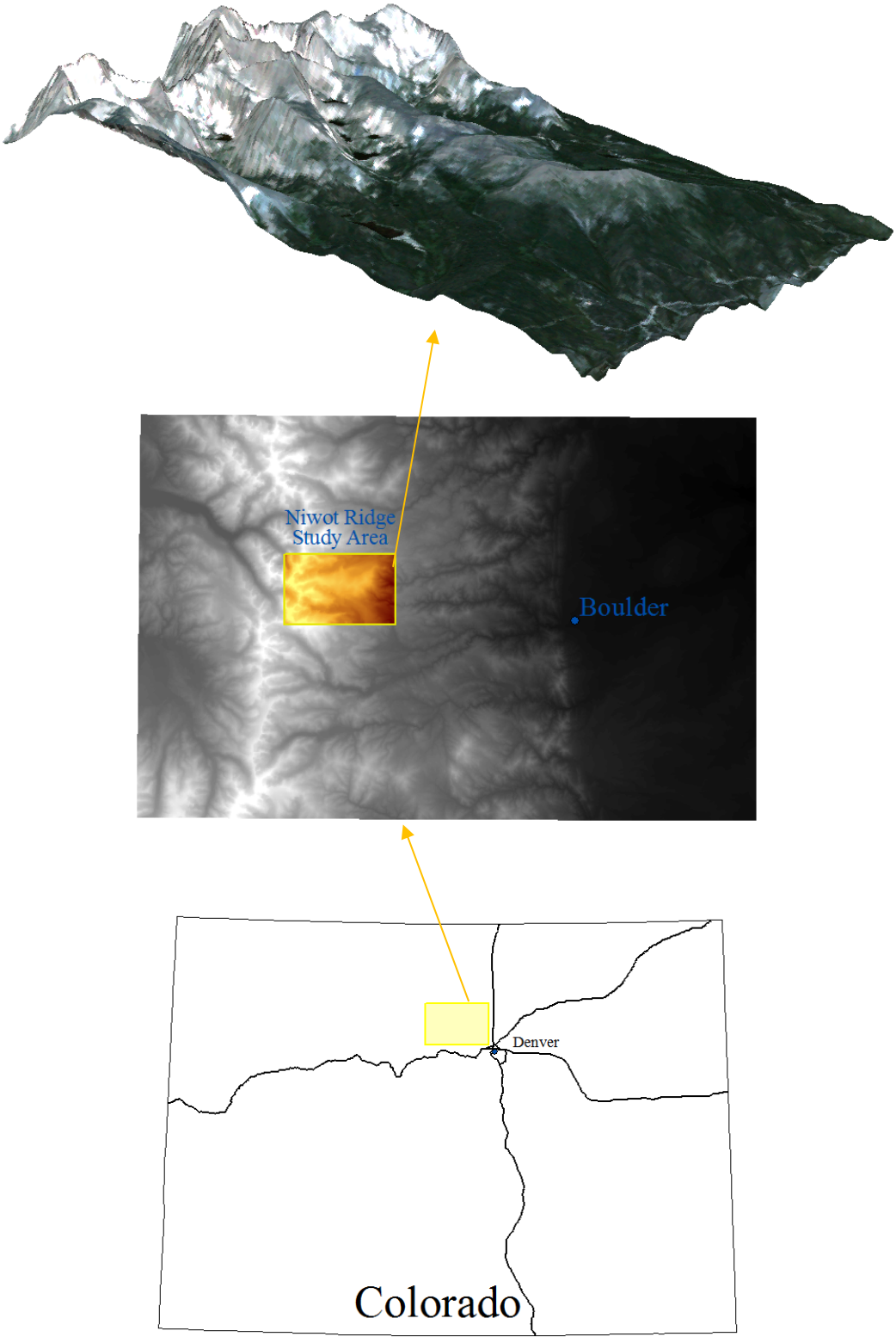

Figure 1.1. Shows the location of the 8km x 13km study region used in this study of Niwot Ridge.

upslope (Figure 1.2). This finding suggests that these two sites, which are separated by the alpine treeline ecotone, are affected differently by mountain weather systems.

Objectives and Organization of this Thesis

This study builds off the work of Blanken *et al.* (2009) to determine whether there was a relationship between the location of alpine treeline and thermally-driven, upslope winds. This study addressed the same question in two ways. First, was to determine whether the extent of thermally-driven, upslope winds was influenced by alpine treeline. The second objective was to look at the question in reverse to determine if the location of alpine treeline was influenced by these thermally-driven winds.

Before these objectives could be completed it was important to identify the meteorological conditions found on Niwot Ridge during 2008 and 2009. In particular, which types of upslope events occurred and what were their temporal and spatial characteristics. These results were critical to completing the main objective of determining the relationship, if any, between alpine treeline and thermally-driven flows. If the frequency of upslope winds was not largely dominated by thermal forcings then special considerations would need to be taken into account before the following analyses could be undertaken.

Analysis of the meteorological conditions yielded similar results to previous findings by Baumann *et al.* (1993), Turnipseed *et al.* (2002), and Blanken *et al.* (2009). Upslope winds did dominate summer daytime periods, compared to synoptic-scale flows and mechanical flows.

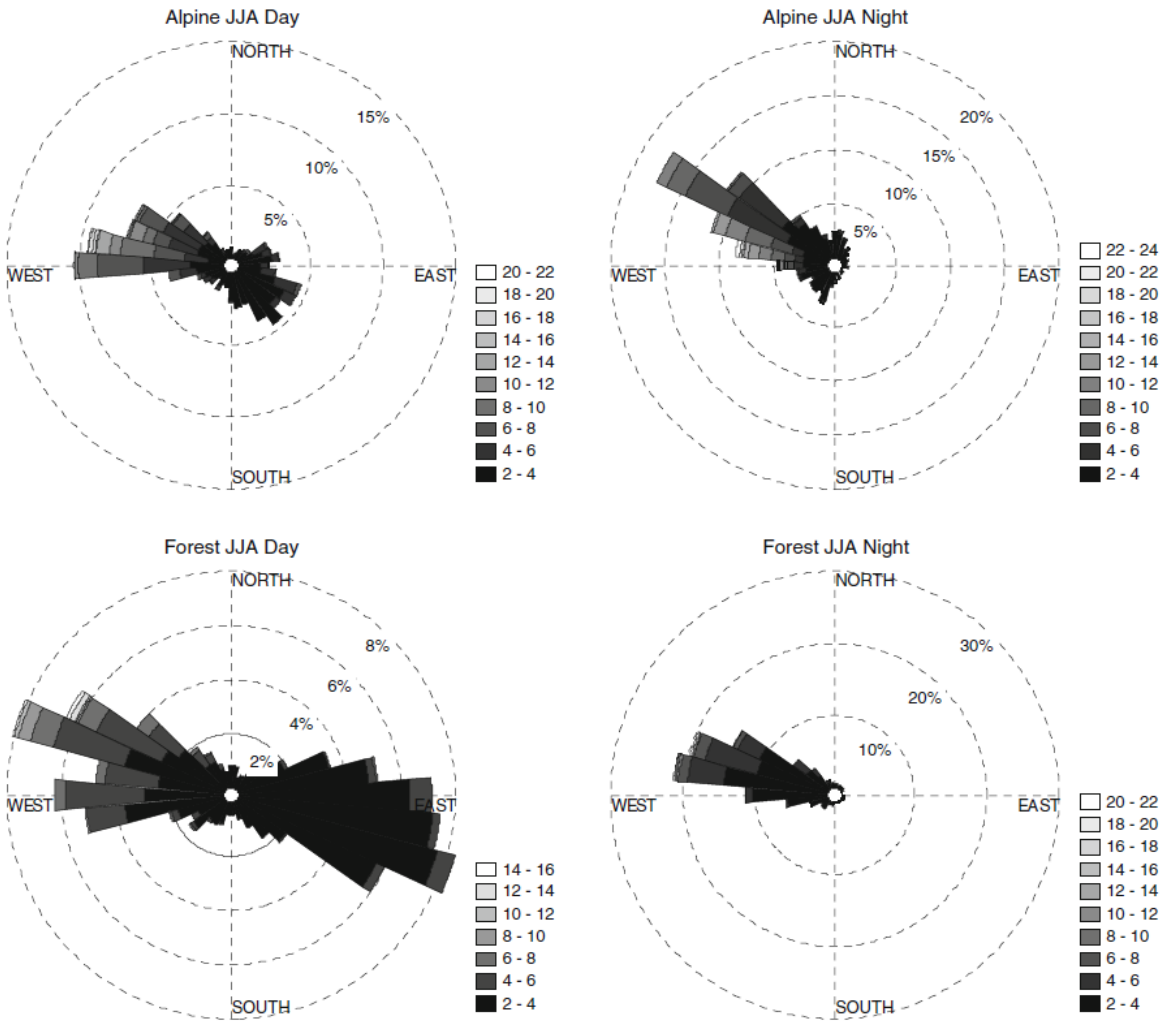

Figure 1.2. Wind roses showing the day (0800-1600 MDT) and night (2000 – 0400 MDT) wind direction and wind speed values at a subalpine forest site and an alpine tundra site on all summer days (JJA) in the period from June 8, 2007 to July 3, 2008 (Blanken *et al.* 2009).

However, it also revealed diurnal differences between the timing of thermally-driven flows in the alpine tundra and the subalpine forest, where the subalpine forest transitioned to upslope flow immediately following sunrise, while the alpine tundra did not see increased frequency of upslope flows until midday.

Finding the difference in the temporal behavior of upslope winds in the tundra versus forest was an important consideration for the first objective. The morning transition to upslope flow in the subalpine forest was considered to be due to anabatic forcings, due to its distinct post-sunrise transition time. However, reasons for the afternoon upslope flows in the tundra required an additional research. It was hypothesized that differential surface and soil temperature (T_s and T_{soil}) distributions on Niwot Ridge, due to different land cover properties, were responsible for creating meteorological conditions suitable to different upslope flow regimes in the alpine tundra versus the subalpine forest. Higher T_s and T_{soil} in the tundra (compared to the forest) were expected to cause land cover-induced, upslope flow, which would explain the afternoon upslope flows in the tundra, coincident with the time of greatest temperature contrasts between tundra and forest.

The last part of this study was to determine whether the airmass composition of upslope winds influenced the location of alpine treeline. Findings revealed that upslope flows were more common in the subalpine forest than in the alpine tundra. Because regions that experienced a greater frequency of upslope flows had greater plant biomass it was hypothesized that the composition of airmasses associated with upslope winds were more beneficial to plant growth than those associate with westerly flows. To address this question, meteorological variables from westerly and upslope wind events were compared to determine if they had distinctive signatures which might explain such differences in vegetation distributions.

Chapter 2

Analysis of the Temporal and Spatial Characteristics of Upslope Flow on Niwot Ridge

Abstract

Studies of mountain environments have characterized a wide variety of different wind patterns that occur in complex terrain. The purpose of this study was to characterize the upslope flow regimes on Niwot Ridge. The first step in understanding upslope flows was to determine which different types of upslope flow exist and to determine the temporal and spatial variability of these flows. The data were examined looking for three types of upslope winds: thermal flows, mechanical flows, and synoptic-scale flows. Analyses presented in this chapter reveal that thermally-driven, upslope flows were most common to summer days, but that they occasionally occurred in winter months. It was also found that mechanically-driven upslope flows, which occurred due to the formation of mountain gravity waves, occurred mainly at night and in the winter. Synoptic-scale influence on upslope flow was found to be minimal, with alignment (simultaneous upslope orientation) between synoptic-scale (500 mb) flows and surface (660 mb, 710 mb), upslope flows usually occurring less than 3.5% of the time. In addition to these three types of upslope flow, convergence events were examined, due to findings by previous studies revealing times when the subalpine forest experienced upslope (easterly flow) while the alpine tundra experienced downslope (westerly flow). It was found that convergence events during the winter and nighttime often appeared to be influenced by mechanical and synoptic-scale forces. On summer days, convergence events were often due to a lag time in thermal, anabatic flow reaching the alpine tundra. The data revealed that upslope winds initiated in the subalpine forest

immediately following sunrise and did not occur until midday in the alpine tundra, only 4 km upslope.

2.1 Introduction

2.1.1 Thermal Flow

Thermal flows refer to winds in which surface heating of a mountain face causes air to flow uphill. These flows are termed anabatic flow, and refer to upslope winds caused by the combination of buoyancy force and horizontal pressure gradient force. The heated surface creates a local horizontal pressure gradient between the slope (surface) air and horizontally adjacent valley air above the surface layer. This force is parallel to a flat Earth's surface (Figure 2.1). The second force is the buoyancy force caused by the reduction of air density at the surface. These two forces combined cause winds to blow uphill parallel to the slope (Kossmann and Fiedler 2000). This upslope wind reverses direction (e.g. downslope) at night due to the boundary layer once again becoming stable, allowing for gravity-driven, katabatic flows to move down slope.

The equation for anabatic flow (u_s) is,

$$\frac{\partial u_s}{\partial t} = -\frac{1}{\rho}\frac{\partial p}{\partial x}\cos\beta + g\frac{\rho_2 - \rho_1}{\rho_1}\sin\beta - f \qquad [1]$$

, where ρ is density, g is gravity, p is pressure, β is the slope angle, and f is turbulent friction (Kossmann and Fiedler 2000). The term on the left-hand-side of equation (1) describes the change in the upslope component of flow with time (t). The first term on the right hand side of equation (1) describes the pressure gradient force (*PGF*), and the second term describes the buoyancy force.

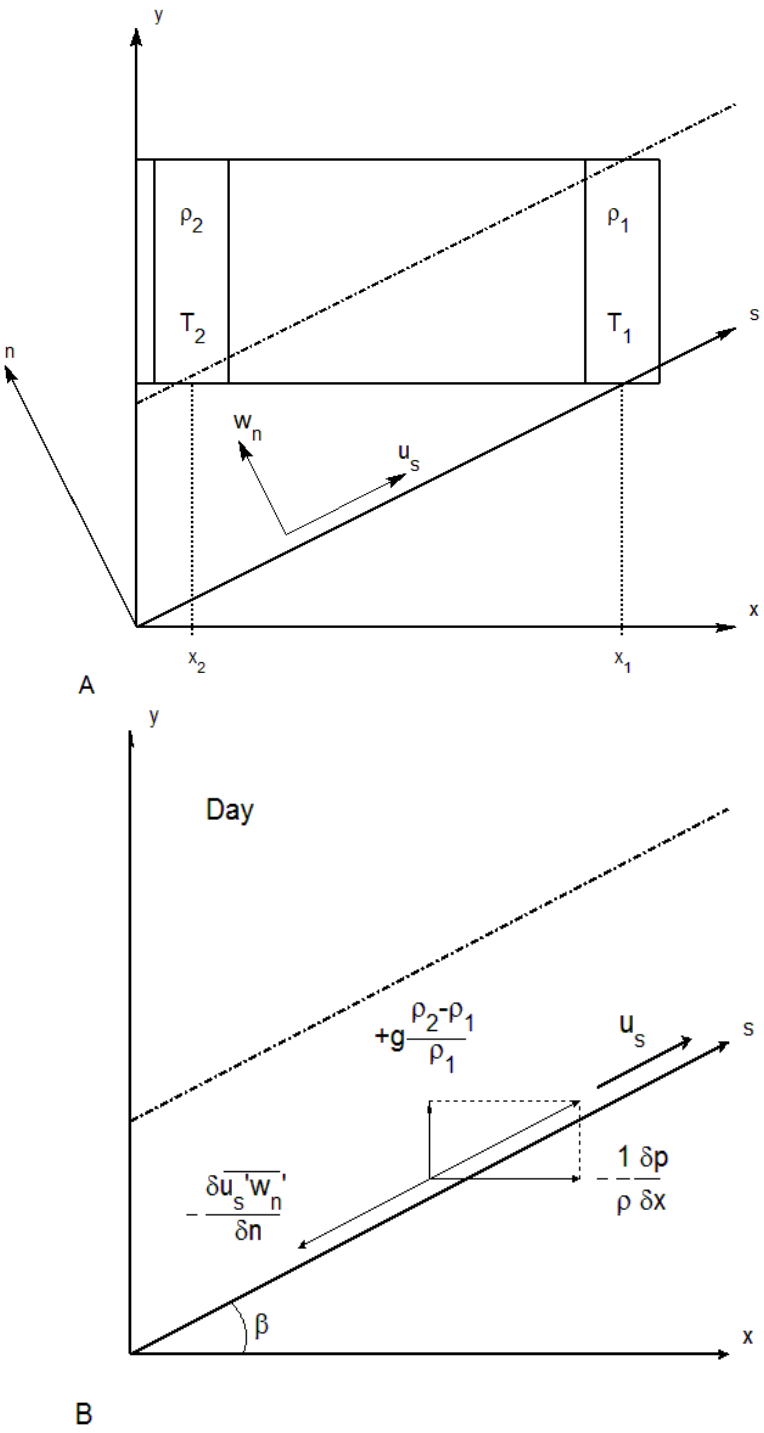

Figure 2.1. The theoretical basis for anabatic flow during the day adapted from Kossmann and Fiedler (2000). The top diagram (a) shows the two theoretical airmasses, one above x_2 and the other above x_1, located on opposite sides of the surface layer (dashed line). The bottom diagram (b) shows the forces involved. The vertical vector represents the buoyancy force, the horizontal vector directed into the slope represents the *PGF*, the downslope vector is *f*, and the upslope vector represents upslope flow.

Since surface heating is the driving mechanism behind thermal flows, these events are mostly summer, daytime events. Many studies have shown an increase in occurrence of upslope flows at these times. Baumann *et al.* (1997) found that in one summer (1993) in the Front Range of the Rocky Mountains, thermal flows occurred roughly ¼ of the time, aligning with proper (weak or non-existent) synoptic-scale conditions. Similarly, Turnipseed *et al.* (2002) and Blanken *et al.* (2009) found that in summer months over the subalpine forest on Niwot Ridge, upslope winds occur 30-40% of the time during the day.

2.1.2 Mechanical Flows

Another phenomenon known to cause upslope flow on Niwot Ridge is leeside gravity waves (Losleben *et al.* 2000, Turnipseed *et al.* 2004). Studies have shown that gravity waves can induce vertical eddies (rotors) which cause winds to flow uphill (Figure 2.2). On the windward side of the wave trough winds will be strong and oriented downslope, while on the leeward side of the trough there are often upslope flows due to rotor winds (Doyle and Durran 2002). Turnipseed *et al.* (2004) found that conditions supported the existence of these mechanically-driven upslope winds 14% of the time in a 4 month winter period on Niwot Ridge.

Mountain gravity waves are created by strong winds flowing over mountain ridges. Under the appropriate conditions, a minimum horizontal wind speed (U) of 8 m s^{-1} must be reached on the ridge top to create these flows (Turnipseed *et al.* 2004). However, U is often much higher. Therefore, downslope windstorms are associated with the formation of mountain gravity waves (Smith and Skyllingstad 2009), causing strongly negative vertical wind speeds (w) on the leeside of a mountain ridge (Doyle *et al.* 2011), often between 5 m s^{-1} and 10 m s^{-1}. Under

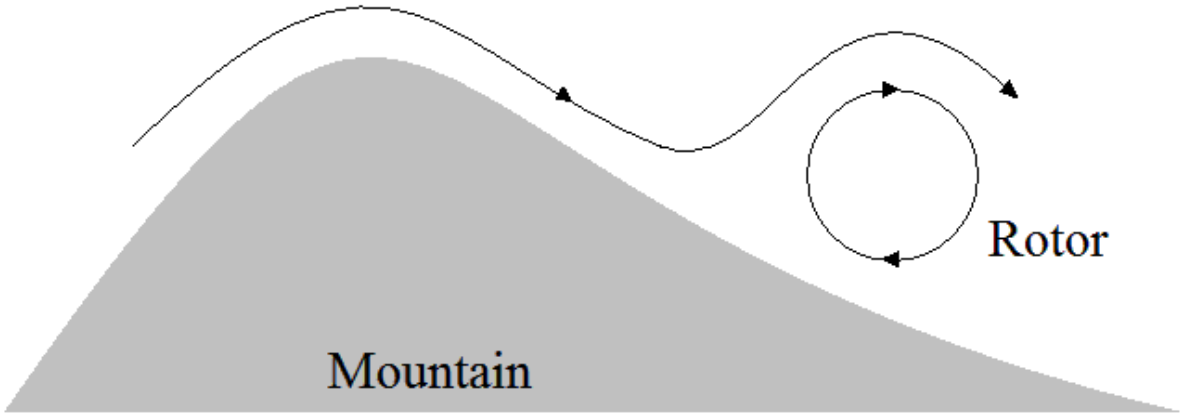

Figure 2.2. Theoretical diagram of leeside gravity wave creating a rotor wind, adapted from Doyle and Durran (2002).

typical conditions mountain environments do not usually experience *w* with magnitudes greater than 1 m s^{-1} (Worthington *et al.* 2001, Loescher *et al.* 2005).

Such windstorms on Niwot Ridge have been found to occur most often during winter months between midnight and 0700 local time (Brinkmann 1974). Studies from other mountain ranges have observed a preference for late afternoon windstorms (Seluchi *et al.* 2003, Grubisic and Xiao 2006). Smith and Skyllingstad (2009) found that mountain waves were most likely to exist under strongly stable conditions of surface cooling, concluding high levels of turbulent kinetic energy (TKE) during the day inhibited formation.

2.1.3 Synoptic-Scale Winds

The existence of upslope flow on a mountain can also be the work of synoptic-scale winds. The Rocky Mountains, due to their mid-latitude location, generally experience westerly synoptic-scale winds (Barry 1973). Niwot Ridge is on the east side of the Continental Divide, and therefore is typically on the leeward side of the prevailing winds. However, under synoptic-scale easterly-flow conditions, Niwot Ridge can experience easterly (upslope) surface flow. In addition, it has been found that winter upslope winds are indicative of synoptic-scale storms that pass to the south rather than thermally-driven winds (Turnipseed *et al.* 2003, Turnipseed *et al.* 2004). When the low pressure centers of the storms advance over the plains southeast of Niwot Ridge the cyclonic flow causes easterly flow at Niwot Ridge (Turnipseed *et al.* 2004).

Suitable synoptic-scale conditions are also important to the existence of thermal flows. It has been found that synoptic-scale westerly winds must be weak or nonexistent in order for upslope winds to form. A study of a surface wind at a subalpine site on Niwot Ridge, Colorado,

found that mountain-valley winds were typical of summer months (Turnipseed *et al.* 2002) when synoptic-scale westerly winds were not as strong (3-4 times weaker) and less frequent in the summer at 700 mb level (Parrish *et al.* 1990)). This means that when synoptic-scale weather systems are strong, thermally-drive winds do not occur.

2.1.4 Convergence

Many studies have suggested the existence of convergence zones near mountain peaks due to thermally-driven flows (Mahrer and Pielke 1977, Toth and Johnson 1985, Wolyn and McKee 1994, Kalthoff *et al.* 2009). These can form either by thermally-driven flows on both sides converging or by thermally-driven flows on one side meeting synoptic-scale prevailing winds. Modeling results have shown that these areas of convergence form on the lee side of the peak (Wolyn and McKee 1994, Fujibe *et al.* 1999, Lin and Chen 2002) instead of being located directly at the ridge top.

The existence of such convergence may have important implications on the local meteorology, as well as pollution transport. Under the right circumstances, this may lead to convective cells and cloud formation (Sasaki *et al.* 2004, Meissner *et al.* 2007, Barthlott *et al.* 2006, Kottmeier *et al.* 2008, Eigenmann *et al.* 2009, Kalthoff *et al.* 2009). Upslope flow is often cited for increasing transport and deposition of atmospheric pollutants to high alpine regions from low-lying plains (Lu and Turco 1994, Kossman *et al.* 1998). However, convergence has been found to lead to an exchange between the atmospheric boundary layer (ABL) and the free troposphere, causing a net export of pollutants out of the regional system (McElroy and Smith 1991, Kossmann *et al.* 1999, Nyeki *et al.* 2002, Henne *et al.* 2005).

On Niwot Ridge, the existence of lee side convergence has been documented by Turnipseed *et al.* (2004). A subsequent study at Niwot Ridge showed opposing summer, daytime wind direction (*WD*) for an alpine site versus a subalpine site 4 km downslope (Blanken *et al.* 2009). This difference in *WD*, westerly winds at the alpine site and easterly winds at the subalpine site, suggests the existence of a convergence zone somewhere between the two sites, possibly where the transition from subalpine forest to tundra occurs.

2.1.5 Objectives

The overall goal of this chapter was to analyze the atmospheric environment of Niwot Ridge during the two years of this study and determine the types of upslope flow present. The temporal and spatial characteristics of these different winds were important considerations for the following chapters which attempt to determine the relationship between alpine treeline and upslope flows regimes. Based on previous research, it was hypothesized that the majority of summer, daytime upslope flows were due to thermal forcings and that nighttime and winter upslope flows, which were expected to be more infrequent, were due to synoptic-scale and mechanical forcings. It was also hypothesized that convergence events would be more common in the summer, when upslope winds were more frequent.

2.2 Methods

2.2.1 Study Sites

Three meteorological measurement stations were used to complete this research (Figure 2.3). For a full summary of the instruments and meteorological parameters collected see Table 2.1. An alpine tundra site was located at 3480 m above sea level (asl) on the top of Niwot Ridge, Colorado (40° 03'11" N; 105° 35'11"W) near the Saddle site. This site is a dry alpine meadow with low snow accumulation, high winds speeds, and dry soil (Blanken *et al*. 2009). The site is dominated by short vegetation with high root:shoot ratios and low leaf area index (<0.5 $m^2 m^{-2}$). It is located on an almost flat surface with a southeasterly aspect (139.7°). This site will be referred to as Tvan.

The station was equipped with two sonic anemometers (CSAT3, Campbell Scientific) spaced 50 m apart on an east-west axis. The anemometer heads were located 3 m above ground level (agl) facing north. Other equipment at this site included an open path gas analyzer (LI-7500, Li-Cor), a shielded temperature/ relative humidity probe (HMP 45C, Vaisala), and a net radiometer (NR-Lite, Kipp and Zonen), all mounted at 3 m agl. The sonic and gas analyzer data were recorded at a frequency of 10 Hz and fluxes were computed as 30 minute averages.

The second station was a subalpine forest site located 3050 m above sea level (40° 01'58" N; 105° 32' 47" W) near the Niwot Ridge C1 site. It is roughly 4 km east of the alpine tundra site. The area is considered a low-productivity subalpine forest and is warmer and drier than the alpine site (Blanken *et al*. 2009). It is located on a ~5% slope with east aspect (87.1°). This site will be referred to as C1. Analyses for both C1 and Tvan will include data from 2008 and 2009.

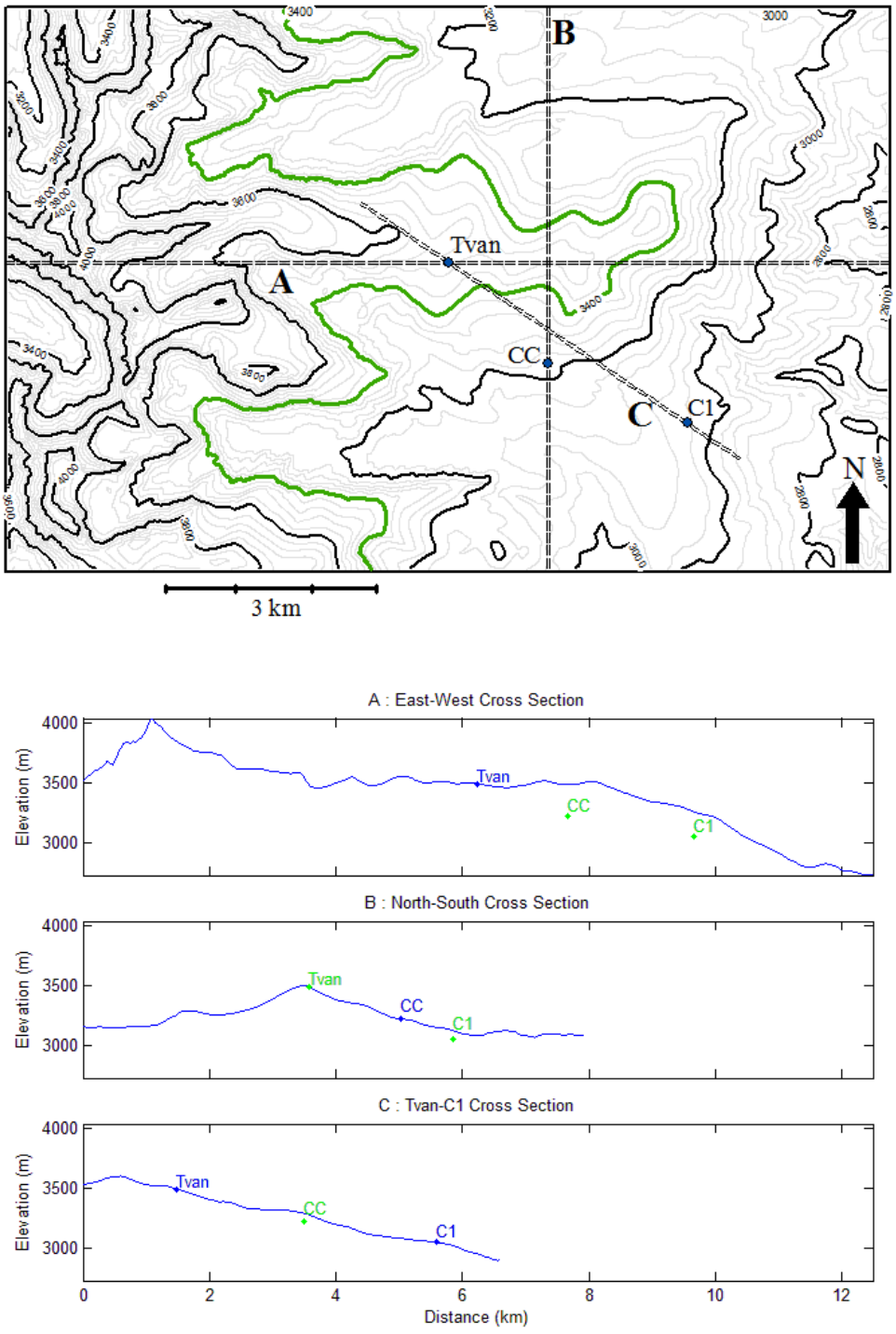

Figure 2.3. Map and cross-sections of Niwot Ridge. Treeline is roughly represented by the 3400 m contour line, highlighted green. Dashed lines on map represent the lines of three different cross-sections below. On the cross-sections locations of the three sites are shown, with blue lettering indicating those sites that fall directly on the line, green representing sites that do not fall on the line.

Table 2.1. List of the meteorological parameters measured at the three sites, the instruments used to collect the data, and the height of the measurements (agl).

Site	Measured Parameters	Instrument	Height (m)
Tvan	Wind Direction	CSAT3, Campbell Scientific	3
	Wind Speed	CSAT3, Campbell Scientific	3
	H2O Flux	LI-7500, Li-Cor	3
	CO2 Flux	LI-7500, Li-Cor	3
	Air Temperature	HMP 45C, Vaisala	3
	Relative Humidity	HMP 45C, Vaisala	3
	Net Radiation	NR-Lite, Kipp and Zonen	3
CC	Wind Direction	CSAT3, Campbell Scientific	2.5
	Wind Speed	CSAT3, Campbell Scientific	2.5
	Virtual Air Temperature	CSAT3, Campbell Scientific	2.5
C1	Wind Direction	CSAT3, Campbell Scientific	21.5
	Wind Speed	CSAT3, Campbell Scientific	21.5
	H2O Flux	IRGA Model #6262, Li-Cor	21.5
	CO2 Flux	IRGA Model #6262, Li-Cor	21.5
	H2O Flux	KH 20, Campbell Scientific	21.5
	Air Temperature	HMP-35D, Vaisala	2, 8, 21.5
	Relative Humidity	HMP-35D, Vaisala	2, 8, 21.5
	Net Radiation	Rebs Q7.1	25.5

The meteorological equipment at this site was located on a 26-m tall scaffolding tower. A sonic anemometer (CSAT3, Campbell Scientific) was situated 21.5 m agl (~10m above the canopy) on a boom 1.8 m off the west side of the tower. It collected wind direction (*WD*) and speed (*U*) data. Temperature (T_a) was also measured at 21.5m (HMP-35D, Vaisala). Fluctuations in water vapor were measured by an open path hygrometer (KH 20, Campbell Scientific) located 36 cm east of the anemometer. Water vapor and CO_2 mixing ratios were measured by an infrared gas analyzer (IRGA Model #6262, Li-Cor; intake 20 cm from anemometer). All values were compiled as 30 minute averages. For a more detailed explanation of equipment settings and data processing, see Turnipseed *et al*. (2002).

A third meteorological station was installed at a site (3218 m asl) roughly halfway in between the other two stations (40° 02' 25" N; 105° 34' 11" W) close to treeline (~ 0.5 km downslope). It was placed in a small clearing (roughly 40 m x 20 m) adjacent to the dirt road connecting Tvan and C1. The clearing itself has a southerly orientation (173.1°), but lies in a general region with an easterly aspect. The surrounding environment is subalpine forest, similar to that at C1. This site had one sonic anemometer (CSAT3, Campbell Scientific), mounted at 2.5 m agl, which recorded wind in the horizontal, vertical, and cross-wind directions (same as the other sites), as well as a virtual (sonic) air temperature (T_v). A CR23X datalogger sampled at 10 Hz and computed 30 minute averages. This site will be referred to as Cabin Clearing (CC). The collection period for CC was shorter than C1 and Tvan, running from 7/29/2009 to 7/8/2010.

The *WD* data from all three sites were oriented with 0^o representing true north. The data from C1 was downloaded with this orientation. For Tvan and CC a correction was applied to change 0^o from magnetic north to true north. For the sake of simplicity the declination from 1/1/2009 (9.583^o) was applied to all *WD* values for these two sites. Also for simplicity the

virtual air temperature (T_v) collected at CC will be used interchangeably with T_a collected from air temperature probes at both Tvan (Vaisala, HMP 45C) and C1 (Vaisala, HMP-35D).

2.2.2 Seasonal Characteristics

The first goal was to determine the seasonal characteristics of upslope wind at the three different sites (C1, Cabin Clearing, and Tvan). The seasonal percentages of upslope winds were calculated for the summer months and winter months, as well as summer days and winter days. Spring and fall were excluded from analysis due to a preliminary analysis which found that the annual maximum and minimum occurrence of upslope flow happens in the summer and winter, respectively. Summer was defined as the months of June, July, and August and winter was defined as the months of December, January, and February. Daytime values were defined as (0800 to 1600 MST). Since C1 and Cabin Clearing had easterly aspects, upslope flow was defined to include all *WD* between 50° and 130° (an 80° range centered on 90°). Because Tvan had an aspect of roughly 140°, upslope winds for this site were defined to include all winds between 100° and 180°. These definitions for upslope flow will be used for the remainder of all upslope analyses, except when otherwise stated.

In addition to these values, the percentage of summer days that experienced different lengths of sustained upslope wind was calculated (for C1 and Tvan). The four different lengths of sustained winds were ½, 1, 1½, and 2 hours. Any day that experienced continuous upslope winds for these lengths of time was selected.

2.2.3 Diurnal Characteristics

The next goal was to determine diurnal patterns in the timing of upslope flow. To determine the time at which winds shifted from westerly (downslope) to easterly/southeasterly (upslope) flow the hourly median *WD* values for summer were calculated and plotted for all three sites. Median *WD* values were used instead of means since averaging *WD* tends to obscure information (i.e. averaging westerly flow and easterly flow yields southerly flow).

A second analysis addressed the lag time between the initiation of upslope flow in the subalpine forest versus the tundra. This analysis used data from only C1 and Tvan. The first step was to isolate all days in which both sites experienced upslope flow (at least two consecutive hours). The time of initiation of upslope flow was found for both sites for each day selected. The percentage of days in which C1 experienced upslope flow prior to Tvan was calculated, as was the percentage of days in which Tvan experienced upslope flow first. The average upslope wind start times at both sites were calculated and compared.

2.2.4 Convergence

The wind patterns on Niwot Ridge often showed some type of convergence. The next analysis was to determine the seasonal and diurnal characteristics of convergence events. To do this the wind direction difference between Tvan and C1 (WD_{Tvan}- WD_{C1}) was calculated. All values falling between 150° and 210° were considered convergence. The number of total convergence events and daytime convergence events that occurred each month (over 2008 and 2009) were found and plotted on a bar graph. Because well over 99% of all upslope flows at both C1 and Tvan have *ws* greater than 0.5 m s^{-1} and over 94% have *ws* greater than 1 m s^{-1} it is

concluded that, on average, these winds do have magnitude and therefore are not just a trick of the non-windy conditions (*ws*=0). Therefore wind speed was not considered for this convergence analysis.

Differences in *WD*, *U*, and T_a between Tvan and C1 were then analyzed during convergence events at different times of day to determine whether there were different causes of daytime and nighttime convergence. The four periods were non-day (1600 – 0800 MST), night (2000 – 0400 MST), day (0800 – 1600 MST), and summer day (0800 – 1600 MST, months: 6-8). Differences were calculated as WD_{Tvan}-WD_{C1}, $|U_{Tvan}$-$U_{C1}|$, and $|T_{Tvan}$-$T_{C1}|$ for each category. In addition, the average *U* during all time periods, for both sites, was calculated for both convergence events and for the periods as a whole.

2.2.5 Tethersonde

To determine the characteristics of the ABL over Niwot Ridge and the temporal characteristics of the breakup of the morning inversion layer, a tethersonde system was used. This allowed for the collection of multiple sets of T_a and air pressure (*p*) profiles over the lowest layer of the atmosphere. The goal was to get readings of the T_a and *p* of the atmosphere before and after sunrise.

The tethersonde was not a traditional commercial product. A homemade tethersonde system was created using a standard 3 m weather balloon and radiosonde attached to fishing line (200m). An MW31 sounding system was used with Vaisala RS92 radiosondes. The MW31 system was installed in a trailer near the C1 tower, with an antenna installed on the roof of the

trailer. The fishing line was secured to a power cord storage wheel so that the radiosonde could be reeled in and out.

The balloon was released manually at a slow and steady rate, and readings were collected for the ascent. The balloon was kept up for roughly 30 minutes before reeling it in. The sounding system was set to manual settings so that the radiosonde would continue collecting readings upon descent. Descent readings were treated as additional soundings.

Due to the close proximity to trees at C1, the balloons were released 0.15 km down the road in a clearing at 40° 1' 57.9" N, 105° 32' 27.1" W. Attempts to collect data on four mornings yielded useable data for only one day due to faulty batteries and loss of balloons as the result of strong winds aloft. On the morning of 8/10/2010, soundings were collected for 0415, 0437, 0504, 0522, 0542, 0603, 0623, 0626, 0634, and 0638 MST.

The T_a values were plotted against altitude (agl) for each sounding to obtain a vertical T_a profile. Because the high winds caused the balloon to oscillate up and down several meters in the course of a few seconds the data were sorted by altitude rather than time, under the assumption that in the course of the minute or two it took to reel out the balloon the conditions were constant. Mean values for readings of duplicate heights were calculated and used in place of the multiple values. Then, a five block simple moving average was applied to the data before plotting.

A second profile was created of potential temperature (θ). T_a, p, and surface pressure (p_o) values were applied to the following equation:

$$\theta = T\left(\frac{P_0}{P}\right)^{R/c_p} \qquad [1]$$

, with gas constant (R) set to 287 J kg^{-1} K^{-1}, and specific heat capacity (c_p) set to 1004 J kg^{-1} K^{-1}. The same five block simple moving average was run for these θ values before plotting.

2.2.6 Synoptic-Scale Winds

The last set of analyses was designed to determine the influence of synoptic-scale flow on upslope winds. Synoptic-scale data were gathered for 2008 and 2009. For this research NASA's Modern Era Retrospective-analysis for Research and Applications (MERRA) data were used, which is free and available online. MERRA is long-term (1979-present), continuous reanalysis data which combines output from meteorological models and observational data for a vast array of climatological variables. The data have a temporal resolution of 3 hours. For this analysis, easterly wind component (U_E) and northerly wind component (U_N) were obtained for the 500 mb level. These values were collected for the four reanalysis points that fell between the longitude 105.6°W and 105.4°W and between the latitude 40.0°N and 40.2°N (Figure 2.4). The U_E and U_N values from the four points were averaged and then converted to *WD* and *U*.

The first analysis was to determine what percentage of local upslope events were coincident with similarly directed synoptic-scale events. Synoptic-scale events with upslope *WD* were isolated. Then these synoptic-scale events were compared to the surface winds at Tvan and C1. All surface upslope wind events that fell within a three hour block centered on the MERRA data hour were considered to be aligned with synoptic-scale flow. Dividing the number of these aligned periods by the total number of local upslope events gave the ratio of how often upslope winds on Niwot Ridge may be directly influenced by synoptic-scale winds.

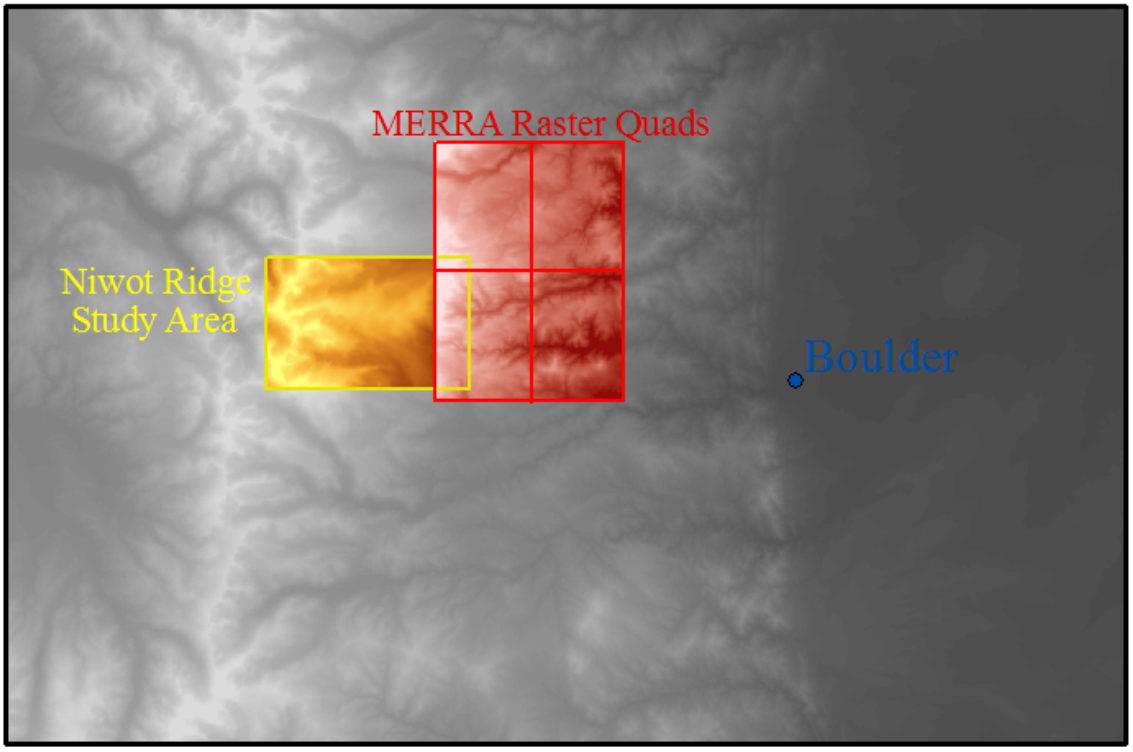

Figure 2.4. The location of the four MERRA reanalysis cells (in red) used for determining the synoptic-scale meteorology on Niwot Ridge.

The second analysis was to determine whether differences in synoptic-scale *U* influenced upslope flow. The median synoptic-scale *U* for the whole dataset was calculated and combined with the *WD* values for Tvan and C1 were used to determine what percentage of upslope flow occurred when synoptic-scale *U* was lower than the median value. This same analysis was run just for the summer to see how many upslope wind events occurred when synoptic-scale winds were below their median summer synoptic-scale *U*.

2.3 Results and Discussion

2.3.1 Seasonal Characteristics

To initially get a sense of the wind patterns between Tvan and C1, a *WD* scatterplot (filtering out $ws < 2$ m s^{-1}) was analyzed (Figure 2.5). The cluster of points in the upper right hand corner (cluster A) showed that both sites typically experienced westerly flow and usually simultaneously. The other distinguishing features are the clusters at *WD* 140^o, 90^o (cluster B) and the cluster around 270^o, 90^o (cluster C). Cluster B represents times when both site were experiencing upslope winds. Cluster C represents convergent times when C1 was experiencing upslope winds and Tvan was experiencing westerly winds. This cluster is interesting because it is just as prominent as cluster B meaning that these times of convergence were just as common as full upslope flow.

The seasonal percentages of upslope winds at the three sites were calculated (Table 2.2 and 2.3). At C1, in 2008 and 2009, there were 2443.5 hours of upslope winds, accounting for 13.93% of all the data. In the summer, the percentage increased to 17.47% and on summer days (defined as 1500 to 2300 UTC, or 0800 to 1600 MST) this percentage increased to 31.62%. This

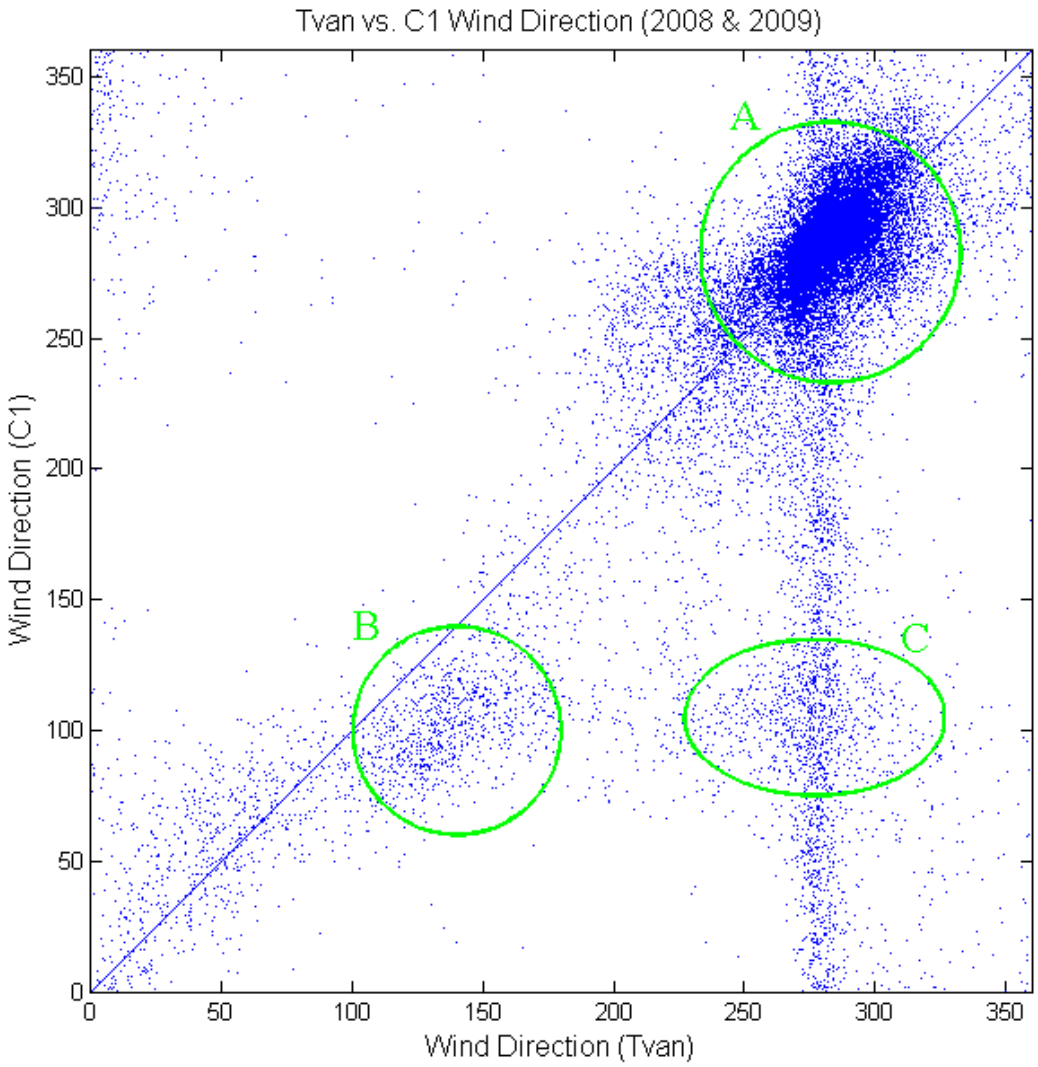

Figure 2.5. *WD* in the tundra versus *WD* in the subalpine forest for all times in which both sites had *ws* greater than 2 ms^{-1} during 2008 and 2009. The solid line shows the line of slope 1. The vertical streak on the right-hand side of the plot shows that during westerly flows at Tvan the wind direction at C1 can be from all directions.

Table 2.2. The percentage of summer days which had at least 0.5, 1, 1.5, and 2 consecutive hours of upslope flow.

Site	Consecutive Hours of Upslope Flow	% of Summer Days
C1	0.5	89.1
	1	75.0
	1.5	64.7
	2	53.8
Tvan	0.5	66.9
	1	54.4
	1.5	41.9
	2	34.8

Table 2.3. The total number and percentage of upslope winds at the three study sites for different times of year.

Category	C1	CC	Tvan
Total Hours of Upslope	2443.5	--	1178
% Entire of Data Collection	13.9	--	6.7
% of Winter	9.1	11.9	2.7
% of Winter Days	12.2	18.5	4.1
% of Summer	17.5	16.9	10.4
% of Summer Days	31.6	27.5	16.2

correlates well with Turnipseed *et al.* (2002) who, at the same site, found that in summer months upslope winds occurred 30-40% of the time during the day. The percentage of days in the summer that experienced at least 0.5, 1, 1.5, and 2 consecutive hours of upslope flow were 89.13%, 75.00%, 64.67%, and 53.80%, respectively. In the winter, upslope winds are more infrequent, occurring only 9.07% of the time overall and 12.19% during the day at C1.

The higher subalpine site (3218 m asl) showed winds characteristic of the lower subalpine forest site. In the roughly one year of data collection (8/1/09-7/8/10) it had upslope flow 16.93% of the time in the summer and 27.50% of the time on summer days. These values are just slightly lower than C1. In the winter upslope flows occurred 11.90% of the time overall and 18.47% of the time during the day. These values were higher than the winter values from the other sites. However, they were obtained from the winter of 2010 and a closer inspection revealed that all sites experienced a higher frequency of upslope winds in the winter of 2010. This shows that these seasonal patterns can have sizable variation from year to year.

The values from the alpine tundra (Tvan) produce the same pattern of increased number of upslope events in the summer and during the daytime. Overall, however, this site showed a lower number of these events. Over the course of two years (2008-2009) there were only 1178 hours of upslope winds (1265.5 hours less than the amount accumulated at C1), accounting for 6.71% of all winds throughout the entirety of data collection. In the winter these winds occurred 2.68% of the time and 4.07% of the time during the day. In the summer these winds occurred 10.41% of the time overall, and 16.20% of the time during the day. The percentage of days that experienced upslope wind events for at least 0.5, 1, 1.5, and 2 consecutive hours were 66.85%, 54.35%, 41.85%, and 34.78%, respectively. At all levels these percentages were much lower than the values collected for C1.

These values revealed that tundra did indeed experience fewer upslope events than the subalpine forest. This is also visible in Figure 2.6, which shows all upslope events at the three sites, as well as synoptic-scale easterly and southeasterly winds that occurred over the course of roughly one year. The number of upslope events decreased with increased elevation/altitude. The synoptic-scale easterly/southeasterly events were infrequent (n=101) and when they did occur, they usually correlated well with strong upslope events across all of Niwot Ridge. However there are many more upslope events on Niwot Ridge than can be explained fully by synoptic-scale conditions.

2.3.2 Diurnal Characteristics

The diurnal patterns of thermal flows were also analyzed to determine the time at which winds shifted from westerly to upslope flow. The hourly median *WD* values for summer revealed that upslope (easterly) winds were first observed in the subalpine forest (C1) starting at 0600 MST (Figure 2.7). The subalpine forest site at 3218 m asl (CC) showed that upslope (easterly) flow typically initiated at 0700 MST. Upslope (southeasterly) winds over the alpine tundra (Tvan) were found to begin much later at 1200 MST. These values showed a general lag in initiation times with increasing elevation. One other noteworthy finding from these values was that Cabin Clearing showed a bimodal distribution of upslope flow marked by a decrease in the frequency at 1000 MST. Upslope winds came back in full at 1200 MST, aligned with the onset of upslope flow in the tundra. This late morning reversal is even visible, though small, in the mean *WD* values at C1 (Figure 2.7 – red line).

The second analysis was run to investigate the lag time between upslope flows in the subalpine (C1) and tundra (Tvan). On days in which both sites experienced two consecutive

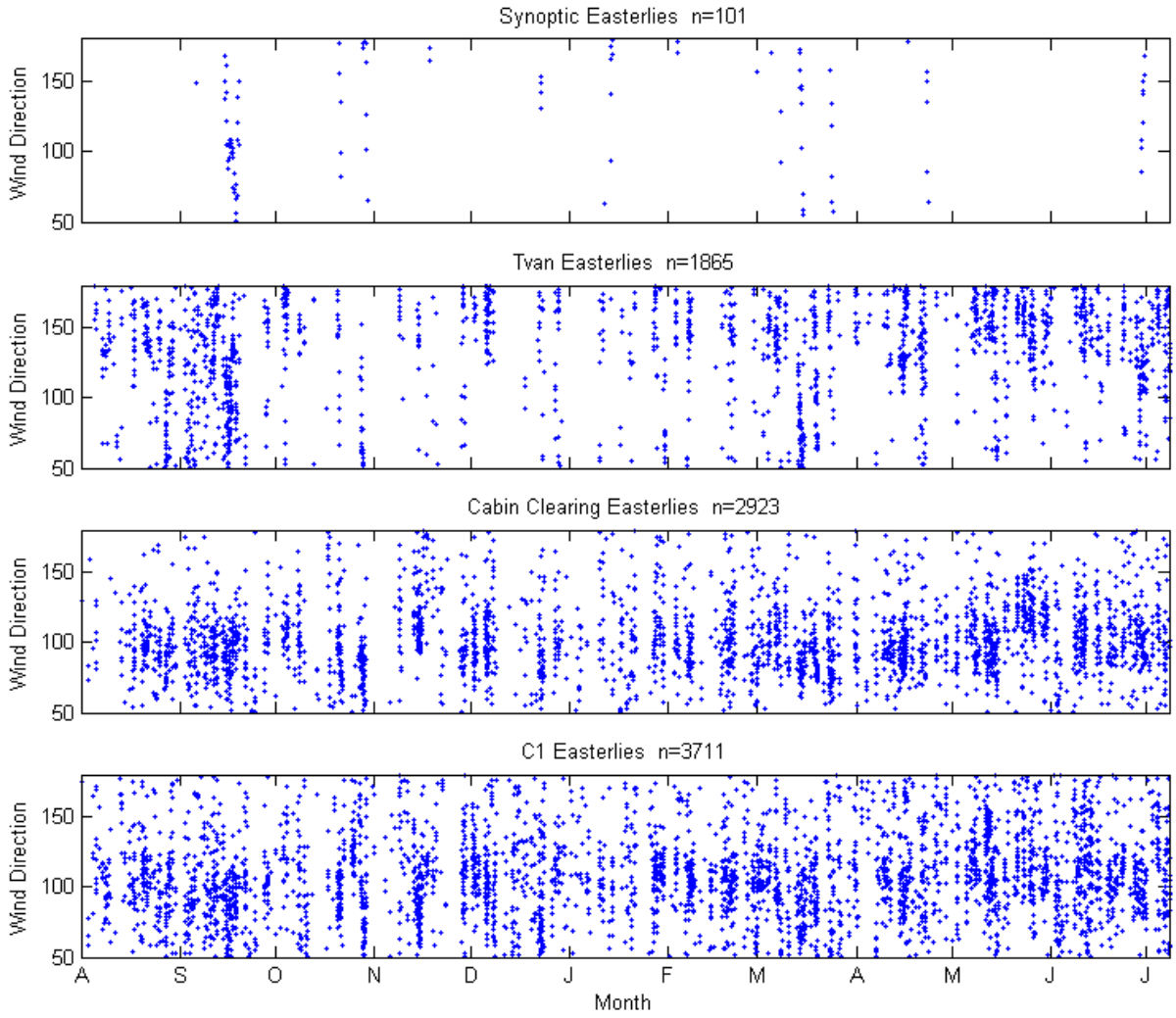

Figure 2.6. Easterly/southeasterly wind events at the three meteorological sites and for synoptic-scale conditions over the 11 months that the Cabin Clearing site was functional (8/10/09 to 7/8/10). The *n* value for each figure records the number of wind events falling between 50° and 180° which occurred over the period. The numbers decreased as elevation increased. Since the synoptic-scale data were recorded every three hours its *n* value is theoretically 6x lower than it would be at the 30 minute intervals of the sites.

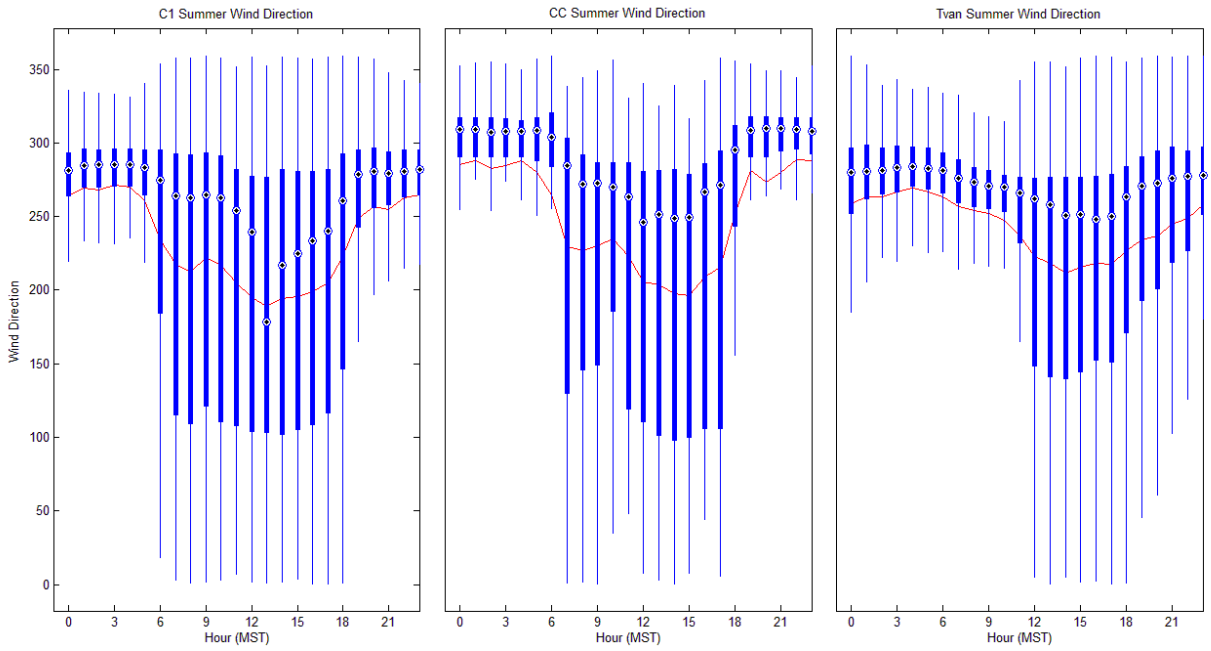

Figure 2.7. Hourly boxplots of *WD* for C1, Cabin Clearing, and Tvan during summers (JJA). Bulleyes represent median values, the edge of the boxes represents 25% and 75% values, and the whiskers show the extent of all values not considered statistical outliers. The red line shows the hourly average *WD*.

hours of upslope flow (days=143), 60.14% of the time upslope winds at C1 precede upslope winds at Tvan. The average time difference between the wind shifts of these events was 3.65 ± 3.29 hours. On 10.49% of days, the transition to upslope winds started during the same half hour measurement. For the remaining 29.37% transition to upslope flow occurred first at Tvan, by an average of 4.49 ± 3.45 hours.

Following up these findings with average time of day at which these events occurred gave more insight into the process. The average time of shift for subalpine preceding tundra was 0830 MST for subalpine and 1209 MST for tundra. For the cases in which the tundra switched first we see that tundra switched at 0337 MST and subalpine at 0806 MST. It is clear that subalpine forest has a very definitive time of upslope initiation in the hours following sunrise. Upslope flows in the tundra were not as well defined, with upslope flow often initiating midday, but sometimes in the middle of the night.

2.3.3 Convergence

From the previous analyses, it is clear that upslope flows occurred much more often in the subalpine forest than in the alpine tundra. A large percentage of the time the alpine tundra was experiencing prevailing westerly flow while the subalpine forest experienced easterly, upslope flow. These convergence events were studied more closely to determine what type of interaction occurred between the two opposing flows.

The first step in answering questions about the mechanics of convergence was to determine when they occurred. Selecting all WD_{Tvan}- WD_{C1} values falling between 150° and 210° as convergence, a minor seasonal pattern was observed, with summers generally having

slightly more convergent events than winter months (Figure 2.8). This was expected as the summers had a higher frequency of upslope flows, allowing for more opportunities for convergence to occur. However, increased frequency of upslope events did not lead to a higher frequency of convergence in the summer.

Analysis revealed that simultaneously to summer upslope flow events at C1, winds were upslope at Tvan 38.57% of the time and convergent (out of the west between 230° to 310°) 38.97% of the time. During the winter upslope flow at C1 was more often accompanied by westerly winds at Tvan at 50.52%, with only 23.70% of winter upslope events at C1 coinciding with upslope events at Tvan. Therefore, subalpine upslope events in the summer were less likely to be part of a convergent system than in the winter months.

The other noticeable feature of convergence on Niwot Ridge was that nighttime convergence was as prevalent as daytime convergence. Over two years there were 1496 total convergence events and 739 daytime convergence events. Defined daytime hours comprise only 1/3 of a day, meaning that the 49.4% of convergence during the day is higher than random prevalence. However, the large percentage of nighttime convergence was unexpected and suggests that there may be multiple causes for opposing flow in the tundra versus subalpine forest.

Days in which weak upslope flow in the subalpine forest occurred simultaneously to strong westerly flow in the tundra provide some insight into the mechanics associated with these convergence events. An example of this type of convergence occurred on the morning of 8/10/2010. Tethered balloons, released between 0415 and 0638 MST at C1, revealed that the complete breakdown of the nocturnal inversion was accomplished within an hour of sunrise

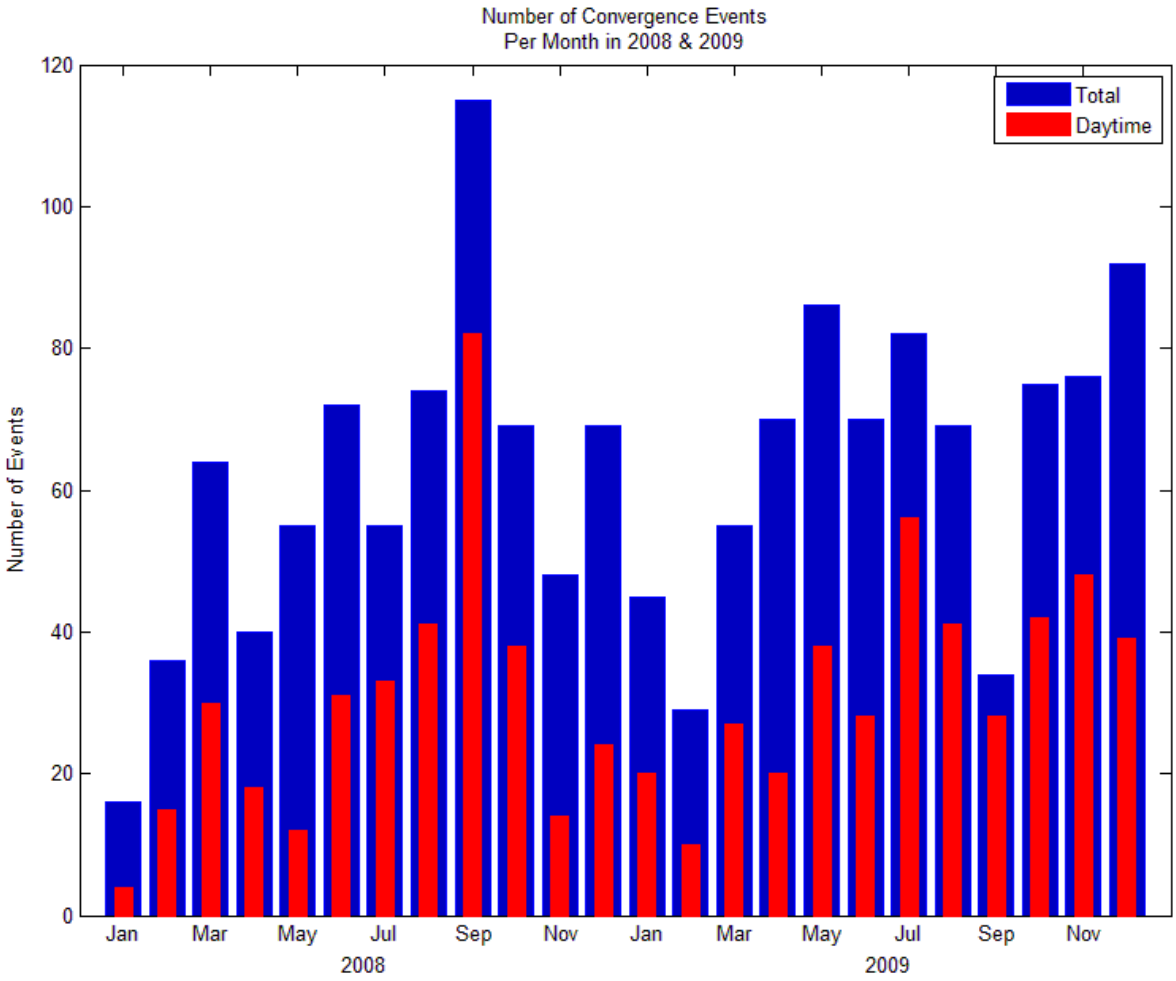

Figure 2.8. Convergence events between Tvan and C1 per month over 2008 and 2009. Blue bars show total values per month, and red bars show only those events that occur during the hours of 0800 to 1600 MST. Convergence was defined as $150° < WD_{Tvan}\text{-}WD_{C1} < 210°$.

(0504 MST), as seen by the neutrally stable, vertical θ profile (Figure 2.9). The surface heating which caused this breakdown suggests that the change to upslope flow, which occurred following sunrise, was due to anabatic forcings.

In the tundra winds remained westerly (Figure 2.10). Wind speed (U) in the tundra increased to 17.63 m s^{-1} in the three hours following sunrise, while the easterly flow in the subalpine remained at roughly 2 m s^{-1}. The flow in the tundra at this time appears to have been strongly influenced by synoptic-scale winds. As U peaked in the tundra, the physical movement of the tethersondes revealed that there was a shear layer at 80 m agl at the subalpine site where weak easterly flow (2 m s^{-1}) transitioned to strong westerly flow (Figure 2.11). This can be seen in the soundings at 0623 and 0626 MST which under full extension (200 m) only rose to heights of 69 m and 85 m, respectively, due to inability to break through this shear layer. This example reveals that there are times when surface conditions in the subalpine forest were decoupled from the winds aloft. This example suggests that under the appropriate surface heating conditions thermally-driven, upslope flows will form regardless of the strength of the winds aloft.

Convergence was also observed in circumstances which suggest a different set of causes. This second convergence scenario is one which may help to explain winter and nighttime convergence. On the night of 6/12/2008 a similar pattern of strong westerly flow in the tundra and weak easterly flow in the subalpine was observed (Figure 2.12).

During the daytime hours, C1 and Tvan exhibited the same patterns in observed variables (WD, U, T_a, net radiation (R_n), sensible heat flux (H), latent heat flux (λE)). While the means are not the same, changes occurred at the same hour, with the same degree of change. The momentum flux (τ) was the only variable that showed disagreement during the day, with Tvan

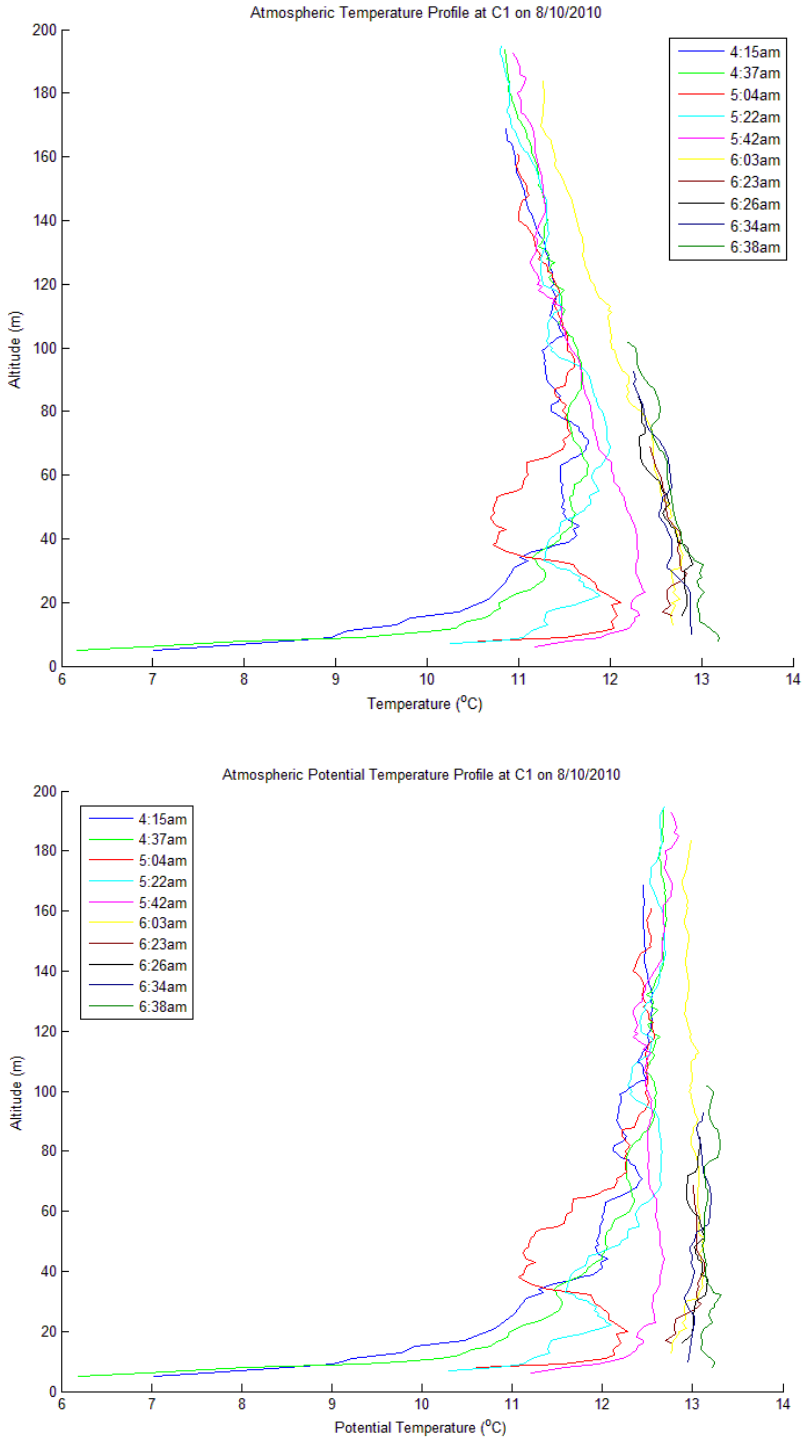

Figure 2.9. The atmospheric T_a profile (top) at C1 on the morning of 8/10/2010 (legend times are in MST). Profiles were created using a five block moving average. Sunrise occurred at 0504 MST. The two soundings prior to sunrise show strong inversions up to 40 m agl. This inversion quickly dissipates after sunrise. The bottom plot shows the θ profile.

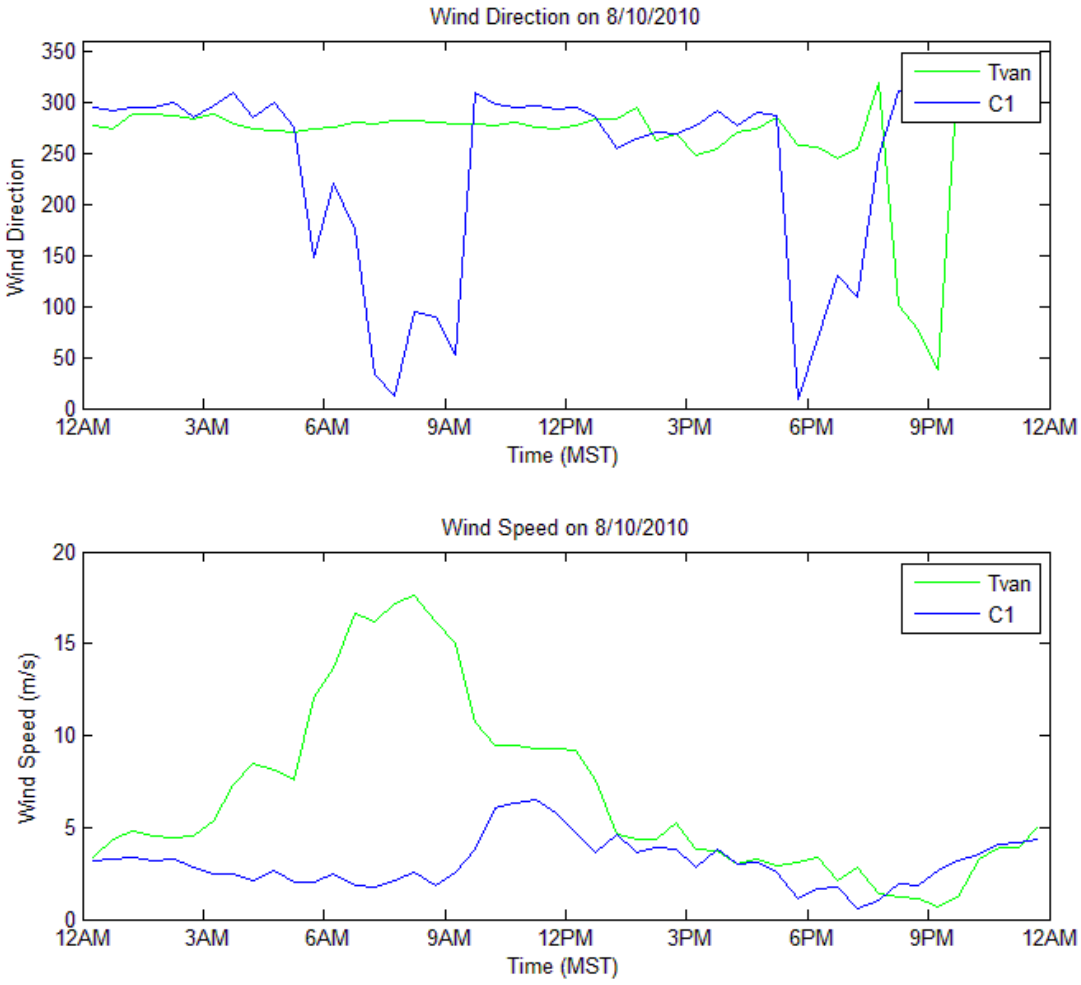

Figure 2.10. The *WD* and *U* values measured on 8/10/2010. There was a very large increase in *U* at Tvan around 0600 MST, which is not observed at C1.

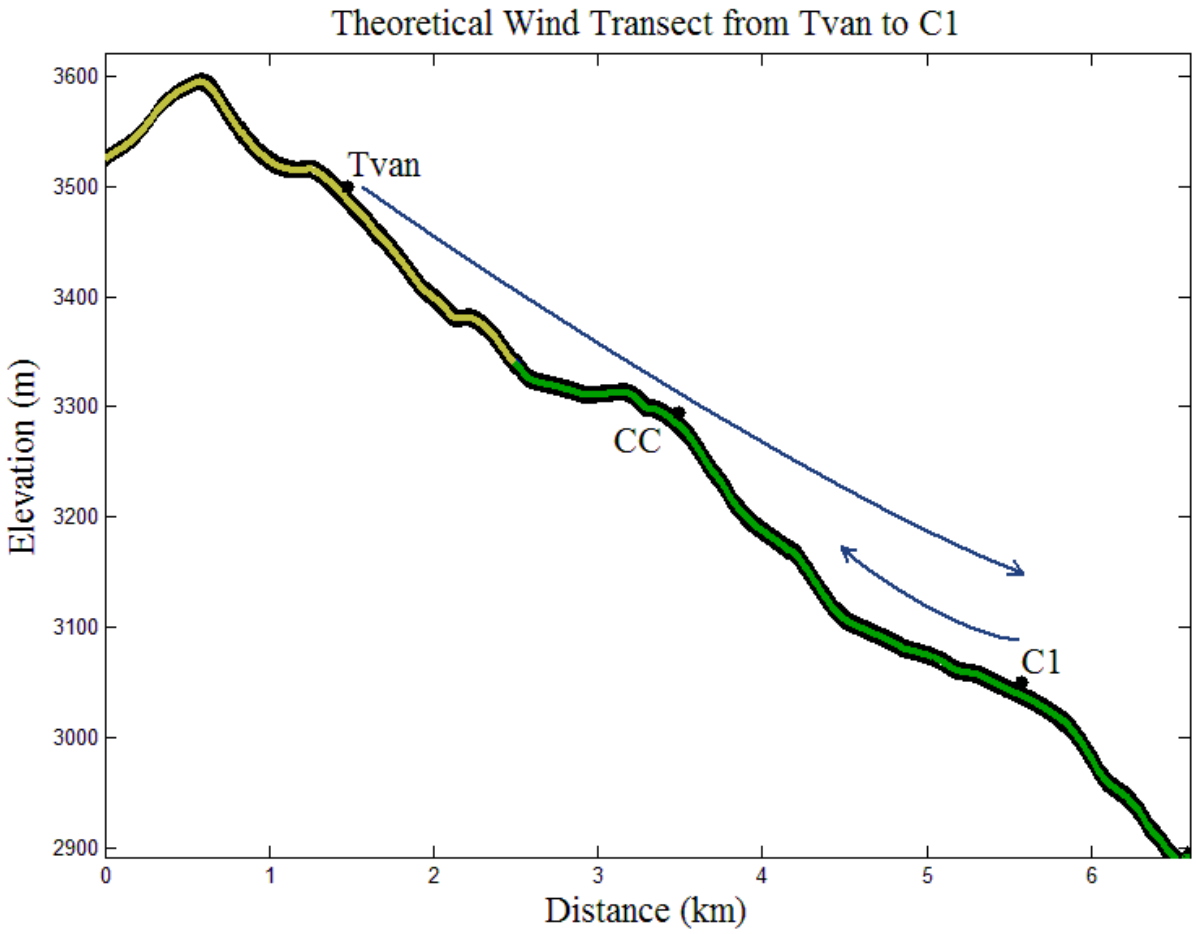

Figure 2.11. The theoretical *WD* plot based on the *WD* and observed at both sites and the maximum height of the 0623 MST sounding. The terrain is a cross-section of the ridge found by extracting elevation data from the line that passes through C1 and Tvan.

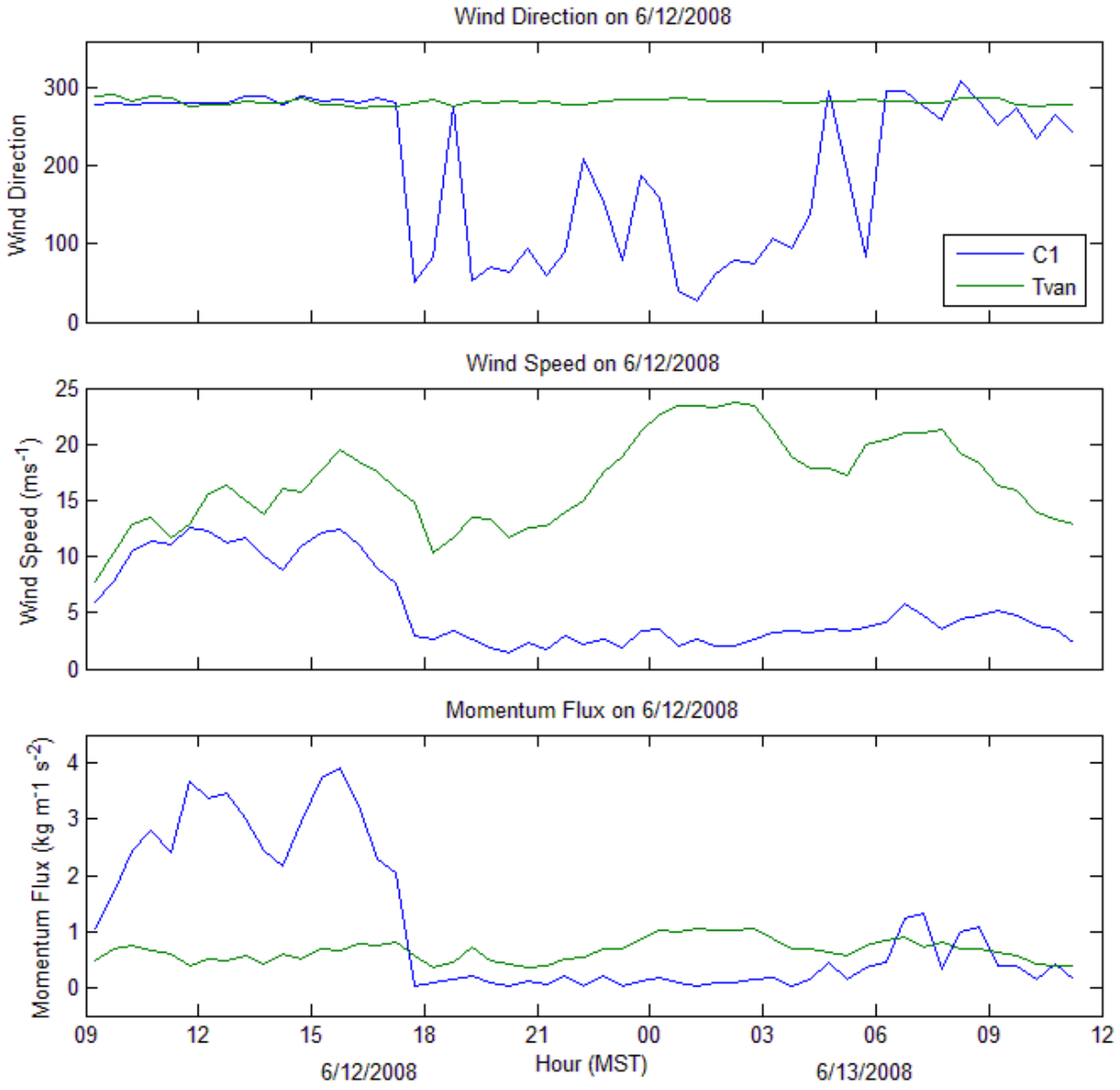

Figure 2.12. The nighttime *WD U*, τ at C1 and Tvan on 6/12/2008, into the morning of 6/13/2008.

experiencing steady τ of roughly 0.66 kg m^{-1} s^{-2}, and C1 experiencing high τ (as high 3.92 kg m^{-1} s^{-2}). At 1800 MST this downward momentum stopped and convergence began, with C1 switching from westerly to easterly flow. C1 experienced very calm winds the rest of the night (1-2 m s^{-1}) while *U* at Tvan increased, reaching a maximum at 0215 MST of 23.68 m s^{-1}.

The meteorological conditions surrounding this event closely resembled the situations described for upslope wind caused by mountain gravity waves (Doyle and Durran 2002, Turnipseed *et al.* 2004). Because there was no thermal mechanism to cause upslope winds at night (the thermal environment supports katabatic flow), and because of the existence of strong downward momentum, it is suspected that the cause of upslope winds may be a result of mechanical forcing.

To quantify these results nighttime convergence events were compared against daytime convergence events to see if meteorological variables showed differences. The variable showing the greatest variation was *U* (Table 2.4). During nighttime (2000 – 0400 MST) convergence events we observed average $|U_{Tvan}-U_{C1}|$ of 11.25 ± 6.00 m s^{-1}. This difference was much greater than the average nighttime $|U_{Tvan}-U_{C1}|$ for the whole dataset of 4.93 ± 4.62 m s^{-1}. This average was also different from the daytime convergence $|U_{Tvan}-U_{C1}|$ of 4.14 ± 4.32 m s^{-1}, and even more so the summer daytime convergence $|U_{Tvan}-U_{C1}|$ of 2.26 ± 2.43 m s^{-1}.

Observing the average *U* for C1 we can see that for all times of day convergence events had lower *U* than average (Table 2.5). However, *U* for Tvan showed a different pattern. During non-day and nighttime events it showed stronger winds than the average for the whole period. For daytime and summer periods convergence events showed weaker than average *U*.

Table 2.4. The average values of *WD* (degrees) for Tvan and C1 and *WD*(degrees), *U*(m s^{-1}), and T_a (^{o}C) differences between Tvan and C1 for convergence events for non-day (1600 – 0800 MST), night (2000 – 0400 MST), day (0800 – 1600 MST), and summer day (0800 – 1600 MST, months: 6-8) periods.

Period	N	WD_{Tvan}	WD_{C1}	WD_{Tvan}-WD_{C1}	$\lvert U_{Tvan}-U_{C1}\rvert$ [conv only]	$\lvert U_{Tvan}-U_{C1}\rvert$ [whole period]	$\lvert T_{Tvan}-T_{C1}\rvert$ [conv only]
Non-day	755	272.29	92.78	179.52	8.72 ±5.90	4.72 ±4.43	2.75 ±1.22
Night	305	271.07	91.19	179.88	11.25 ±6.00	4.93 ±4.62	2.76 ±1.01
Day	649	273.31	97.22	176.1	4.14 ±4.32	3.86 ±3.77	2.38 ±1.58
Summer-Day	187	272.05	96.46	175.59	2.26 ±2.43	2.04 ±2.45	1.92 ±1.17

Table 2.5. Average *U* (m s^{-1}) for Tvan and C1 for convergence events during the periods: non-day, night, day, and summer day, as well as the average *U* for those periods as a whole.

Period	U_{Tvan} [conv]	U_{C1} [conv]	U_{Tvan} [period]	U_{C1} [period]
Non-Day	10.47	2.25	9.23	5.01
Night	13.2	2.38	9.44	5.06
Day	6.14	2.33	8.64	5.12
Summer-Day	4.38	2.42	5.14	3.49

2.3.4 Synoptic-Scale Winds

The last part of this study determined the role, if any, synoptic-scale flow played in causing upslope flow. The first analysis was to find the frequency of easterly/southeasterly synoptic-scale flow and to determine whether local flows aligned with these events. The second analysis observed the relationship between synoptic-scale *U* and local, upslope flow.

Our analysis revealed that over two years the surface upslope flow ($50° < WD_{C1} < 130°$, $100° < WD_{Tvan} < 180°$) aligned with like synoptic-scale flow 3.24% of the time over the alpine tundra and 3.42% over subalpine forest. Narrowing the parameters to include only summer (JJA) days easterly flow on the ground aligned with easterly synoptic-scale conditions 1.28% of the time in the tundra, and 4.94% of the time above the subalpine forest. The lack of large scale easterly and southeasterly flow was visible in the synoptic-scale wind roses (Figure 2.13) which showed that the vast majority of all winds were westerly, falling between 240° and 300°, with a slight increase in northwesterly flows during the winter months. Because only a small percentage of upslope flows aligned with similar synoptic-scale conditions, it is concluded that synoptic-scale winds were not responsible for the vast majority of upslope flows.

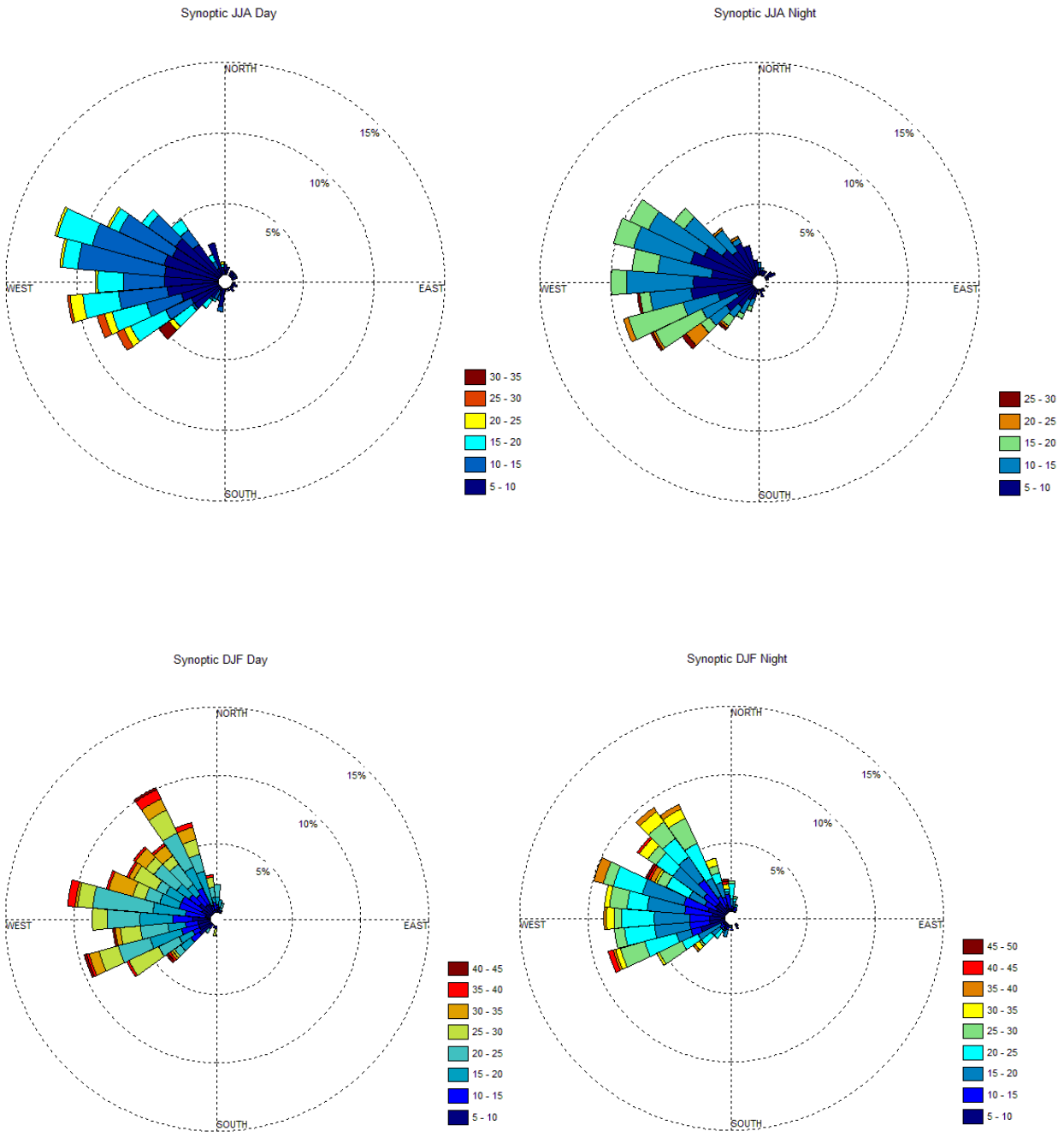

Figure 2.13. Wind roses of the summer and winter synoptic-scale *WD* (day and night) using MERRA reanalysis data. Wind roses on the following page show the summer *WD* (day and night) for Tvan and C1. The wind roses show *WD* combined into 10^{o} blocks and shown as percentage of all winds, and *U* in m s^{-1}.

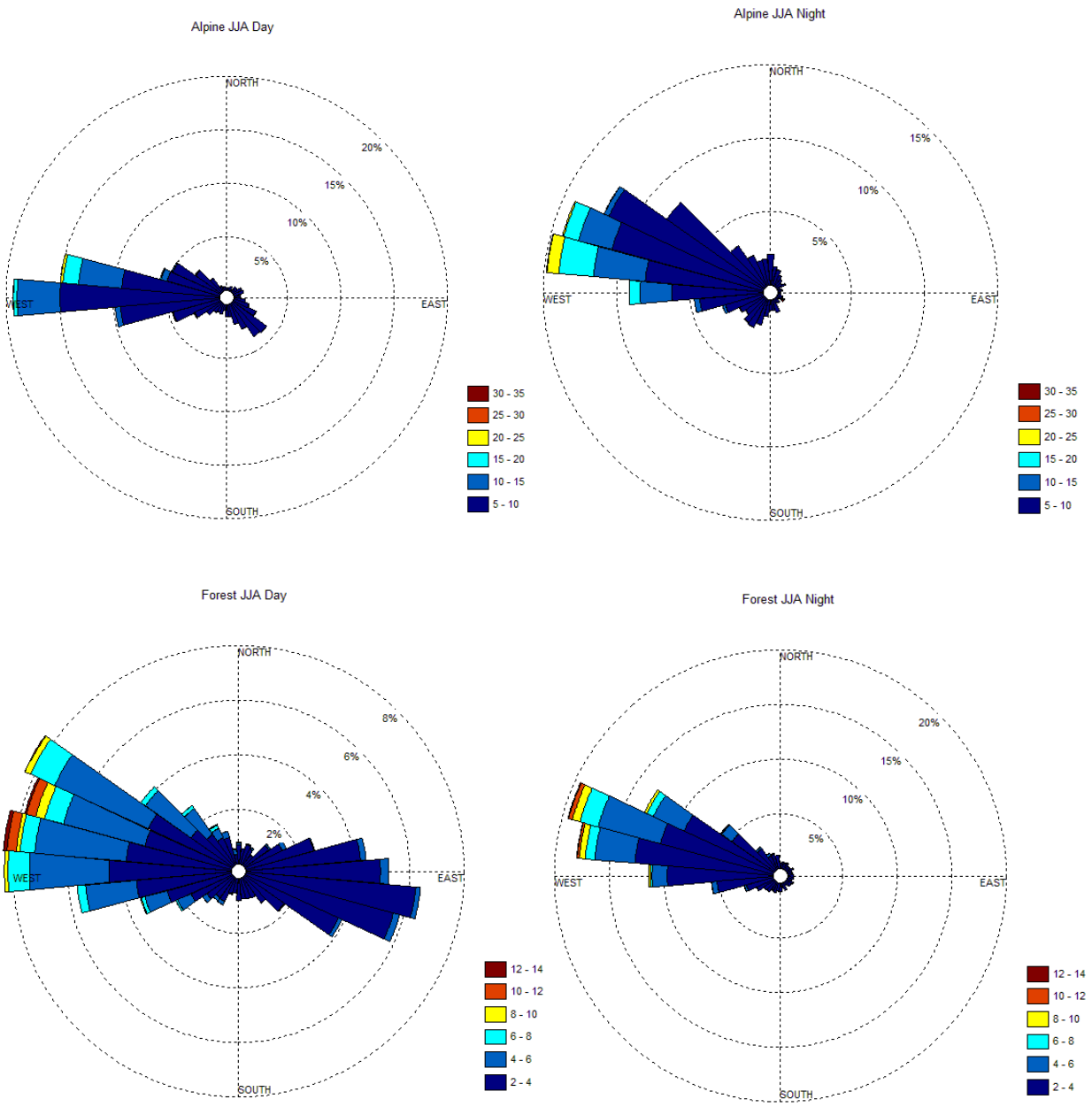

Figure 2.13 continued.

Synoptic-scale *U* was also analyzed for influence on upslope flow regimes. Results showed that 61.49% of upslope winds in the alpine tundra and 60.85% of upslope winds in the subalpine forest occurred when the synoptic-scale *U* (500 mb level) was less than its median value of 15.28 m s^{-1}. Throughout the year, *U* was lowest during the summer (Figure 2.14), with 78.9% of summer hours below the yearly median *U*. During this 78.9% of summer hours 84.64% of tundra and 76.52% of forest summer upslope winds occurred. During the 50% of summer hours lower than the median *summer* synoptic-scale *U* (10.9 m s^{-1}), 50.38% of tundra and 49.48% of forest upslope wind events occurred. These findings show that throughout a year, synoptic-scale *U* had only a modest relationship with the existence of upslope winds.

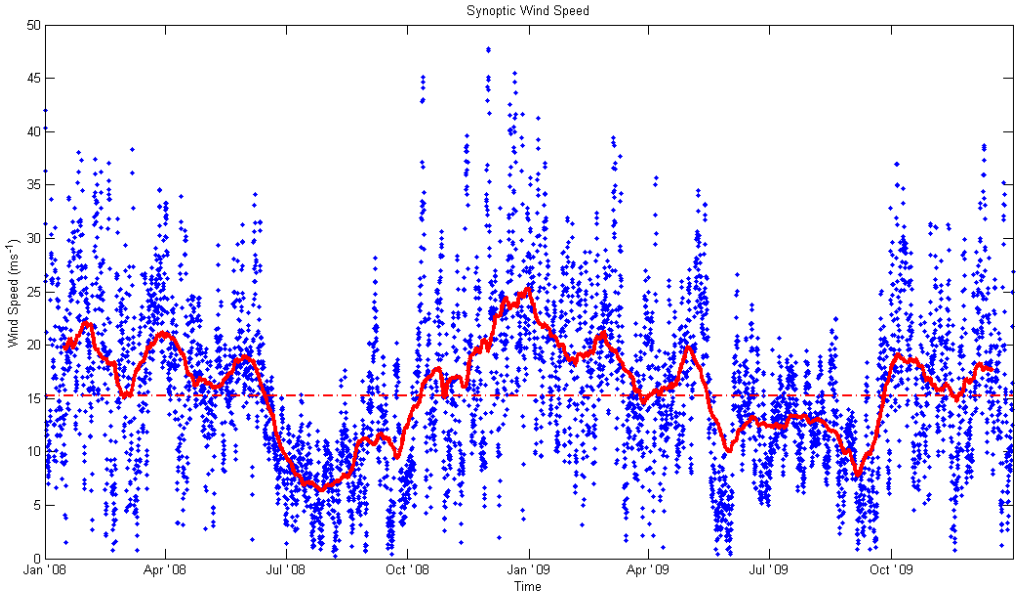

Figure 2.14. The synoptic-scale *U* values at the 500 mb level above Niwot Ridge for two years (2008-2009). The red line shows the 30 days moving average of the *U* data. The dashed red line shows the median *U* value (15.28 m s^{-1}) of the whole data set.

2.4 Conclusions

This study of Niwot Ridge found the presence of upslope winds due to thermally-driven flows, mechanical forces, and synoptic-scale weather. The goal of this study was to distinguish the temporal and spatial characteristics of these separate flows.

Mechanical flows were found to be winter and nighttime occurrences. They were distinguishable by strong downdrafts preceding upslope flow in the subalpine forest and by high *U* over the alpine tundra. These convergence events showed large differences between alpine and subalpine *U* and are believed to be responsible for causing the large discrepancies between nighttime convergence $|U_{Tvan}-U_{C1}|$ (11.25 ±6.00 m s^{-1}) and total nighttime period $|U_{Tvan}-U_{C1}|$ (4.93 ±4.62 m s^{-1}). The finding that $|U_{Tvan}-U_{C1}|$ during daytime convergence events was lower than normal daytime conditions suggests that mountain gravity waves are not common to this time of day.

The analyses also revealed that the influence of 500 mb level flow in the creation of upslope flows was minimal. Alignment of these upper level winds and with local upslope flows occurred less than 3.5% of the time at both Tvan and C1 over the two years of data collection. Even under persistent (days long) easterly/southeasterly synoptic-scale wind events, local sites exhibited katabatic (westerly) flow during nighttime hours. This suggests that these winds did not strongly influence local winds.

While these analyses did not reveal strong synoptic-scale influence, this result is not conclusive. There are many upslope wind events that cannot be explained by mechanical or thermal forcings. It is believed that such wind events may still be due to large-scale weather

patterns. One possibility is that such events were unaccounted for due to inaccuracies in the broad scale meteorological model. Another possibility is that the use of the 500 mb level for determining synoptic-scale flow may have simply been too high an altitude to gain an accurate account of how large-scale weather patterns behave closer to the surface.

In addition, weak synoptic-scale flow has often been described as being an environmental requirement before thermally-driven, upslope flows can occur. This is usually cited because thermally-driven, upslope flows occur in the summer and *U* is lower in the summer (Turnipseed *et al.* 2002). While upslope flows and weak synoptic-scale winds are temporally correlated they may not be directly related. Observations during summer showed that moderate fluctuations in synoptic-scale *U* did not play a large role in altering upslope flow. This is shown by the finding that in both the tundra and forest roughly 50% of upslope winds occurred above and 50% below the median *summer* synoptic-scale *U* value (10.9 m s^{-1}). It was also found that 84.64% of tundra and 76.52% of forest summer upslope winds occurred in during the 78.9% of summer hours in which synoptic-scale *U* was below the *yearly* median (15.28 m s^{-1}). This means 15.36% of tundra and 23.48% of forest summer upslope wind events occur in the 21.1% of time in which summer *U* was *above* the yearly median, indicating upslope wind events occur regardless of synoptic-scale *U*. This was supported by the tethersonde experiment, where the surface was experiencing anabatic flow and the tundra was experiencing strong westerly winds. This suggests that it is not high *U* in the winter that limits thermal flows, but the correct thermal environment.

While the thermal environment in the winter is not as suitable for thermally-driven, upslope flows, with upslope flow largely dominated by synoptic-scale and rotor winds, these thermal flows may occasionally develop. This was concluded due to the higher frequency of

upslope flow in the daytime in winter months, compared to nighttime. These flows may be due to heating of the subalpine canopy. In the winter snow does not remain on the canopy, which allows for high sensible heat flux over the subalpine forest. The negligibly higher frequency of daytime versus nighttime upslope flow in the tundra is due to the lack of canopy, since snow cover greatly reduces sensible heat flux.

During the study period thermally-driven, upslope flows showed the highest frequency during summer days. It was found that a majority of summer days in the subalpine forest (~90%) and alpine tundra (~66%) experience some degree of upslope winds. In the subalpine forest these winds appear to be due to anabatic flows given their propensity to initiate in the hours just following sunrise.

In the alpine tundra, the initiation of upslope flow was not strongly tied to sunrise. It was found that there was a lag time between upslope flow at C1 and Tvan, with upslope flow not typically developing at the tundra site until midday. In addition, a deviation from upslope flow in the late morning hours at Cabin Clearing reversed at 1200 MST concurrent with the start of upslope flow at Tvan. The long lag time for the tundra site suggests that there is a second criterion, beyond anabatic forcings, required for upslope winds to initiate here.

Lastly, convergence on Niwot Ridge was observed in all months, with a slight preference for summer months. However, it was found that an individual upslope event in the subalpine forest was less likely to be a convergence event (e.g. westerly flow in the tundra) in the summer than it was in the winter. This suggests that mountain gravity waves and synoptic-scale events, which are more dominant in the winter, are more conducive to creating convergence than thermally-driven flows.

The main goal of this work was to determine when thermally-driven, upslope flows occurred in the study region. This information was used to inform the following sections which attempt to determine the role of alpine treeline in altering thermally-driven flows and to identify the different airmass composition of upslope versus downslope winds. This research found that mechanical upslope winds were common to winter and nighttime and that there was minimal synoptic-scale influence on upslope flows. Therefore the following chapters will consider all summer, daytime upslope events to be the result of thermal forcings and disregard mechanical and synoptic-scale winds.

Chapter 3

Land Surface Temperature Distribution over Niwot Ridge, Colorado and its Effect on Thermally-driven, Upslope Flows

Abstract

Upslope thermally-driven flows are common to mountainous terrain. The development of daytime upslope flows is caused by incoming short-wave radiation disproportionately increasing the sensible heat flux on the slope oriented towards incident solar radiation (Orville 1964). These heated surfaces create a local horizontal pressure gradient causing wind to blow uphill. Because of the role of surface heating, thermally-driven flows are mainly summer phenomena (Baumann *et al.* 1993, Turnipseed *et al.* 2002, Blanken *et al.* 2009). While it is known that there is a higher frequency of upslope flows in the summer, this study separates the thermal flows into two main categories: anabatic flow and land cover-induced flow. Anabatic flow was defined as any flow caused by surface heating creating an upward buoyancy and a horizontal pressure gradient across all heated surfaces of the mountain. Land cover-induced flow was defined as flow which was specifically created by the differential surface heating of two distinct yet adjacent land covers; subalpine forest and alpine tundra. By these definitions anabatic flow was expected to occur over a whole mountain face, while land cover-induced flow would develop at treeline before expanding outwards. By determining the spatial and temporal surface temperature (T_s) distribution across the ridge it was determined that anabatic flow was more common overall, with particularly high frequency in the mornings. Land cover-induced flows showed a low frequency of occurrence due to the fact that even with disproportionately high tundra soil temperatures (T_{soil}) the sensible heat flux (H) and surface pressure (p_o) values

rarely became conducive to generating upslope flow. However, it appeared that the differential land cover heating may still play a role in increasing the frequency of afternoon upslope flow.

3.1 Introduction

3.1.1 Thermally-Driven Flows

Anabatic flow refers to upslope flow caused by the combination of buoyancy force and horizontal pressure gradient force (*PGF*). The mechanics of these winds were discussed in Chapter 2.

Anabatic flows are influenced by a host of different environmental factors such as steepness of the slope, the magnitude of the ratio of H to latent heat fluxes (λE) (the Bowen ratio; $\beta = H/\lambda E$), and synoptic-scale flow (Whiteman and Doran 1993). Previous studies have shown that slope angle may influence thermally-driven flows. Whiteman and Doran (1993) point out shallow valleys do not often produce strong enough pressure gradients to overcome geostrophic pressure gradients. Conversely, Kossmann and Fiedler (2000) point out that on very steep slopes *PGF* becomes negligible compared to buoyancy force, reducing the likelihood of horizontal advection. Equation 1 (page 8) illuminates this relationship between slope angle and both buoyancy force and *PGF*. Niwot Ridge falls in this zone of moderate grade (with typical slope angles of ~5%). In addition, being in a dry climate on the lee side of the Continental Divide, the typical β (1.60 in the tundra, 1.32 in the subalpine forest for summer (JJA) midday periods (1200 - 0100 MST)) for Niwot Ridge is very conducive to thermal flows. Since the steepness and β of Niwot Ridge are suitable for anabatic flow, we expect that this type of wind is often present.

Another force known to influence local wind patterns, often associated with mountain environments, is land cover differences. Land cover surfaces often have their own unique environmental signature, showing different albedos, transpiration rates, responses to insolation, surface energy, radiation (R_n), and water balances, etc. These differences, specifically H differences, can create local wind patterns.

This type of local wind (aka mountain/valley breezes) has been well documented in scientific literature. The modeling results of Pielke and Vidale (1995) claimed that the average daily difference in H of 50 W m^{-2} between the boreal forest and arctic tundra was large enough to cause the formation of arctic fronts, thus influencing synoptic-scale weather patterns. Chase *et al*. (1999) found that a conversion from natural grassland to irrigated cropland caused an increase in λE over H, effectively reducing the magnitude of upslope flow. In their mountain/valley flow model, Lee and Kimura (2001) set the mountain as a homogeneous forest and the low-lying plains as grasslands. They argued that the increased surface heating of low-lying grasslands (compared to forests) was responsible for weakening or reversing anabatic flow in the afternoon, since it would create a pressure gradient force in which winds would travel from the mountain to the plains. These studies all point to the fact that different land surfaces can initiate winds on a local and regional scale depending on the size of the land cover regions in question.

On Niwot Ridge there is a forest/grassland transition seen in the alpine treeline ecotone similar to that in the studies described above. The modeling results described above, showing that the grassland warms to greater maximum T_s than the forest, suggesting that the transition in land cover should create a local heat distribution capable of generating upslope flows. A recent study on Niwot Ridge found that in the summer tundra has the highest T_{soil}, followed by krummholz soil, and lastly followed by forest soil (Withington and Sanford 2006). Because

higher T_{soil} leads to a higher H (Garratt 1992, Kondo and Ishida 1997) it follows that such a T_{soil} distribution would promote upslope flows.

While there is solid theoretical basis for the upslope/downslope flows on Niwot Ridge being influenced by the sharp difference in land cover across the forest-tundra ecotone, there are also some contradictory findings. As presented in Chapter 2, there was a greater frequency of upslope flows above the subalpine forest than above the alpine tundra during the summer months (also shown by Blanken *et al.* 2009). Therefore, if land cover was responsible for inducing flow, we would expect that the tundra would experience a similar frequency of upslope flows, if not greater, since it would be experiencing both anabatic flow and land cover-induced flow. In addition, a previous study by Blanken *et al.* (2009) found that H was nearly always higher over the subalpine forest than the tundra, contradicting the land cover-induced flow theory.

Mountain environments are considerably more complex than the idealized, flat land versions used in several meteorological models. Therefore, an in-depth investigation of the spatial and temporal distribution of T_s and T_{soil} on Niwot Ridge was undertaken to determine whether treeline influences heating or whether some other factor(s) is (are) at play in complex terrain. The environmental variables, aspect, slope, elevation (defined as meters above sea level), and NDVI ($\frac{r_{NIR}-r_{red}}{r_{NIR}+r_{red}}$; where r is spectral reflectance) were observed to determine which had the strongest influence on T_s and T_{soil}. The goal was to determine whether factors other than land cover differences played a role in the distribution of T_s and T_{soil} and consequently thermally-driven flows.

While aspect, slope, elevation, and NDVI undoubtedly influence T_s and T_{soil}, land cover was expected to have a strong influence (based on the previous findings by Withington and

Sanford (2006)). Therefore, land cover was quantified and T_s and T_{soil} distributions based on the land cover classification were found. These temperature distributions were analyzed to determine how they influenced H and p_o on both sides of the alpine treeline. This allowed us to determine whether or not anabatic flow or land cover-induced flow was more influential in generating upslope flow.

It was hypothesized that when the T_s and T_{soil} differences between the tundra and forest (e.g. $T_{s\,tundra} - T_{s\,forest}$) were greatest, there would be a higher H above the tundra on the ridge top. At such times anabatic flow and land cover-induced flow should work together to draw air upslope. On days in which the temperature differences were not great, because of low insolation, we expected that land cover-induced flow would not exist and that only anabatic flow would exist. Therefore the hypothesis was that land cover-induced flow most likely exists after a threshold T_s (or T_{soil}) difference has been reached. Upslope flow at times when there was small T_s difference between tundra and forest would suggest the existence of only anabatic flow.

3.1.2 Land Surface Temperature

The estimation of T_s is important to many different areas of climate research. Today there are several satellites with capabilities for determining T_s and emissivity (ε) (e.g. ASTER, AVHRR, MODIS, Landsat, etc.). In theory, all satellites obtaining thermal infrared imagery can be used to estimate T_s, however, there are many factors which influence the accuracy of such estimations, making certain sensors much more effective than others.

The theoretical basis for converting thermal infrared irradiance to T_s lies in Planck's Function. Planck's function relates radiated energy emitted by a black body to its effective

temperature. For a non-black body (graybody, $\varepsilon < 1.0$) the function is multiplied by ε, or the ratio of radiance emitted at a specific wavelength to the radiance emitted by a black body at the same temperature (Dash *et al.* 2002) and is written as:

$$R(\lambda, T) = \varepsilon(\lambda)B(\lambda, T) = \varepsilon(\lambda)\frac{c_1}{\lambda^5\left(e^{c_2/\lambda T}-1\right)} \qquad \text{[Pu } et\ al. \text{ 2006]} \qquad [2]$$

Where $\boldsymbol{R}(\lambda, T)$ is spectral radiance of a non-black body, λ is wavelength, $\varepsilon(\lambda)$ is emissivity of a body at λ, T is temperature, and c_1 and c_2 are constants. Since the satellite sensor measures spectral radiance, we can derive T_s by rearranging equation (2):

$$T = \frac{c_2}{\lambda \ln\left(\frac{(\varepsilon(\lambda)\, c1}{\lambda^5 R}+1\right)} \qquad [3]$$

This equation is further simplified to:

$$T = \frac{k_2}{ln\left(\frac{k_1 * \varepsilon}{R}+1\right)} \qquad [4]$$

, where k_2 (1260.56 Kelvin) and k_1 (607.76 $Wm^{-2}sr^{-1}\ \mu m^{-1}$) are constants (Chander and Markham 2003, Li *et al.* 2004).

The theory behind the conversion of thermal infrared radiance to T_s works only under an exact set of ideal conditions. The three major effects that must be accounted for in any reliable T_s estimation are atmospheric, angular, and emissivity effects (Dash *et al.* 2002). The most important correction of the three is accounting for atmospheric effects. The atmosphere can affect T_s calculations in three major ways. The molecules of the atmosphere can absorb radiance leaving the Earth's surface before it reaches the sensor. Second, the atmosphere can contribute its own signature to the sensor reading by upward atmospheric emission. And third, the atmosphere can reflect irradiance back to the surface (Franca and Cracknell 1994).

In the thermal infrared region (8-12 μm) the effect of aerosols on the above three atmospheric effects is negligible (Prata *et al.* 1995), with water vapor being the single most important atmospheric molecule influencing the T_s calculation. This is because of the spatial and temporal distribution of water vapor compared to other aerosols. While O_3 and CO_2 also have partial absorption bands in the thermal infrared regions they vary slowly (temporal homogeneity) and are evenly distributed (spatial homogeneity) (Dash *et al.* 2002). This allows for their contributions to act as more of a constant in the algorithms accounting for atmospheric effects. Because water vapor varies on short time scales and is poorly mixed, it is the most important gas for which to correct.

In addition to water vapor, the other major atmospheric contribution to altering T_s is the vertical air temperature (T_a) profile. According to Dash *et al*. (2002) the top of the atmosphere brightness temperature (T_b) derived from the reverse Planck function method is generally lower than the actual T_s. However, this is reversed, causing overestimation of T_b, when the atmosphere is warmer than the surface (i.e. when there is a temperature inversion). Therefore, the T_a profile is important because it can slightly influence (positively or negatively) the surface thermal infrared radiance as it passes through. Prata *et al*. (1995) found that the range between calculated T_b and T_s under different atmospheric temperature profiles is generally between 1K and 5K.

There are two generally accepted methods used to account for both T_a and water vapor profiles. The most accurate and most labor intensive method is to obtain radiosonde-based T_a and humidity profile data. The problem with using radiosondes in this context is that soundings must be collocated and synchronous to satellite measurements (Dash *et al.* 2002). The other method is to use vertical sounders (on satellites) which can estimate the water vapor and T_a profiles of the atmosphere.

Angular effects and emissivity are the other two main corrections for T_s. Angular effects must be taken into account because the path length of surface radiation to the sensor will be different depending on the angle of view. As described above, the atmosphere inputs its own signature onto the radiance observed at the sensor. Therefore, the path length will be critical to how much attenuation or emission occurs within the atmosphere. Angular effects, however, are not always taken into consideration. Under circumstances where the zenith angle view of the satellite is small, for example 8.55 ^{o} on ASTER, angular effects are often ignored (Pu *et al.* 2006).

The emissivity correction is used to convert T_b into actual T_s by assigning the ratio of radiance to blackbody radiance for each different land cover on the map. However, in general, is not as important as the other two corrections, exhibiting much less influence on the accuracy of results (Becker and Li 1990, Qin *et al.* 2001), with some studies altogether ignoring it (Pu *et al.* 2006).

3.2. Methods

3.2.1 Surface Temperature

Land surface temperature (T_s) on Niwot Ridge was found using Landsat 5 Thematic Mapper thermal imagery obtained from USGS Global Visualization Viewer. Band 6 data were used, which spans from 10.4 to 12.5 μm. Landsat 5 is a sun-synchronous near polar orbiting satellite that has a return interval of 16 days, thus limited the overall days that could be studied. In addition, only days with minimal cloud cover could be used, since clouds interfere with the transmission of thermal emission from the surface. After these selection criteria were met only

nine days were selected for analysis: 3/3/05, 3/8/01, 3/11/08, 4/17/04, 6/15/08, 6/21/10, 8/5/09, 8/21/09, and 9/11/05.

The satellite images were imported into ENVI where radiance was derived from digital numbers (DN) representing brightness using ENVI's Calibration Utilities Landsat TM tool. While ENVI does have an Emissivity Normalization tool it was not used for these data because they had only one thermal band. To get emissivity a split window approach using a multiband dataset would have been required. Because emissivity is the most insignificant of the corrections it was ignored, and all data points were assigned an emissivity of 0.96. As Li *et al.* (2004) explain, precise emissivity values are only required when exact T_s are needed. For the purposes of this research, exact temperatures were not required, only knowledge of the relative T_s distribution.

In addition, no angular or atmospheric corrections were used. Lack of an angular correction should not have a large impact on T_s estimates as Landsat 5 has a constant viewing angle and this correction is only necessary if an atmospheric correction is applied. The lack of an atmospheric correction may be responsible for significant inaccuracies, however over a region as small as our study site (8 x 13 km) it is assumed that the influencing atmospheric components will be distributed homogeneously. Under this assumption the relative temperature distribution should still remain accurate.

At this point all information for a single channel T_s estimate were applied to the approximated inverse Planck function (equation 4). To solve this equation the band math tool was used, yielding georeferenced T_s data of Niwot Ridge at 120 x 120 m resolution. Since atmospheric effects were not corrected for these T_s values are actually T_b (at satellite

temperatures) and should range between ± 1 K to ± 5 K from true T_s values depending on the atmospheric environment (Prata *et al.* 1995).

The data were exported as an ascii file and imported into ArcMap for the remainder of the analysis: comparing T_s distribution to a digital elevation model (DEM) and land cover. The 10-m DEM of Niwot Ridge was over an 8 x 13 km area obtained from the Niwot Ridge LTER online database. The DEM was used to find the relationship between T_s and elevation, slope, and aspect. In addition to these three variables, NDVI was also found using the band math tool in ENVI. The environmental categories were broken into 50 equal intervals (Reclassify tool). T_s averages for each category were obtained using zonal statistics in ArcMap. This analysis was repeated for each of the nine scenes collected. These averages were plotted for each category and each day and analyzed to find the strongest patterns influencing T_s distribution on Niwot Ridge.

In order to accurately compare T_s data of different elevation, potential temperature (θ) was derived by using:

$$\theta = T\left(\frac{P_o}{P_o\left(\frac{zL}{T_o}+1\right)^{-g/LR}}\right)^{R/c_p} \qquad [5]$$

, where z is height agl, L is the lapse rate (-6.5°C/km), R is the gas constant (287 $Jkg^{-1}K^{-1}$), c_p is specific heat capacity (1004 $Jkg^{-1}K^{-1}$), g is gravity, T_o is T_s at sea level, and P_o is the pressure at sea level. Because surface pressure values were not available for each cell of the satellite data, P_o was obtained using the elevation and a standard lapse rate of -6.5°C/km. Variables T_o and P_o were set to the temperature and pressure of the lowest elevation (instead of sea level). While not the standard definition of θ, this calculation allowed for the comparison of temperature in the

study region without the influence by elevational differences. The θ for each of the fifty elevation groups was calculated and plotted against elevation.

3.2.2. Land Cover

In addition to categorizing the study region in terms of elevation, aspect, slope, and NDVI, land cover classes were also determined. ENVI classification tools were used on the satellite data from 8/21/ 2009 for land cover classification because it was in the middle of the growing season and there was no snow cover. Since unsupervised classification techniques yielded results that did not appear close to reality, the Minimum Distance Supervised technique was used. Homogeneous regions of different land cover types were outlined so that ENVI could extrapolate these over the whole map based on their spectral signatures.

The satellite data for the study region were compiled to include six of seven bands in one file. The reflectance values were calculated for each band (band 6 was excluded because the thermal infrared band measures emission, not reflectance). Including the maximum number of bands allowed for a more detailed spectral signature to be obtained, thus allowing for greater accuracy of results. The second step was to map out the Regions of Interest (ROI) in ENVI. This was completed by isolating the most homogeneous regions of land cover type from a true color composite map of the region. Once this was completed, the Minimum Distance Classification tool was applied to differentiate the selected ROIs on the map. At this point the files were exported as ascii and imported into ArcMap where the average T_s for each category was obtained. These land cover classes were also compared to the four environmental categories to see how elevation, aspect, slope, and NDVI varied across different land cover types.

3.2.3. Soil Temperature

For an additional investigation at the T_s distribution across Niwot Ridge, T_{soil} was measured. Thirty-six battery-powered temperature sensors (ibuttons, Embedded Data Systems, Lawrenceburg, KY) were placed using systematic random sampling across a 3 km x 4 km area on the south side of Niwot Ridge. Three randomly placed sensors were added to each square kilometer (except where they overlapped with the restricted City of Boulder Watershed) and placed at 10-cm depth (Figure 3.1). For the summer period (7/7/09 to 9/30/09), these sensors were set to record T_{soil} once at hour. For the winter period, the sensors were set to collect once every three hours. The sensors have an accuracy of ± 1^{o}C and a resolution of 0.5^{o}C as reported by the manufacture, although an independent test of the ibutton has shown the accuracy to be ± 0.21^{o}C (Hubbart *et al.* 2005).

Upon data collection only 27 out of the 36 remained functioning, so only these were used. These T_{soil} values were used to corroborate T_s findings from the satellite thermal imagery. In addition, the T_s data were divided into their respective land cover class. Hourly temperature averages for these different land cover types were calculated to determine how T_{soil} varied throughout the day under different canopies.

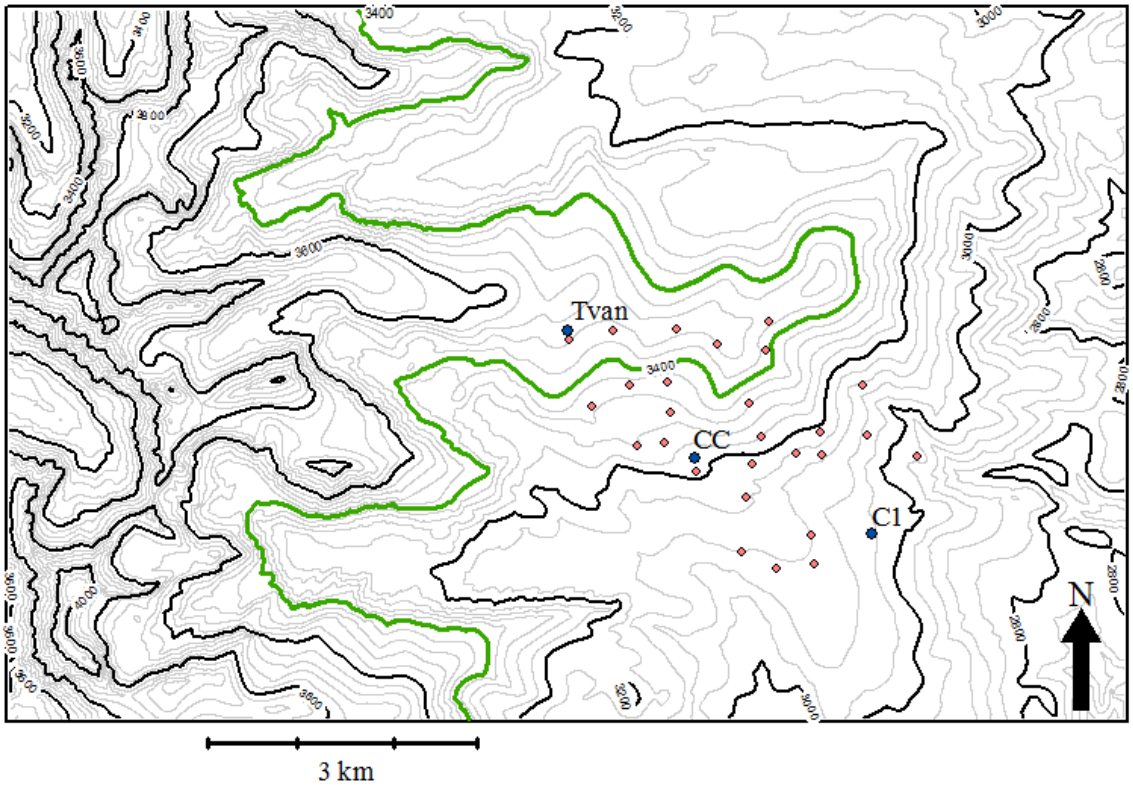

Figure 3.1. Topographic map showing Niwot Ridge. The extent is equivalent to the T_s analysis (8 x 13 km), with heavy contour lines every 200 m and light contour lines every 40 m. The pink dots represent the placement of the 27 soil probes. The blue dots represent the location of the three meteorological stations. The 3400 m contour roughly represents the location of alpine treeline (highlighted green).

3.2.4. Sensible Heat Flux and Pressure

The last part of this analysis was to determine how H and p_o varied over the tundra and the subalpine forest, since both of these variables are important to local thermal flows. Wind direction (*WD*), H, and p_o variations were observed under different T_{soil} distributions. Days were divided into three main categories based on their T_{soil}. The first category included all days in which the T_{soil} in the tundra was at least 10^{o}C higher than the forest at some point throughout the day (17/68 days; 25%). The second category was for all days in which the tundra T_{soil} was at least 5^{o}C higher than the forest at some point throughout the day (26/68 days; 38.2%). This category excluded all days that exceeded a 10^{o}C difference (first category) as well as the days from the final category. The last category selected all days in which the T_{soil} in the forest was greater than the T_{soil} in the tundra at any time during the day (20/68 days; 29.4%). The remaining 5/68 days were days where tundra T_{soil} remained between 0^{o}C and 5^{o}C were excluded from this analysis. The mean hourly *WD*, H, and p_o for each category were obtained.

3.3. Results

3.3.1 Environmental Variables

The T_s analysis described in *section 3.2.2* attempted to determine whether elevation, slope, aspect, or NDVI played the largest role in influencing T_s. Breaking down each of these categories into fifty separate, equally spaced groups we observed whether or not there were distinct T_s differences/patterns for each category.

A few basic patterns in T_s were observed in regards to elevation, aspect, slope, and NDVI (Figure 3.2). T_s generally decreased with elevation; this relationship was strongest during the

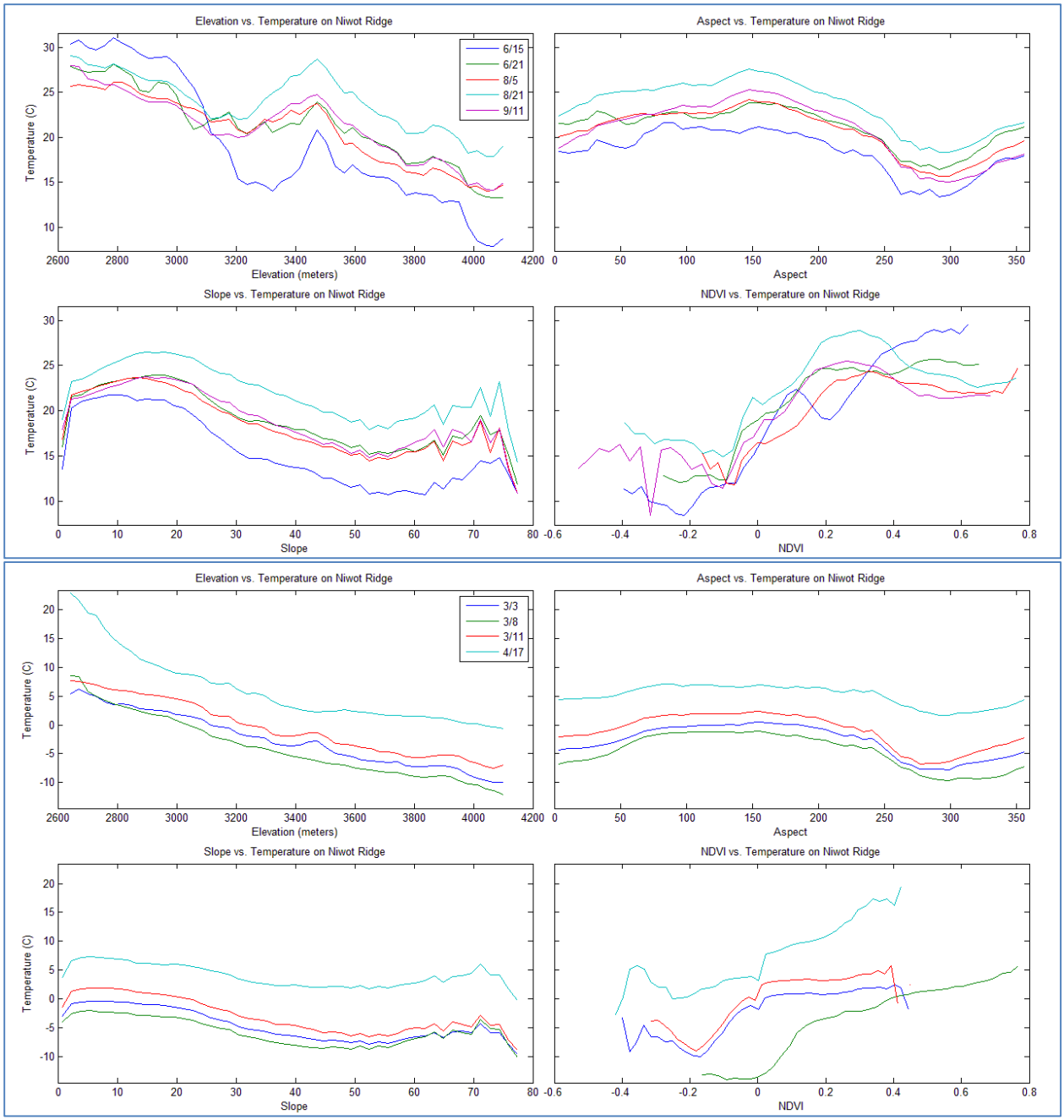

Figure 3.2. This plot shows the average T_s on Niwot Ridge for elevation, aspect, slope, and NDVI classes on winter/spring days. Using ArcMap reclassification tool elevation, aspect, and slope were divided into 50 equal interval classes and NDVI into 41. Then zonal statistics were run to calculate the mean T_s of each class for each day. Negative NDVI represent water and snow surfaces. The top set of plots shows the summer days: 6/15/08, 6/21/10, 8/5/09, 8/21/09, and 9/11/05. The bottom set shows the winter/spring days: 3/3/05, 3/8/01, 3/11/08, and 4/17/04.

colder months. However during the warmer months, the decrease in T_s with increasing elevation was interrupted at around 3200 m with a distinct reversal of T_s over several hundred meters, with a local maximum at 3400 m. This appears to be the result of the transition from subalpine forest to tundra.

The distribution of T_s according to aspect also shows a definite pattern. South-facing slopes had the highest T_s on all days observed. These high T_s values existed not just for due south aspect, but remain relatively constant for all aspects from roughly 60^o to 240^o. The lowest T_s values occurred around 270^o to 300^o on all days. Given that the readings occurred at 1030 MST it was expected that southeast slopes would have the highest T_s and that northwest slopes would have the lowest T_s.

The temperature analysis of slope angle showed that in general lower slope regions (0^o to 20^o) have the highest T_s, while higher slopes (40^o to 60^o) show the lowest values. Based on slope grade alone this does not fit with the predicted outcome. The sun elevation at 1030 MST at this mid-latitude site was between 38^o (on 3/3/05) and 64^o (on 6/21/2010). Therefore, considering that direct, perpendicular rays from the sun have a greater capacity to heat a surface, we expect that if slope were the only variable influencing T_s then the complementary angle to the sun elevation angle on any given day should have the highest T_s.

In general we see that NDVI varies with with T_s, with low NDVI land cover, such as snow and water, exhibiting low T_s and highly vegetated regions exhibiting high T_s. However, during summer days we see an additional relationship. For these days there is a slight decrease in T_s for the highest values of NDVI, suggesting that the places with the highest T_s are those which are lightly vegetated (i.e. tundra and krummholz, with a low leaf area index).

While the previous analysis did yield information on T_s distribution it is difficult to separate the variables and get independent causal relationships, since the variables have multiplicative effects. Calculating θ for these T_s distributions allowed us to determine whether p_o differences due to elevation were influencing the T_s distributions of the environmental factors. Accounting for the influence of the lapse rate on temperature gave a clearer indication of how the T_s distribution of each variable actually changed across their individual spectrums.

For aspect the average T_s differences over the nine days of observations change little between T_s and θ (Figure 3.3). This means that the average elevation of 50 different aspect classes were not much different from each other.

The slope and elevation categories both showed distinctly different patterns of heating using θ instead of T_s. For the elevation category θ, under the influence of no other variables, by definition should reveal a completely equal temperature pattern across Niwot Ridge. However, while we do not observe large differences in θ it is not completely insensitive to elevation, meaning that there are other factors affecting temperature.

Slope also has large differences in temperature distribution once it is corrected for lapse rate. For this category we observe an increase in uniformity of θ (compared to T_s) across all slope regions. This means that slope classes were highly differentiated by elevation. The uniformity in θ indicates that slope as a variable did not greatly influence heating.

NDVI also had a slight change in the temperature distribution after accounting for changes due to lapse rates. Because the regions of highest NDVI are located at the lower elevations, θ was not very different from actual temperature. However the areas in the study site

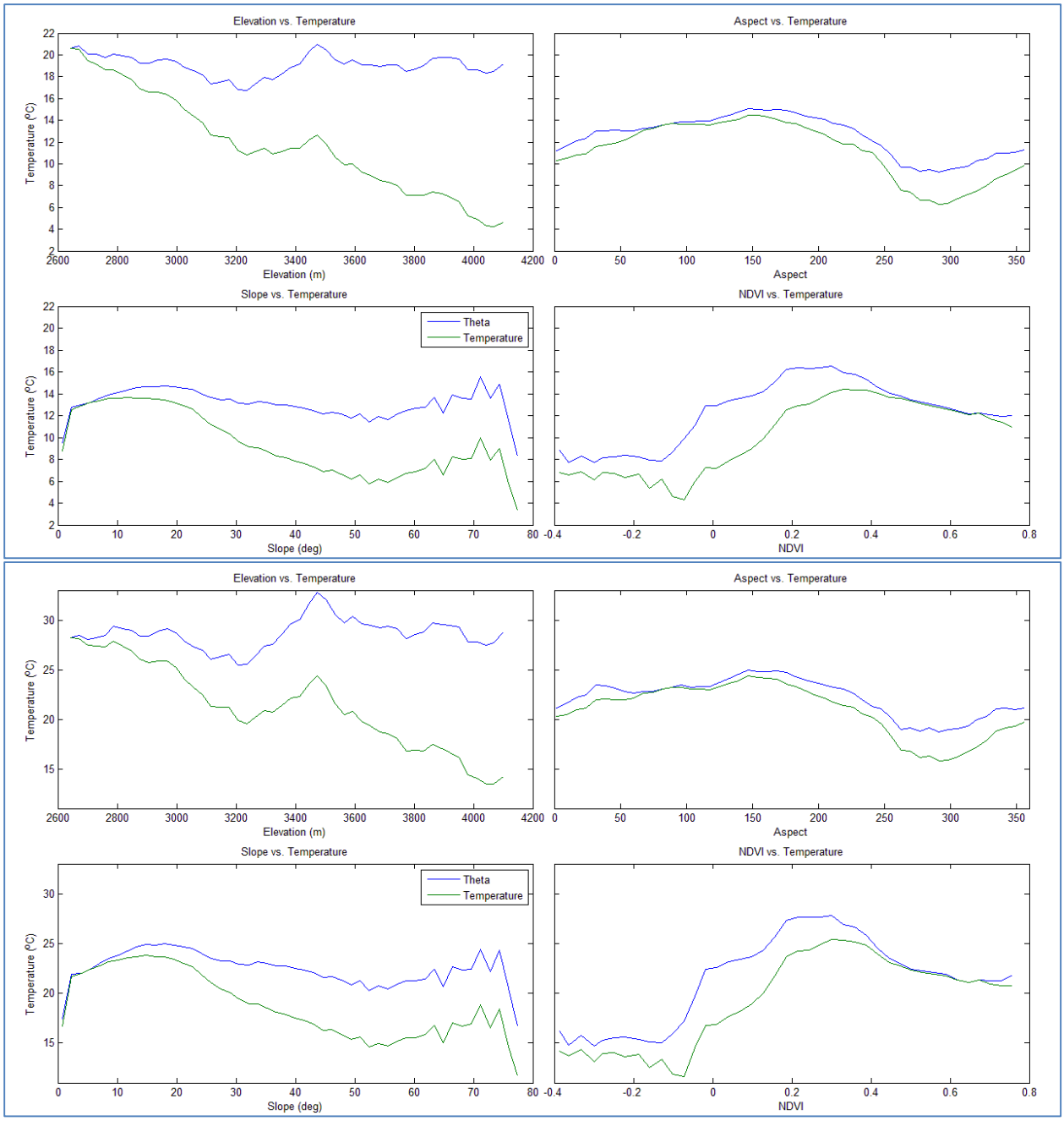

Figure 3.3. The θ for each category was calculated and plotted on the same plot as T_s. The top set shows the averages for all nine days. The bottom plot shows the averages from summer days: 6/15/08, 6/21/10, 8/5/09, 8/21/09, and 9/11/05.

with lower NDVI do exhibit increases in the conversion from T_s to θ. This has the effect of enhancing the pattern where the highest temperatures are in regions of moderate NDVI values (around 0.2).

The analysis above averaged θ over all nine days. However, it was also calculated for only summer days. The patterns between T_s and θ for these days changed little for aspect and slope. NDVI showed a slight enhancement of its peak between 0.2 and 0.3. The most prominent difference between the total average and summer average was an amplification of the θ peak at 3450 m for the elevation category.

To better view how elevation influenced the temperature distribution on Niwot Ridge for the nine days, temperature versus elevation plots winter and summer were created. These plots placed elevation on the y-axis, and T_s and θ on the x-axis (Figure 3.4), making them similar to atmospheric T_a profile, but for surface data. It was observed that the winter had a roughly vertical θ distribution with elevation. This suggests that the T_s will be neutral in regards to altering p_o gradients across Niwot Ridge, probably the result of snow cover reducing the heating differences between different land surfaces. However, the summer θ plot showed a distinct peak in θ at an elevation of 3450 m, near the ridge top. Since high soil T_s can increase H (Garratt 1992, Cellier *et al.* 1996), and since high H values can reduce p_o (Orville 1964, Kossmann and Fiedler 2000), regions with the highest T_s should result in rising, heated air. Because it was cooler above and below 3450 m, we expected to see wind converging at this elevation, traveling down slope from above and upslope from below, moving from regions of high to low pressure.

Observing *WD* measured on four of the five summer days (Figure 3.4) over the tundra (3480 m asl) and the subalpine forest (3050 m asl) during the day both sites experienced upslope

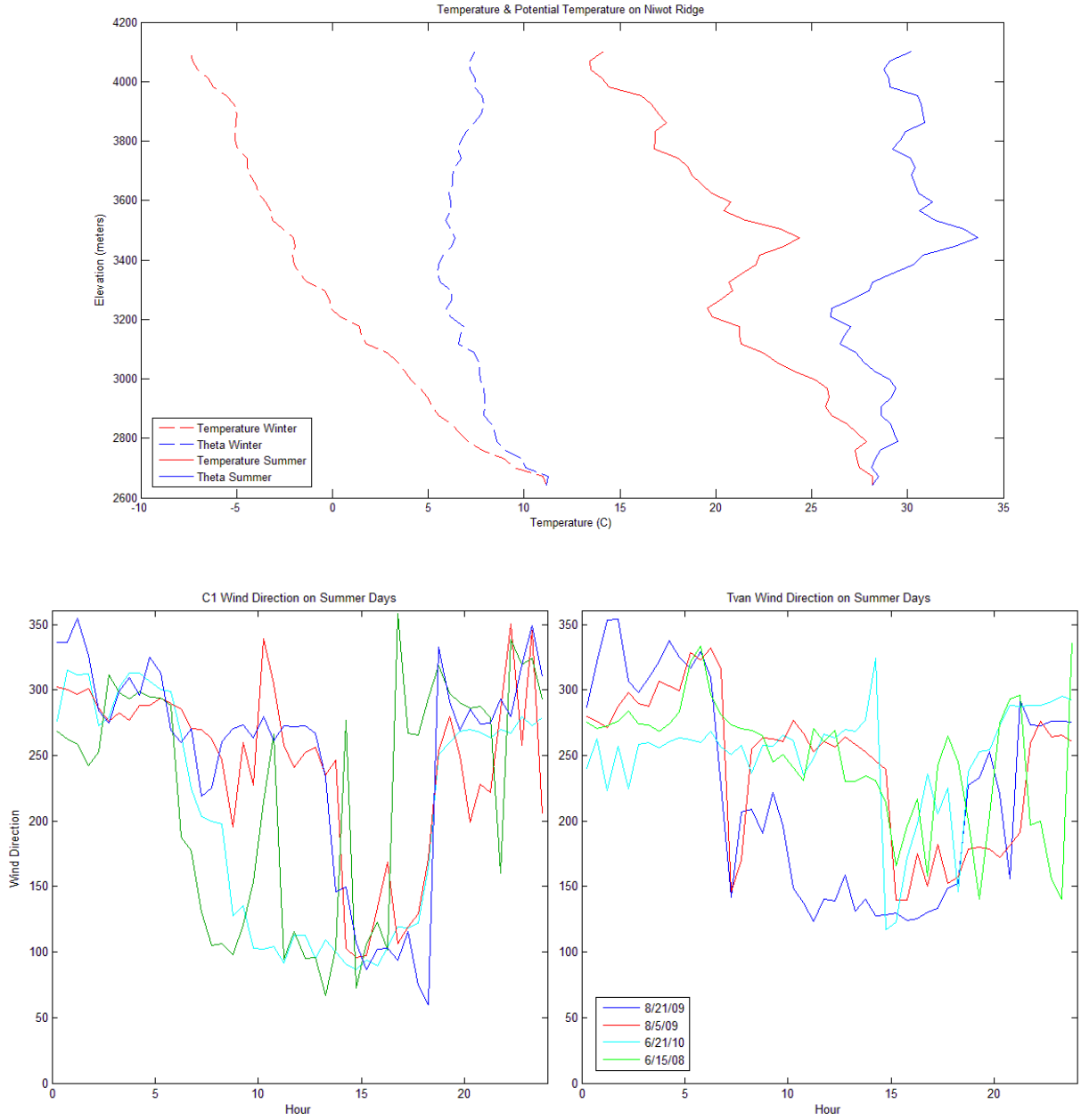

Figure 3.4. The average T_s and surface θ of Niwot Ridge (top) during winter days (3/3/05, 3/8/01, 3/11/08, and 4/17/04) and summer days (6/15/08, 6/21/10, 8/5/09, 8/21/09, and 9/11/05). The bottom plot shows the *WD* at C1 and Tvan on four of the five summer days observed.

flow. Upslope flow in the subalpine was directly from the east (90^o) because of its easterly aspect, while upslope flow at the tundra site was southeasterly (~145^o) due to its southeasterly aspect.

The previous analysis showed the seasonal difference in the distribution of temperature over different elevations. To get a sense of the spatial distribution of T_s values over the study area temperature maps were plotted (Figure 3.5). Two maps, one representative of summer T_s distributions (8/5/09) and one representative of winter T_s distributions (12/11/09), were plotted and overlaid on a digital elevation model (DEM). The summer map showed the highest T_s values centered over Niwot Ridge, while in the winter these markedly high T_s values did not appear. This zone of high T_s appeared to be strongly correlated with tundra regions. The absence of high T_s values over Niwot Ridge in the winter was most likely due to snow cover in the tundra.

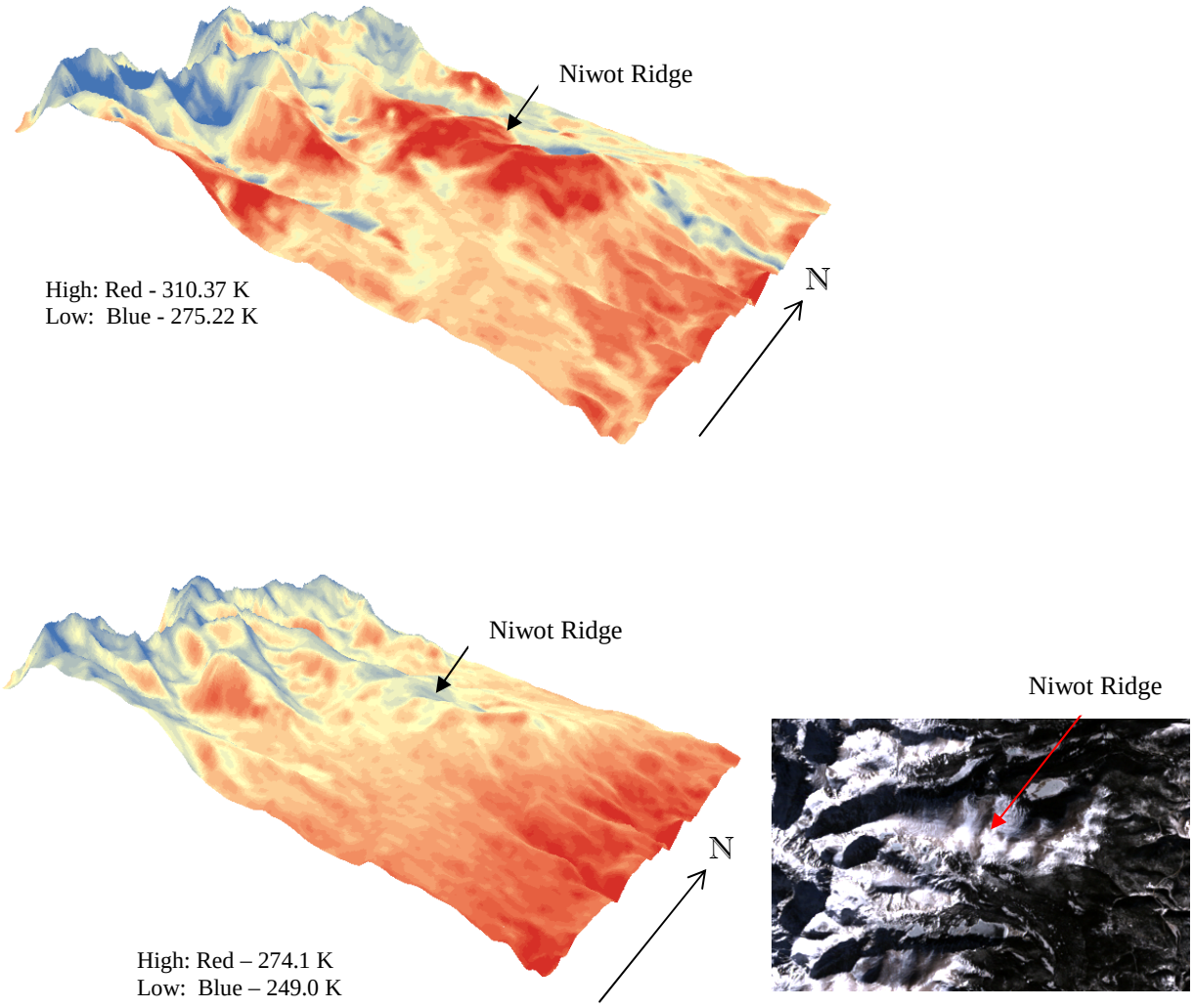

Figure 3.5. T_s data obtained via Landsat 5 thermal infrared imagery for 8/5/09 at 1030 MST (top) and 12/11/09 at 1030 MST (bottom) draped over a DEM. It is clear that during this season the high T_s over Niwot Ridge seen in the summer is absent. From the color composite image it is clear that the alpine tundra is covered with snow (bottom right).

3.3.2. Land Cover

The next analysis was to determine the nature of land cover difference with regard to the four environmental factors described above. In addition, land cover itself was subject to the same T_s analysis as above. As stated above, the first part of classifying land cover required ROIs to be selected. A supervised classification technique was used, meaning that the number of land cover regions needed to be specified in advance. The regions were picked based on broad knowledge of the terrain, keeping the number minimal due to a satellite resolution of 30 m. An initial analysis used six classes (rock, water, snow, tundra, krummholz, forest).

After classifying the whole study site with six classes (Figure 3.6) it became apparent that this method had a few inherent problems. One of the problems of this analysis was that the topographic slope of areas classified as water was 12.14^{o} (it should have been close to 0^{o}). The map was investigated and it appeared the low-lying lakes were correctly positioned. However, it was also observed that some of the water on the land cover map was located on very high, steep, west-facing slopes.

The second problem was that the bare rock class was selected only on the west side of the Continental Divide. In reality, there is bare rock exposed on the east side of the divide too, yet under this analysis it was classified as tundra. Therefore, it appeared that something in the spectral signature of bare rock on the west side of the divide was different than on the east side. Because the data are from the morning (1030 MST) it seems likely that a difference in the angle of incident radiation caused large differences in the reflectance values.

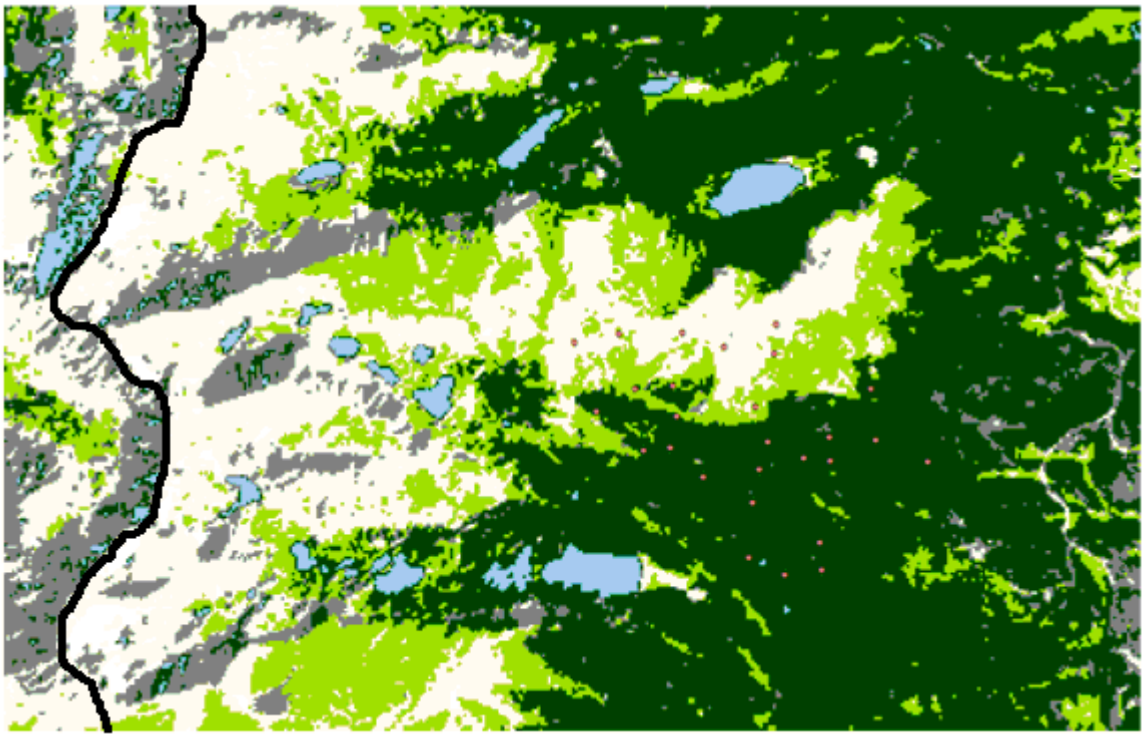

Figure 3.6. Six land type categories extrapolated throughout the study region using the supervised minimum distance classification tool in ENVI. Dark green represents forest, light green represent krummholz, tan represents tundra, gray represents bare rock, white represents snow, and blue represents water. The pink dots show the position of the 27 T_{soil} probes. The black line on the left side represents the Continental Divide.

Due to the problems associated with the six-category land cover approach the land cover analysis for the whole study region was completed using eight different land cover types. To address the water classification-slop problem, two water categories were created. One region was limited to known low-lying lakes, while the other was selected by placing a new ROI over the questionable region on the west side of the divide. The bare rock problem was solved by creating two rock categories: one for easterly aspects, the other for westerly aspects. The spectral signatures of these land cover regions were calculated across six bands (bands 1-5 and band 7) and used by the ENVI classification tool to extrapolate land cover across the map.

The water reanalysis showed that the two water regions have different characteristics. The most clarifying discovery was that the spectral signature of these high elevation regions is similar to the edges of the lakes below, as seen by the fact that all of the low-lying lakes are ringed by this new water category (Figure 3.7). This suggests that these regions are likely regions of soil that have high water content (i.e. moist, sandy banks). In addition, the west side of the divide probably still has morning dew, as the sun had not been directly illuminating its surface for very long. Water has a very distinct spectral signature in that it reflects very little near- and mid-infrared radiation. The derived spectral signatures reveal that this wet soil, which will be referred to as mud, has very low reflectance values overall, yet has slightly higher values than water, particularly in the infrared range (Figure 3.7), meaning its reflectance falls between land and water values.

Dividing bare rock into two different categories also seemed to improve results; bare rock was now detected on both sides of the mountain ridge. In addition, it was found that bare rock on the east side of the divide had higher reflectance values than the rock on the western side.

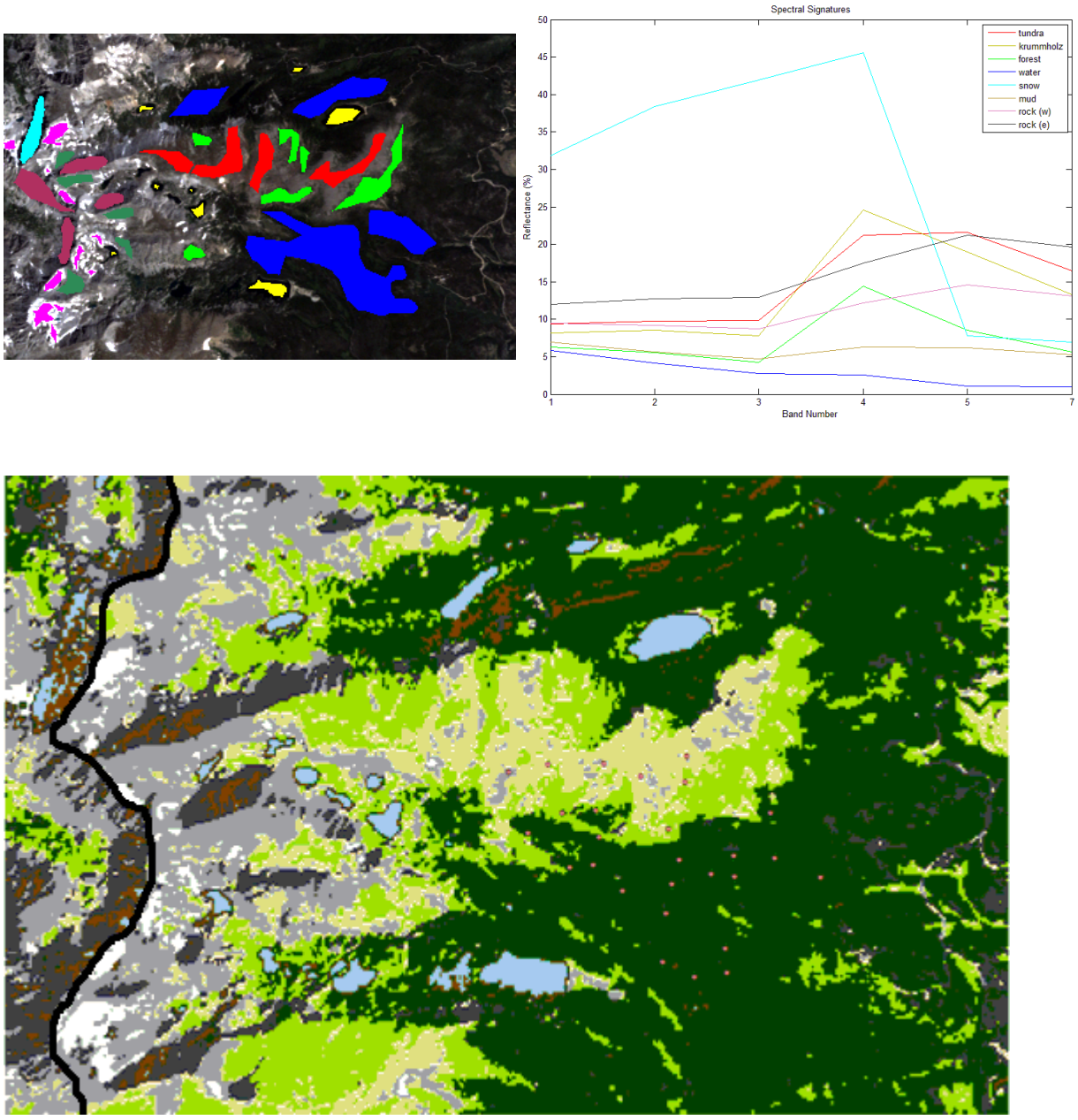

Figure 3.7. Selected ROIs (top left), the spectral signatures of each of these ROIs (top right), and resulting 8 land type categories extrapolated throughout the study region using the supervised minimum distance classification tool in ENVI. Dark green represents forest, light green represent krummholz, tan represents tundra, light & dark gray represents bare rock, white represents snow, blue represents water and brown represents mud. The pink dots show the position of the 27 T_{soil} probes. The black line on the left side represents the Continental Divide.

This fits our hypothesis that incidence of incoming solar radiation played a role in spectral differences. The low incidence on the western side allows for the sun's rays to be reflected, but not necessarily back towards the satellite sensor, while the east side, being hit more directly, reflected radiation back to the sensor.

After classifying the land cover, the areas were analyzed to determine their characteristics with regard to aspect, slope, elevation, and NDVI. These findings were important considerations when looking at land cover T_s distributions on Niwot Ridge.

The average elevation of the different land cover classes showed that snow, rock, and mud are the highest (Figure 3.8). These are followed by tundra and then krummholz, with water and forest averaging the lowest elevations of the study area. The analysis of aspect showed that mud and rock (west) are predominantly westerly facing, and that forest, tundra, and krummholz all average southeast facing aspects. This is expected since these classes are all on the east side of the range. Snow and water-dominated surfaces both had easterly aspects. This makes sense for snow, because the east side of the ridge is the most likely to have snow remaining in August. The water category still has problems, since it should read -1 for aspect, since this is the value that ArcMap assigns flat regions.

The land class averages for slope show that the highest elevation classes (snow, mud, and rock) also had the highest slopes. Slope decreased from tundra to krummholz to forest, with water having the lowest slope. While a slope of 8.46^{o} is still unexpectedly high for water (probably due to pixel contamination), under the eight land cover class analysis it has at least becomes the lowest slope of all the land cover regions.

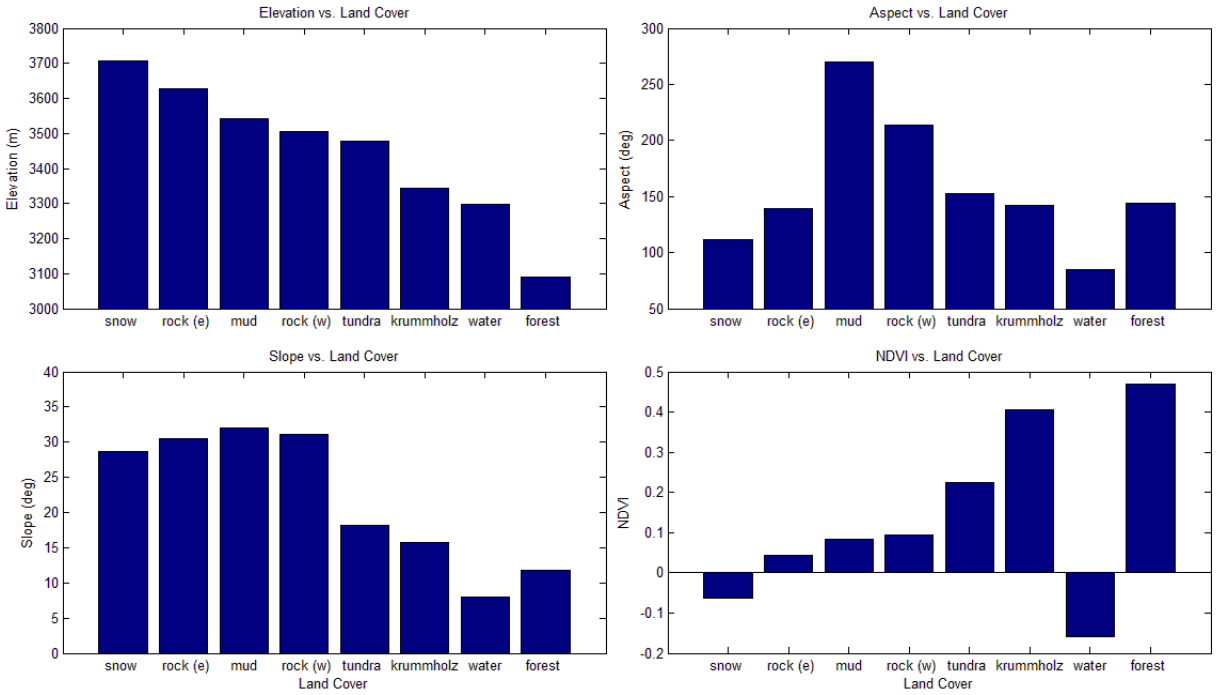

Figure 3.8. The average aspect, slope, elevation and NDVI for each land cover class.

Lastly, the mean NDVI was found for each of the land cover classes. The previous variables were all derived from a DEM and therefore were fixed throughout the year. The values of NDVI, however, change throughout the year. To gain a sense of the maximum vegetation coverage during the growing season the NDVI from 8/21/2009 was used. It was found that, with the exception of water surfaces, NDVI increased with decreased elevation. The forest had the highest NDVI at 0.468, krummholz next at 0.405, and tundra the lowest at 0.224.

This breakdown of environment characteristics by land cover class was followed by a T_s analysis across the classes. The total T_s average across the nine days was found, as well as an average for winter and summer. To account for the effect of the lapse rate on T_s the θ was found for each category using the same method described above. This meant that the class with the lowest average elevation (forest; 3091.6 m asl) was considered the zero elevation and all other categories were modified so θ was comparable to this elevation.

The average of all days revealed that the T_s for tundra, krummholz, and forest were all roughly the same at around 14^{o}C (Figure 3.9). However, the θ calculation shows that once the lapse rate was considered, the tundra had the highest temperature, followed by krummholz, and then by forest. Isolating the winter days, T_s for tundra and krummholz were much lower than the forest. For these days the θ for tundra and forest were roughly equal, with krummholz still lower. The summer showed a very different pattern, with the actual T_s going from high to low for tundra, krummholz, and forest respectively. Therefore, once the influence of the lapse rate on T_s was considered, the gap between these values increases and tundra clearly shows the highest values, with even the high elevation bare rock (east) showing greater θ values than the subalpine forest.

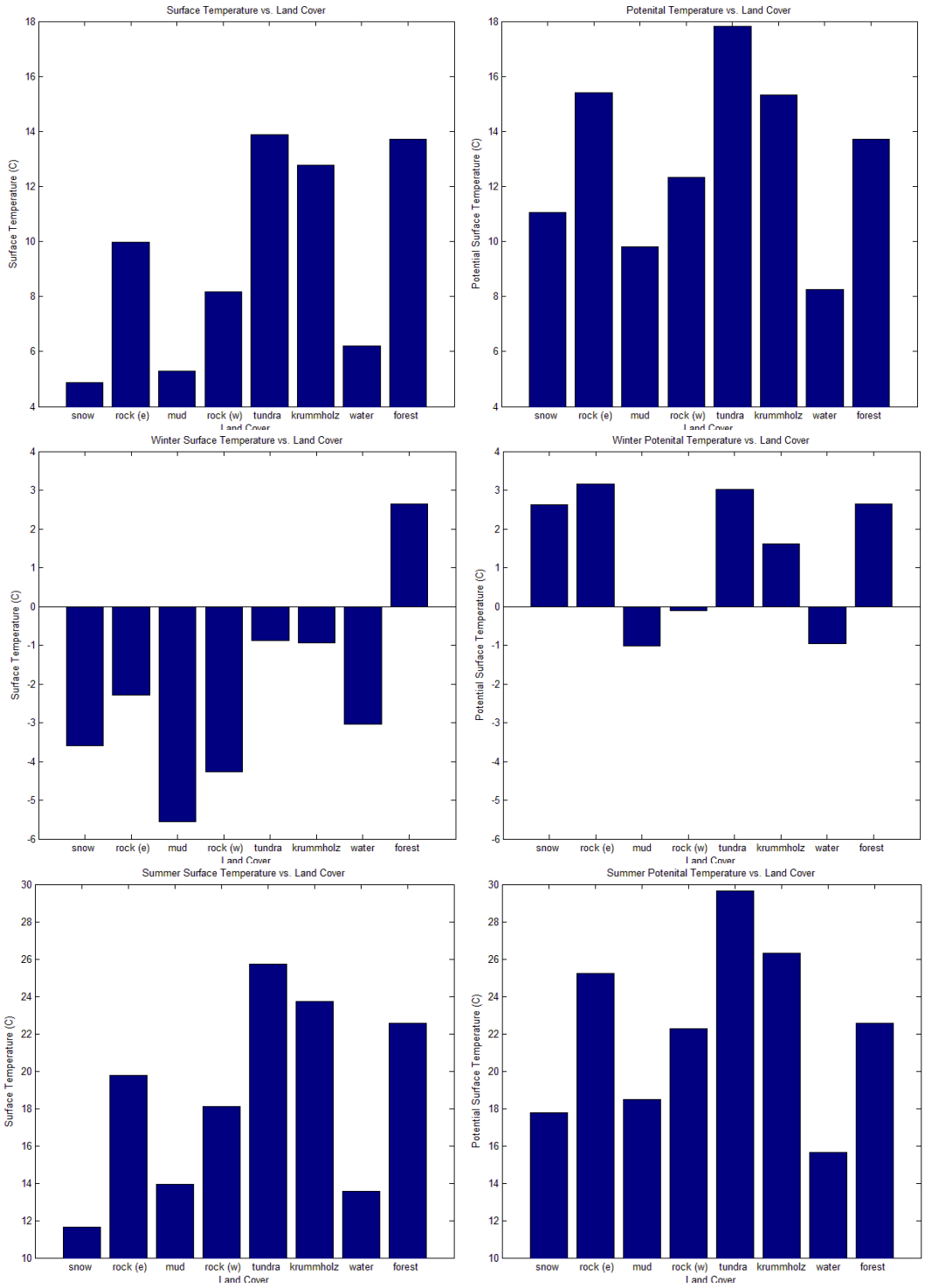

Figure 3.9. The average T_s (left side plots) and θ (right side plots) of the nine days observed (top row), winter days (middle row), and summer days (bottom row).

3.3.3. Soil Temperature

Following the T_s analysis attention was turned towards T_{soil}. The two main objectives were to determine whether there was a relationship with T_s distribution and to determine how T_{soil} varied across the different land cover classes.

For the first objective, the T_s versus elevation plots were compared to T_{soil} versus elevation plots. A problem with this analysis was that there were only two days with simultaneous satellite and T_{soil} measurements (Aug 5, 2009 and Aug 21, 2009). The T_s and T_{soil} for these days were then plotted together to determine whether similarities existed between temperature and elevation. The most obvious difference between T_{soil} and T_s was that T_{soil} was much lower than T_s (Figure 3.10). This is expected as the mid-morning time (surface – 1030 MST, soil - 1000 MST) of the recording of this data means that the soil to 10-cm depth has not fully heated.

To view the temperature patterns T_{soil} were split into two categories: forest points and tundra & krummholz points. Least-squares trend lines were added for both groups to show their trend with increasing elevation (Figure 3.10). The results showed that as forest sites decreased in T_{soil} they increased in elevation. In reverse, the krummholz and tundra sites showed increased T_{soil} with elevation. This is the same pattern as the T_s profile, as can be seen by their alignment with the shifted T_s profile. The elevation at which forest transitions to krummholz (3300 m asl) appeared to roughly aligned with the local temperature minima of the T_{soil} and T_s plots. In addition, the elevation of the tundra sites with the highest T_{soil} (3499.6 m asl) aligns with the elevation of the local temperature maxima of the T_{soil} and T_s plots. From this analysis, it appears that the pattern of T_{soil} distribution was similar to the pattern of T_s distribution. It is important to

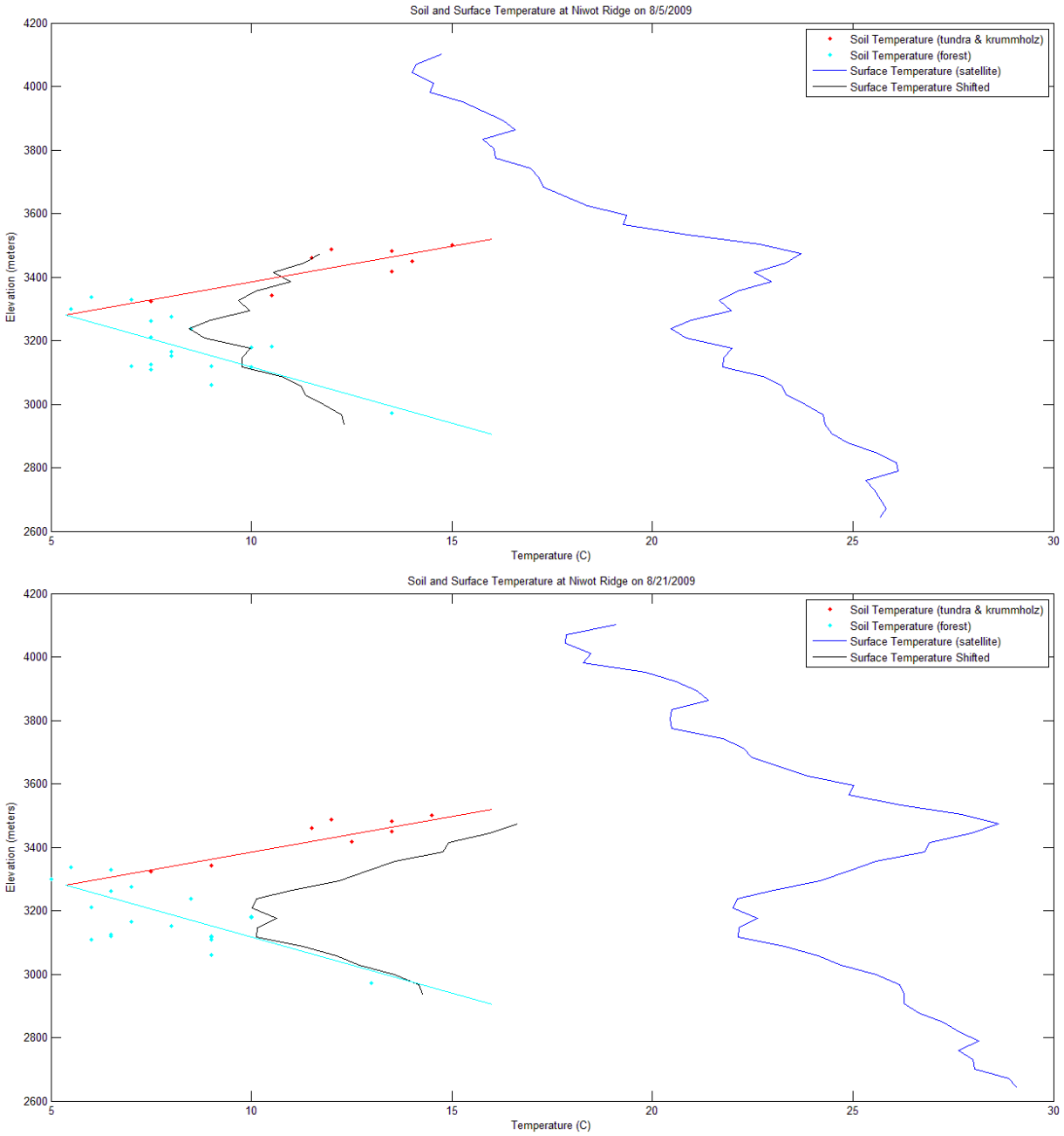

Figure 3.10. The T_{soil} and T_s of Niwot Ridge on 8/5/2009 at 1000 MST and 1030 MST respectively. The in-situ T_{soil} readings closely align to the pattern of T_s (derived using Landsat 5 thermal imagery and plotted according to elevation class averages) in the same elevation range, although it appears the magnitude of the T_{soil} changes are greater.

note that at 10 cm below the surface T_{soil} values were expected to be lower than T_s due to the heat capacity of the overlying soil, however the distributions of T_{soil} and T_s were expected to be similar.

3.3.4. Mean Hourly Soil Temperature

The second analysis of T_{soil}, after determining the spatial patterns, was to determine the temporal patterns. To do this, the mean hourly T_{soil} for each land cover class was found.

The results from the five tundra sites revealed that they had the largest daily fluctuation in T_{soil}, followed by krummholz, and lastly forest, which showed the least difference between the average daily maximum and minimum T_{soil} (Figure 3.11). It was found that tundra maximum was the highest with 17.7^{o}C, followed by krummholz at 12.1^{o}C, and lastly forest with 8.85^{o}C, all occurring at roughly 1500 MST. The average daily T_{soil} minimums followed the same pattern but were much closer in value, yielding 8.32^{o}C, 7.65^{o}C, and 6.91^{o}C for tundra, krummholz, and forest respectively (occurring at roughly 0630 MST).

The next step was to find whether days with greater differences in T_{soil} between tundra and forest showed different wind patterns. Using the three T_s category method described above it was observed that all categories had a small decrease in *WD* from roughly due west (270^{o} to 280^{o}) in the early morning to southwest (220^{o} to 230^{o}) at around 0600 MST (Figure 3.12). For the third category ($T_{tundra} < T_{forest}$) the *WD* stayed around this zone for the remainder of the daylight hours, switching back to westerly flow at 1900 MST. The second category ($T_{tundra} > T_{forest} + 5^{o}$C)

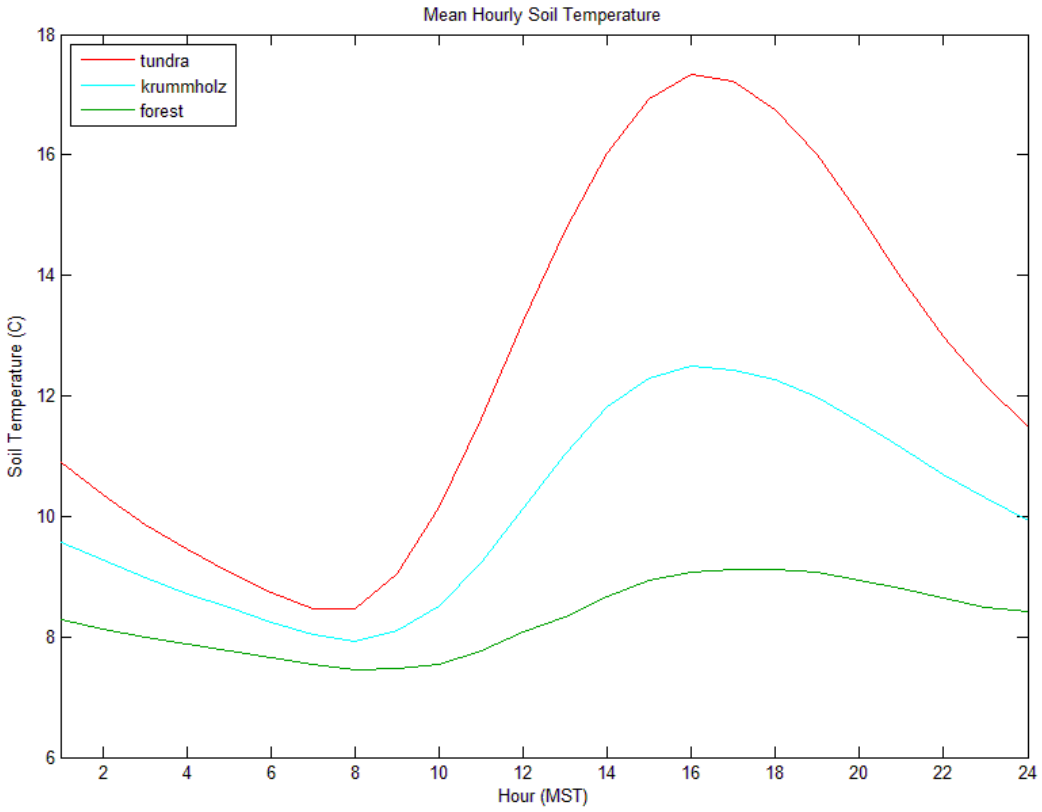

Figure 3.11. Mean hourly T_{soil} for different land cover surfaces (tundra, krummholz, and forest) from July 6 to September 30, 2009. The land cover categories were determined via the ENVI classification procedure described above. It yielded 5 tundra sites, 3 krummholz, and 19 forest sites. Tundra has the largest fluctuations in daily T_{soil}, as well as the highest values, even at its T_{soil} minimum.

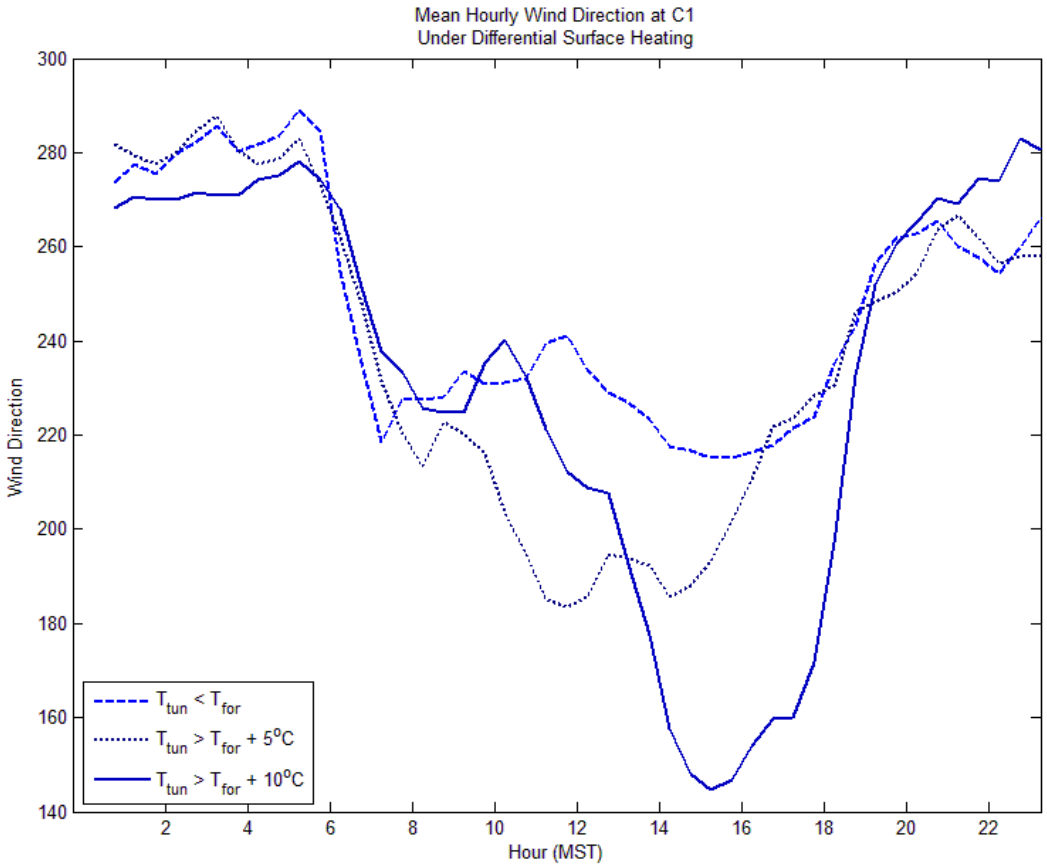

Figure 3.12. *WD* for different T_{soil} gradients on Niwot Ridge. The three categories selected were days in which the average maximum T_{soil} for tundra sites exceeded the average maximum T_{soil} for forest by 10°C, days in which tundra exceeded forest by 5°C (excluding days from other two categories), and days in which tundra was cooler than forest. The days with the greatest differences in T_{soil} between tundra and forest showed the largest drop in *WD*. The *WD* is shown here as a simple moving average with a lag of three.

dropped slightly throughout the day to reach a minimum *WD* of south southwest flow (185^{o}) at 1130 MST. The first category, however, the day with the greatest difference between T_{soil} of tundra and forest ($T_{tundra} > T_{forest} + 10^{o}C$), had *WD* decrease all the way to southeasterly flow (145^{o}) at 1530 MST. While none of these days averaged complete easterly flow (90^{o}) it is important to note that these *WD* values were averages of all days in the category. Therefore, any days with westerly flow (270^{o}) increase the average.

The previous analysis showed that days with greater T_{soil} differences between tundra and subalpine forest had an increased frequency of upslope winds in the afternoon, coincident with the time of greatest T_{soil} difference. To determine whether these winds were a result of land cover differences the *H* and p_o from the two main meteorological stations were analyzed.

For the first analysis, *H* was compiled into the same groups as for *WD* analysis (the three T_{soil} categories). It was found that on days with little to moderate T_{soil} difference between tundra and forest sensible heat flux was roughly 80 Wm^{-2} higher over the forest during the day than the tundra (Figure 3.13). On days in which T_{soil} was at least 10^{o}C greater in the tundra the sensible heat flux over the forest was 180 Wm^{-2} greater than the tundra. Interestingly this is opposite of the expected result. Since the tundra has higher T_{soil} and lower T_{air} its temperature gradient should promote *H*.

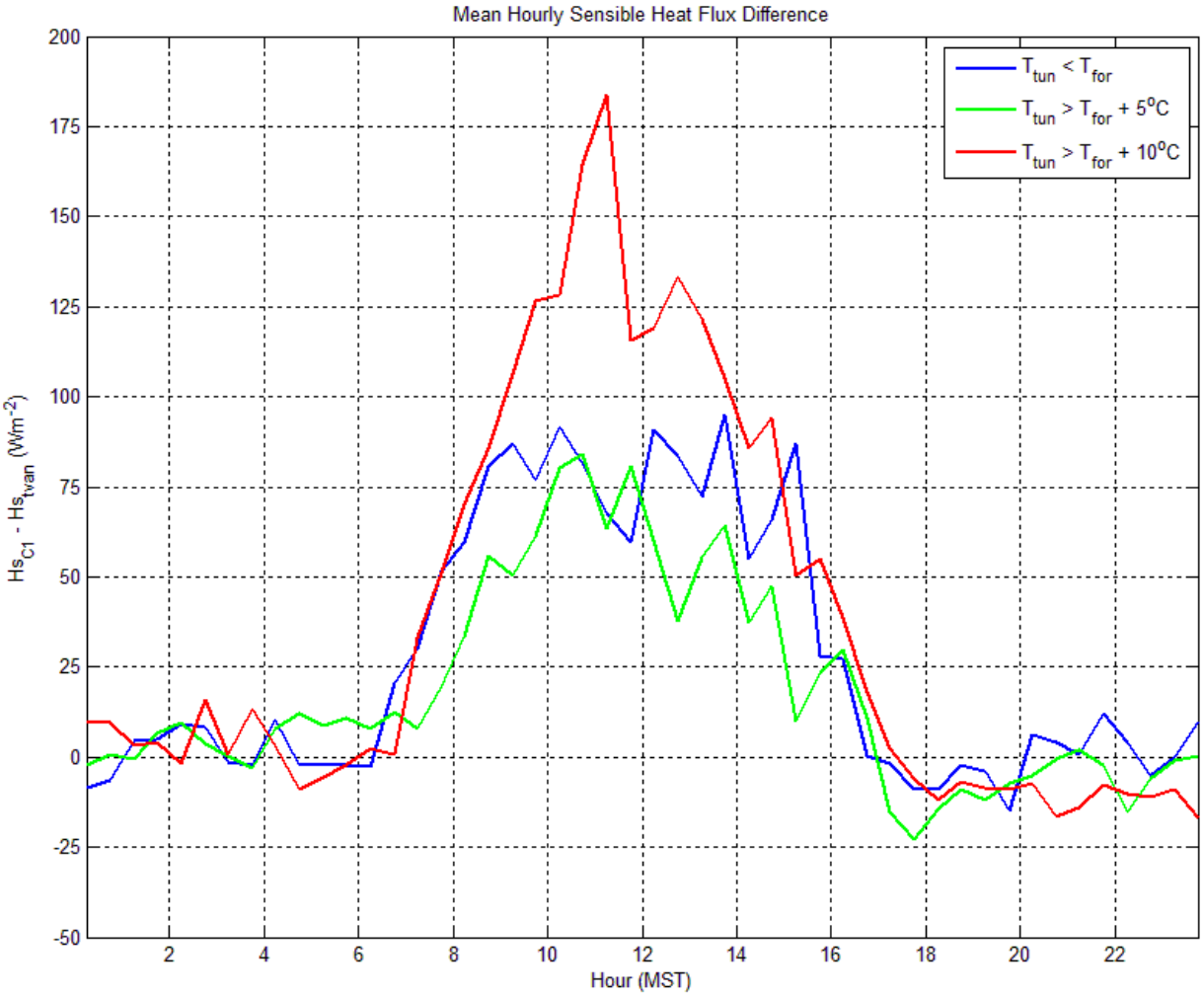

Figure 3.13. Same as Figure 3.12 for *H*, except that *H* is plotted as H_{C1} - H_{tvan}. Also, no moving average was applied.

Daily p_o fluctuations were shown as deviation from the minimum average hourly p_o (which occurred at 0400 MST for both sites). It was observed that both sites, the increase in p_o after sunrise until 1100 MST (Figure 3.14). The tundra site p_o increased at a faster rate in late morning, causing it reach a greater maximum deviation at midday. Surface pressure (p_o) at both sites decreases at roughly the same rate from 1100 MST to 1800 MST.

The second p_o analysis was the same differential T_{soil} analysis as was used for *WD* and *H* above. It revealed that all three categories of T_{soil} differences have the same pattern of daily p_o differences – at night the difference between tundra and forest ($p_{o\ C1}$-$p_{o\ tvan}$) is greatest and dropping throughout the day to a minimum at 1600 MST. It was also found that p_o differences were lower for the days of in which tundra had greater T_{soil} than C1. On these days the p_o at both sites was higher than average, but the tundra shows even higher than average increase.

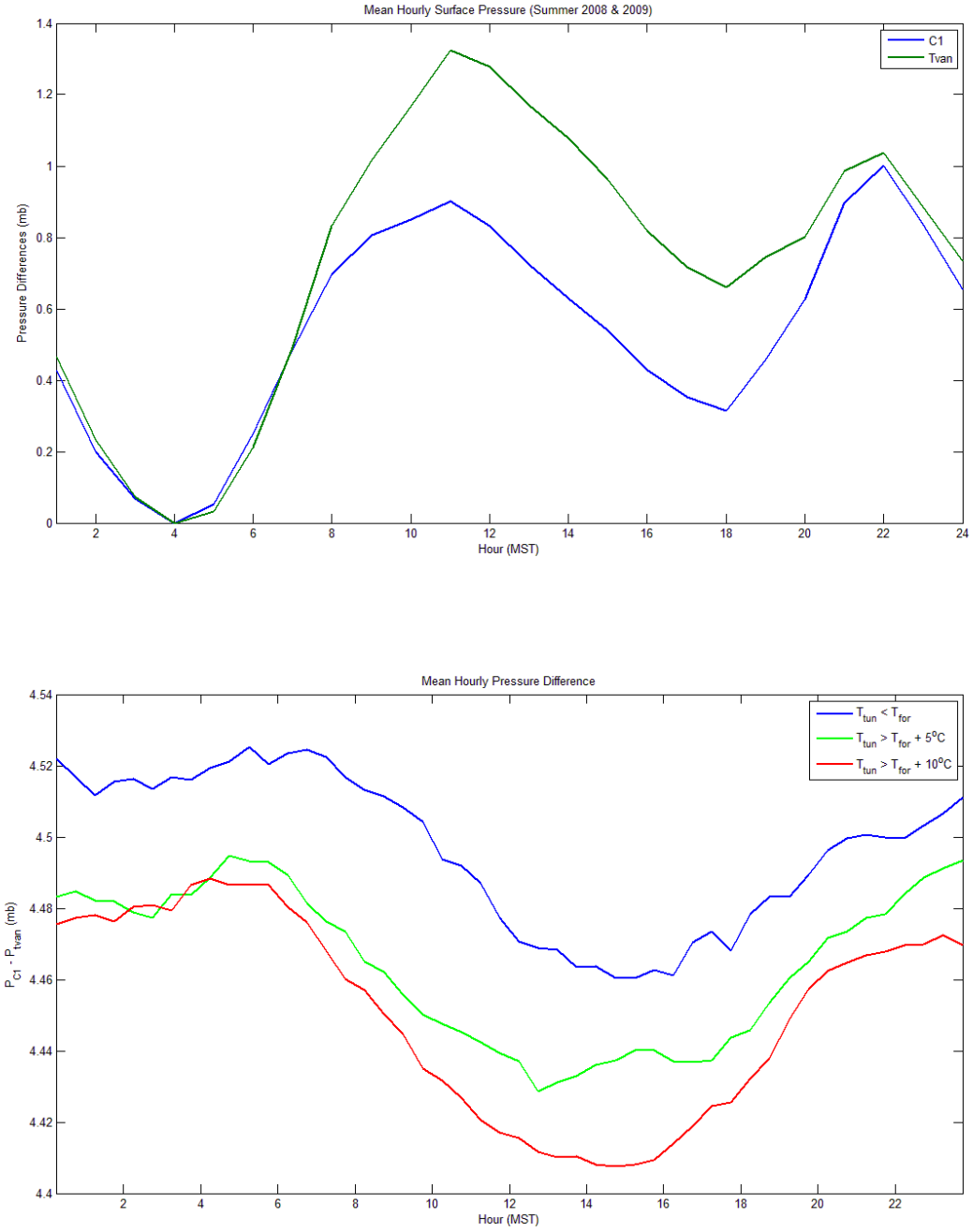

Figure 3.14. The top plot shows the average hourly p_o of the tundra (2 m agl) and the subalpine forest (12 m agl) for the summers (JJA) of 2008 and 2009. It shows the deviations from the minimum hourly p_o at 0400 MST. The bottom plot is the same as Figure 3.12, except for p_{o_C1}-$p_{o\ tvan}$.

3.4. Conclusions

The main conclusions from this chapter were that NDVI and land cover had the greatest influence on T_s and T_{soil}. Temperature differences between tundra and forest peaked in the afternoon and coincided with increased frequency in upslope air flow. The T_s and T_{soil} differences suggest that land cover-induced this directional flow. However, H and p_o told a different story. On days with the greatest difference in T_{soil} ($T_{tundra} > T_{forest} + 10^oC$) these meteorological variables acted to oppose upslope flow, with tundra experiencing higher than average p_o and lower H compared to the forest.

Of our four original environmental variables (elevation, aspect, slope, and NDVI) elevation and NDVI had the largest impact on T_s. Aspect had very little impact on T_s differences across its range, with the exception of low values from 270^o to 300^o. Since these aspects are almost nonexistent on Niwot Ridge, aspect probably played a small role in T_s distribution. After calculating θ we found that slope also plays a very small role in temperature differences. Potential temperature (θ) also revealed a more uniform temperature distribution throughout the elevation classes, which by definition was to be expected. However, the elevation classes still showed a maximum at roughly 3400 m. This we expect is attributable to the NDVI and land cover type.

The second part of this analysis was to more definitively break down the four environmental variables by land cover class. This revealed that mean elevation and NDVI of tundra matched the T_s maximums for both the elevation and NDVI categories (~3400m, 0.2). Calculating T_s for land cover classes directly revealed that tundra did in fact have the highest values, particularly in summer. This apparent correlation between maximum temperature of NDVI (0.2) and land cover (tundra) makes sense because NDVI and land cover should be

correlated. This assumption hinges on the fact that both NDVI and land cover categories were determined by spectral signatures, NDVI with near infrared and red reflectance, and land cover on 6 bands of reflectance, including near infrared and red.

Soil temperature (T_{soil}) yielded similar results. The T_{soil} versus elevation plot had the same pattern as the T_s profile. Breaking the data points into their respective land cover classes showed that the reason for the decrease in T_s up to 3200 m was related to the fact that T_{soil} and T_s under forest canopy decrease with increased elevation. However, because tundra T_{soil} was found to increase with elevation, the rise in T_{soil} and T_s from 3200 m to 3450 m was due to the transition from forest to tundra at 3200 m. This led to a local maximum T_{soil} and T_s at roughly 3450 m.

This difference in T_s distribution on Niwot Ridge is likely a key factor governing the existence of upslope, thermally-driven flows in the summer. Since the tundra experiences greater heating during this season, heating which is notably absent in the winter, it appears to lead to the increased occurrence of these flows. Observing the *WD* patterns on days with greater differences in T_{soil} between tundra and forest revealed that this does indeed increase the frequency of easterly flow.

The main goal of this research was to determine whether the location of alpine treeline was influencing thermally-driven flows. More specifically, to determine which of the two thermally-driven flows (anabatic or land cover-induced) was responsible for upslope winds and when they occur. It was difficult to determine when anabatic flows were occurring because of a lack of information about the vertical temperature profile and therefore the atmospheric stability. To determine these flows multiple towers, collecting temperature and density data at multiple

heights would have been required. To determine land cover-induced flows T_s, p_o, and H were observed over tundra and forest.

Because T_s differences are minimal in the morning we assume that the initiation of upslope flow at sunrise is due to anabatic forces. However, from Chapter 2, we know that upslope flow in the morning is limited to the subalpine forest (both C1 and Cabin Clearing). This may be due to the lower elevation of these sites placing them horizontally adjacent to colder, denser valley air, thus increasing the strength of their horizontal pressure gradient force. The tundra, being more exposed to synoptic-scale winds, most likely avoids such pressure forces.

The other main finding from Chapter 2 was that anabatic flows decreased in frequency above the forest site near treeline (Cabin Clearing) in late morning. When the frequency of upslope flow increased again at noon it coincided with the start of upslope flow in the tundra. Because of the loss of upslope flow at Cabin Clearing at 1000 MST it appears that the winds are caused by two separate forces, and not just a lag time between sites.

At first glance the original hypothesis that differential T_s of a specific threshold will cause land cover-induced flow appeared to be correct, as frequency of upslope flows increased on days with higher tundra T_{soil} (relative to forest). Under this hypothesis the upslope flow regime is one in which Niwot Ridge experiences anabatic flow in the morning hours, switching to land cover-induced flow in the afternoon when T_{soil} in the tundra was high.

However there were a couple major flaws with the theory of land cover-induced flow. The tundra site, which would theoretically see the highest sensible heat flux, due to having the largest $T_{soil} - T_{air}$ values (Kondo and Ishida 1997), almost never has higher H values during daytime hours. In fact, under the differential T_{soil} analysis it was found that on days of greatest T_s

difference ($T_{tundra} >> T_{forest}$) the *H* over the forest was 180 Wm^{-2} greater than the tundra, compared to a more common 80 Wm^{-2}. In addition, on these days the p_o of the tundra was higher than average compared to the forest. Both of these findings suggest that the increased T_{soil} of the tundra should force winds down slope.

Therefore, it is concluded that upslope, land cover-induced flow does not actually occur on Niwot Ridge. However the increased frequency of upslope flow when T_{soil} differences are great ($T_{tundra} >> T_{forest}$) still strongly suggests that T_s and T_{soil} played a role in upslope flow. A likely possibility is that the high tundra T_{soil} values in the afternoon cause anabatic flow, rather than land cover-induced flow, to initiate over the tundra. In the morning, the exposure to strong, westerly, synoptic-scale flow may be too great for the anabatic pressure gradient to overcome in the tundra. However, by the afternoon increased turbulent mixing and atmospheric boundary layer (ABL) depth may slightly protect the tundra site from prevailing winds, allowing anabatic winds to develop. The ABL height, combined with higher T_s and *H*, may be the cause of these afternoon flows.

Appendix

It is important to note that the conclusion that land cover-induced flow was determined mainly by the p_o and *H* readings at the two meteorological stations (C1 and Tvan). These sites do not measure these two variables at equivalent heights above the surface. The subalpine forest site measures p_o at 12 meters and *H* at 21 meters, while the tundra site measures both variables at 2 meters.

However, it does not appear that these differences influenced the results. Pressure (p_o) will be slightly higher at a lower elevation above ground level, however it is unlikely that 10m will greatly alter the value. In addition, whether it does alter it or not, the differential surface heating analysis of p_o showed P_{C1}-P_{tvan}. The finding that Tvan p_o is closer to p_o at C1 under greater heating of the tundra heating will remain regardless of a blanket change p_o at C1.

Sensible heat flux (H) should be almost constant with height within the surface layer (Luhar and Rayner 2009), above which H will decrease with height (Pan and Li 2008). Therefore there is no reason to believe that the higher H over the forest is due to the height, because if anything it would be expected to be slightly lower due to its higher elevation above ground level.

An important follow up study to this one would look at the variables causing the lower H values in the tundra (particularly when its T_{soil} is high and its air temperature is low).

Chapter 4

The Effect of Upslope Winds on Atmospheric Variables and Airmass Composition along Colorado Front Range

Abstract

The previous chapters have outlined the details regarding thermally-driven, upslope flows at Niwot Ridge, with Chapter 2 discussing when and where, and Chapter 3 discussing possible causes for these flows. The focus of this chapter will be to show why these different flow patterns are important to study. How different meteorological variables are influenced by these flow patterns and the possible implications are described. Findings show that these summer, upslope flows have very distinct effects on the airmass composition at Niwot Ridge. The most obvious effects observed are a decrease in air temperature and an increase in humidity when sites experience a transition from westerly to upslope air flow. These effects in turn play a role in influencing the surface energy balance and carbon fluxes at the site in the short term and possibly the spatial distribution of vegetation in the long term.

4.1. Introduction

It has been shown by previous studies and this study that upslope wind events are common phenomena on summer days along the Front Range of Colorado. It has also been shown that these airmasses often contain higher levels of pollutants (Parrish *et al.* 1990, Veltkamp *et al.* 1996). What has not been studied has been whether distinct differences in the compositions of prevailing westerly flows versus upslope flows help explain the location of alpine treeline. In this chapter, air temperature (T_a), relative humidity (h), dewpoint temperature

(T_d), sensible heat flux (H), latent heat flux (λE), net radiation (R_n), and the CO_2 flux were characterized for variations in airmasses from the west (downslope) and east (upslope).

4.1.1 Upslope Winds as a Source of Moisture

Airmasses have different characteristics with factors such as T_a, h, and aerosol concentrations (organic and inorganic) changing depending on the area of origin (Eleftheriadas *et al.* 2008). It is known that the origin of air can create very different weather patterns. For example, maritime airmasses formed over large bodies of water are relatively warm and moist (Pang *et al.* 2004, Teitelbaum *et al.* 2008) while continental airmasses are cold and dry (Kassomenos and McGregor 2006).

While the above examples refer to large-scale air movements such differences in airmass composition also occur on local scales. Gerbush *et al.* (2008) found that local heterogeneity in ice thickness on Lake Erie had significant effects on heat and moisture fluxes to the boundary layer air, and in turn played an important role in the cloud formation and lake effect snow. This shows that local surface characteristics can influence airmass composition. In their study of air flow on Mt. Kilamanjaro in Kenya, Duane *et al.* (2008) found that thermally-driven, upslope winds caused a net export of moisture from the subalpine forest to the upper regions of the mountains. The export of the moisture (from the high evapotranspiration rates of the forest) was found to be the single most important source of moisture for these upper regions of the mountains.

4.1.2 Effect of Strong Winds on Vegetation

Strong winds have been known to increase stress on trees in a variety of ways. They create mechanical stress, causing trees to streamline their form to avoid damage directly from wind, as well as damage from debris and ice pellets carried by the wind (Holtmeier and Broll 2010). In addition, strong winds have a desiccating effect on mountain vegetation creating an even greater stress on vegetation. This was seen in mountainous regions of southern Tibet where the increasing strength of foehn winds has caused the retreat of plant relicts from a higher humidity past (Miehe 1996).

It has been found by previous studies that consistently strong winds during the growing season can effectively impair the development of trees, particularly impeding the growth of needles and shoots on the windward side (Grace 1977, Holtmeier 1980, Telewski 1995). In addition, under these same stresses tree cuticles may fail to fully mature. According to many studies this incomplete process during the growing season, which makes the trees more vulnerable during the winter season, is the most important factor controlling treeline (Tranquillini 1980, Sowell *et al.* 1982, Barclay and Crawford 1982, Delucia and Berlyn 1984, Cairns 2001).

We know that vegetation on Niwot Ridge is affected by strong winds as the physiognomy of krummholz and trees in the treeline ecotone show the influence of wind. Flagging of trees (the preferential growth of leaves on the downwind side of a tree trunk) is a wind driven adaptation (Holtmeier and Broll, 2010) which is common in Niwot Ridge treeline vegetation. If strong westerly flow is controlling treeline it would have the effect of pushing treeline eastward, down the slope.

It was also found that the subalpine forest experiences a lower frequency of strong winds than the alpine tundra (measured above canopy). Convergence events are a common occurrence on Niwot Ridge and are characterized by times of weak, upslope flow over the subalpine forest and strong, synoptic-scale, westerly flow over the subalpine forest. Chapter 2 showed during one of these events that the surface layer of the subalpine forest was decoupled from these synoptic-scale flows by a shear layer that existed 80 m agl. This finding suggests that upslope flows may create a kind of barrier against damaging strong winds.

4.1.3 Objectives

The hypothesis of this study is that the composition of upslope airmasses enhances tree growth and helps create enough growth in the summer season to support a permanent treeline. We predict the same general pattern of increased *h* of upslope flows, as observed by Duane *et al.* (2008), will exist on Niwot Ridge due to the enhancement of airmass moisture from advection across the subalpine forest. Increased *h* and reduced wind speed (*U*) that exist under upslope flow should reduce stresses on vegetation and create a more suitable environment for subalpine forest. It was already found that upslope winds occur 32.62% of all summer daytime hours above the subalpine forest (at C1) and only 16.20% of all daytime hours above the tundra (at Tvan) (see Chapter 2). It is predicted that the high frequency of upslope wind events over the subalpine forest is an important feature controlling alpine treeline at Niwot Ridge.

4.2. Methods

The goal of this work was to test how meteorological variables where influenced by upslope flows, namely to determine whether we see different meteorological conditions on days with upslope flows versus days without upslope flow. To do this three main methods were employed, each of them attempting to yield information about meteorological variables by finding their average characteristics with and without upslope flow. The first method was to indentify all days with upslope flow (at least four consecutive hours) and find the hourly mean for each meteorological variable through these days versus days not selected. The second was to indentify every individual upslope wind reading (30 minute blocks) throughout two years of data, indentify its time of day, and then find the upslope and non-upslope mean for each time block throughout the study period. And the third method was to find the precise moment upslope flow events (minimum 4 hours) started on different days and then take the mean for the hours prior to and following the initiation of upslope flow. Each of these methods yields a slightly different view of how these flows influence the airmasses of Niwot Ridge. These analyses are completed for C1 and Tvan, but exclude CC because of a lack of meteorological data.

4.2.1 Hourly Means

Hourly means of meteorological variables were calculated for all days exhibiting upslope flow. This allowed an assessment as to whether these days differ from days with westerly flow. The determination of days with 'upslope flow' was done by finding all days in which both C1 and Tvan experienced at least one four-hour period of upslope flow, defined as 50^{o} to 130^{o} at C1

and 100^{o} to 180^{o} at Tvan (definition used throughout analyses). Wind speed was not considered. Since upslope flow is much more common in the summer months (see Chapter 2) these averages showed summer characteristics. To make the westerly flow averages (control group) comparable to the upslope flow days only summer values were observed. Summer was defined as June, July, and August. This left 184 total days to use from the Tvan and C1 datasets from 2008 and 2009. The control group for this analysis was comprised of all days not selected by the 'upslope flow' criteria. A limitation of using this as a control was that it inevitably contained some days with upslope flows – events not long enough in duration to be selected.

After running this analysis as stated above, the same method was rerun changing the criteria for determining the 'upslope flow' group. For this analysis upslope days were isolated as days in which *only* C1 experienced four consecutive hours of upslope flow. The days selected in the previous analysis, which showed strong upslope flow at both sites, were not selected under this new criterion. To prevent the westerly control group to be corrupted by the upslope conditions on these non-selected days they were discarded from the analysis completely.

4.2.2.Upslope Blocks

The second method for distinguishing the characteristics of meteorological variables under different flow regimes was the upslope blocks method. This method dissected days into their individual hour blocks that experienced upslope winds. For each of these 24 daily data blocks two wind direction indices were created – one for all summer (JJA) upslope flow events and one for all other summer flows. From here means for different meteorological variables were calculated for both groups and for each hour. This analysis allowed for a comparison of the

influence of upslope versus westerly flows on meteorological variables at different times of the day. For example, does upslope flow at 0900 MST have a different influence on wind speed or T_a than it does at 1600 MST?

4.2.3 Initiation Method

The final averaging method was used to determine if any discernable patterns could be observed at the transition point from westerly to upslope flows. To do this the exact start time of upslope flow events were identified. This analysis was done for both Tvan and C1 sites individually. Upslope events were defined as any event that showed sustained upslope flow (same definition as previous analyses) for four consecutive hours at the site in question. Then after the initiation times were assembled block means were taken for each 30-minute measurement six hours prior to and following initiation. This allowed for a much more distinct point in which to observe airmass composition. While similar to the first method, this one lined up starting points, not just days with upslope flows, therefore avoided the problem with the first method that upslope flow can initiate at various times during the day. Therefore averages in the first method are prone to masking that this method circumvents.

This method also needed a control group for comparison. This presented a problem since the initiation times were at different times on different days. Therefore it had a smoothing effect on the means, not encountered when averaging variables aligned by time of day. In order to have a meaningful control variable means were found for 24 hours prior to the initiation event. This created a control in which each mean value had an equivalent collection of different times

contributing as the upslope flow means in question. The same process was repeated for a second control 24 hours after the initiation event.

4.2.4 Normalized Difference

The last method used to compare composition was a normalized difference between variables at Tvan versus C1 under different atmospheric circumstances. The normalized difference equation was $(Var_{Tvan} - Var_{C1})/ (|Var_{Tvan}| + |Var_{C1}|)$ and was plotted against wind difference values ($WD_{Tvan} - WD_{C1}$). All the above mentioned variables were run through this analysis for the summers (JJA) of 2008 and 2009. The analysis would attempt to conclude whether there were meteorological differences between Tvan and C1 under divergence ($WD_{Tvan} - WD_{C1}$ near -180^o), convergence ($WD_{Tvan} - WD_{C1}$ near 180^o), and at times when both sites exhibited comparable wind directions ($WD_{Tvan} - WD_{C1}$ near 0^o). A second analysis was overlaid on the original which found the median value of normalized difference points in each 10^o block from -360^o to 360^o (excluding blocks with fewer than 10 data points). Finally, a least-squares trend line was added for these block medians.

4.3. Results

The main findings common to each of the three averaging methods above were that upslope flows had the effect of reducing T_a and increasing h compared to westerly flow. These effects appeared to directly influence λE and T_d. However there were only modest differences between westerly and upslope flow for the remaining meteorological variables (R_n, H, *and* CO_2 flux).

4.3.1 Hourly Means

These differences were clearly visible by the first method described above – the *hourly means* method. Using this method we can see how the meteorological variables at C1 and Tvan, on days with 4 consecutive hours of upslope flow, at both C1 and Tvan, had different characteristics than normal. Figure 4.1 shows that on these days *WD* at C1 typically transitioned from westerly to upslope flow at around 0700 MST and remained upslope flow until roughly 1800 MST. At Tvan *WD* did not fully transition to upslope flow until 1200 MST and typically remained upslope flow until roughly 2200 MST. The *U* on days with upslope winds were lower than average at both sites, with C1 showing a marked decrease at the transition times, as should be expected since the magnitudes of opposing flows (west and east) were canceled out.

Also notable was a distinct difference in T_a patterns. At C1, T_a on days with upslope flows was lower overall, with a noticeable plateau in T_a starting at 1000 MST and lasting seven hours. At Tvan, T_a followed the average pattern of increased T_a in the morning, however began to decrease at 1100 MST, which was two hours earlier than normal. Relative humidity (*h*) patterns were also found to differ between days with upslope flows and days without, with both sites experiencing higher *h* on days with upslope flows. To determine whether high *h* was due solely to lower T_a a closer investigation was undertaken and it revealed these days did indeed exhibit higher vapor pressure.

Surface fluxes also showed patterns on these days at C1 (surface fluxes at Tvan were not observed due a high degree of noise in the data). There was a slight decrease in *H* at roughly 1100 MST (Figure 4.2). In addition, R_n values were slightly lower, as were CO_2 fluxes, during midday hours on days with upslope winds compared to days without. The most prominent

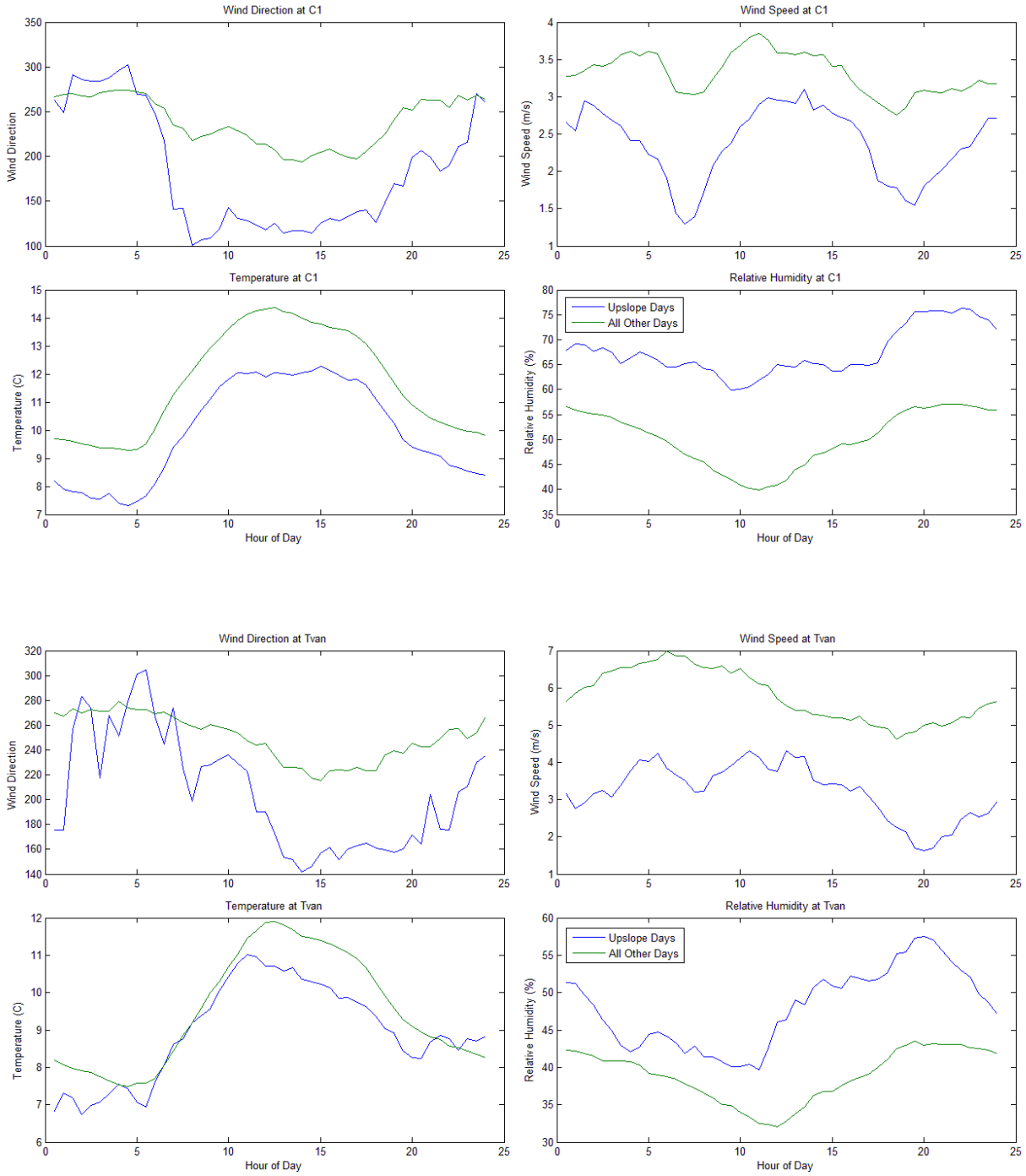

Figure 4.1. *WD*, *U*, T_a, and *h* at C1 on summer days (JJA) during 2008 and 2009 for days with upslope flow versus the remaining days. Upslope flow days were defined as all days in which both C1 and Tvan experienced at least one four-hour period of uninterrupted upslope flow (C1-50^o to 130^o, Tvan 100^o to 180^o). Only 23 of 184 days met these conditions, the remaining 161 are used for the 'All Other Days' mean values. Since the criteria are selecting only days with the strongest upslope flows the 'All Other Days' group does include days with varying, lower degrees of upslope flow as can be seen by the notable drop in *WD* during the daytime hours for this group.

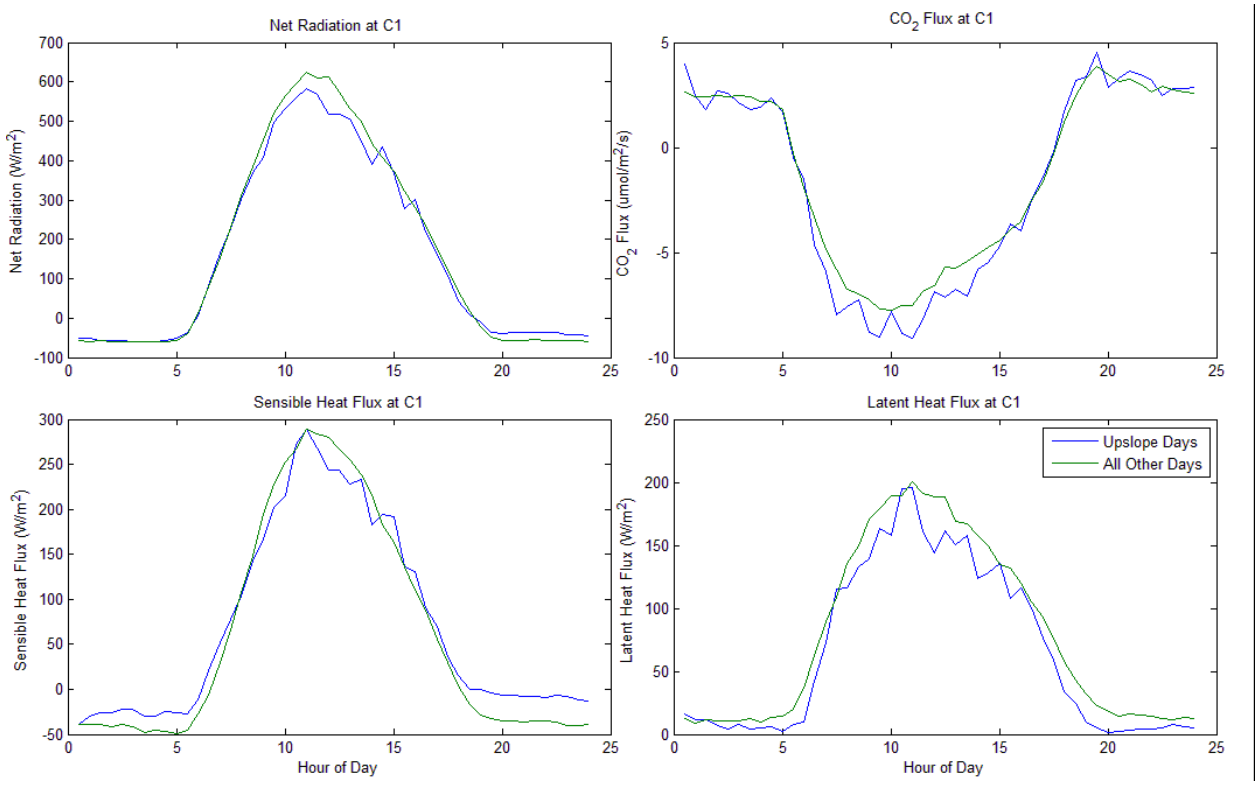

Figure 4.2. Same as Figure 4.1 except for R_n, H, λE, and CO_2 flux. Tvan data were excluded from this analysis because of noise.

difference was observed for λE, which showed distinctly lower values on days with upslope winds. From these patterns it appears there were several factors at work. The slightly lower R_n during the day suggested the formation of clouds over Niwot Ridge. This appeared to play a role in the lower T_a and H values. The drop in λE was most likely in response to the increased h of the new airmass reducing the humidity gradient between the soil and the air.

When the analysis was repeated for days in which *only* C1 experienced four consecutive hours of upslope flow, the same findings were found (Figure 4.3). Under this criterion R_n and H on upslope flow days had nearly identical averages to westerly flow days in the morning hours, but dropped more precipitously at midday, causing them to have lower values in the afternoon. Temperature (T_a), remained lower on upslope flow days, but lost the distinctive plateau from the first analysis. Latent heat flux (λE) also followed a similar pattern, with upslope flow days exhibiting values well below normal due to high h. The sharp decrease in R_n and H on days with upslope flows suggests that these winds may increase the propensity for cloud cover. Conceptually this makes sense, as the upslope flows carry cool, moist air to higher altitudes above the ridge top, leading to greater cooling of the airmass and an increased likelihood for T_d to be reached and condensation to begin.

4.3.2 Upslope Blocks Analysis

The next analysis used to observe differences in airmass composition was the *upslope blocks* method. This method allowed for differences in composition of airmasses to be compared for upslope winds that occurred at all times of day; to determine, for example, whether upslope winds that occur at night have different signatures than upslope winds during the day.

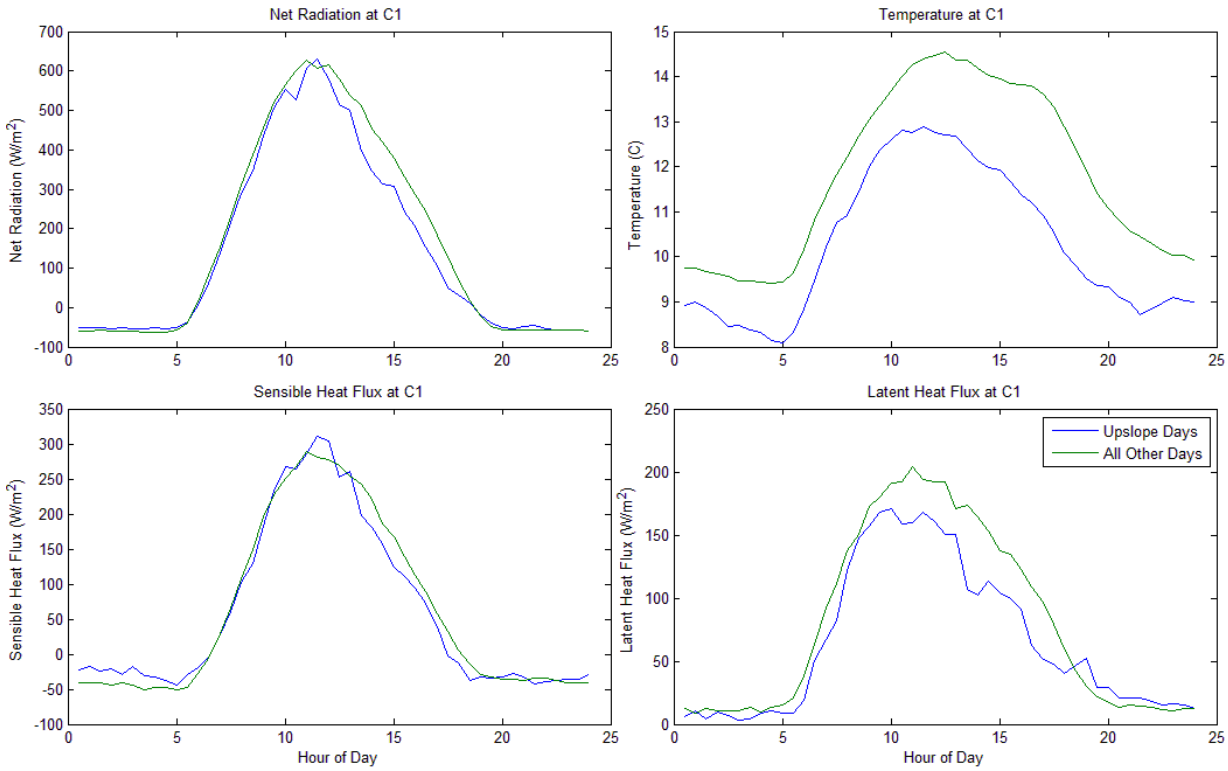

Figure 4.3. The above plot follows the same general pattern as the Figure 4.1 for R_n, T_a, H, and λE. Days with upslope flow were defined as days when C1 experienced four consecutive hours of upslope flow *and Tvan did not* (the 23 days from the previous analysis are not included in either group of this analysis). There are 16 days which meet the upslope criteria of a possible 161 days.

Theoretically there should be a difference since a sizeable percentage of daytime, upslope flows were due to thermal forcings, while such should not be the case at night when thermal forcing leads to katabatic flow.

The first step for the upslope blocks method was to locate each upslope wind event that occurred during the summer months (JJA). These were then sorted into groups with all other upslope winds that occurred at exactly the same time of day. The frequency of upslope flows at these different times of day varied greatly (Figure 4.4). C1 showed a much higher frequency of upslope flows than Tvan, particularly in the hours before noon. Also, at both sites the daytime hours had many more occurrences of upslope flow, with upslope flows in the early morning hours almost nonexistent.

From here the mean *WD*, *U*, R_n, and T_a of both upslope and non-upslope flows for both sites were found (Figure 4.5). Please note that there is no temporal linearity between consecutive points (i.e. neighboring points, connected by a line, are not calculated from the same group of days).

It is clear from the *WD* plot that the groups were successfully separated, with the non-upslope means showing westerly flow and upslope means showing easterly/southeasterly flow. It is also clear that *U* was lower for upslope flow. For both sites upslope flow showed lower R_n than non-upslope flow. Air Temperature (T_a), however, did not show an equally strong signal. For both C1 and Tvan, nighttime upslope flows had a lower T_a than nighttime non-upslope flow. During the day the pattern between Tvan and C1 differed, with Tvan showing equivalent T_a for upslope flows and non-upslope flows and C1 showing slightly lower T_a values for upslope flows

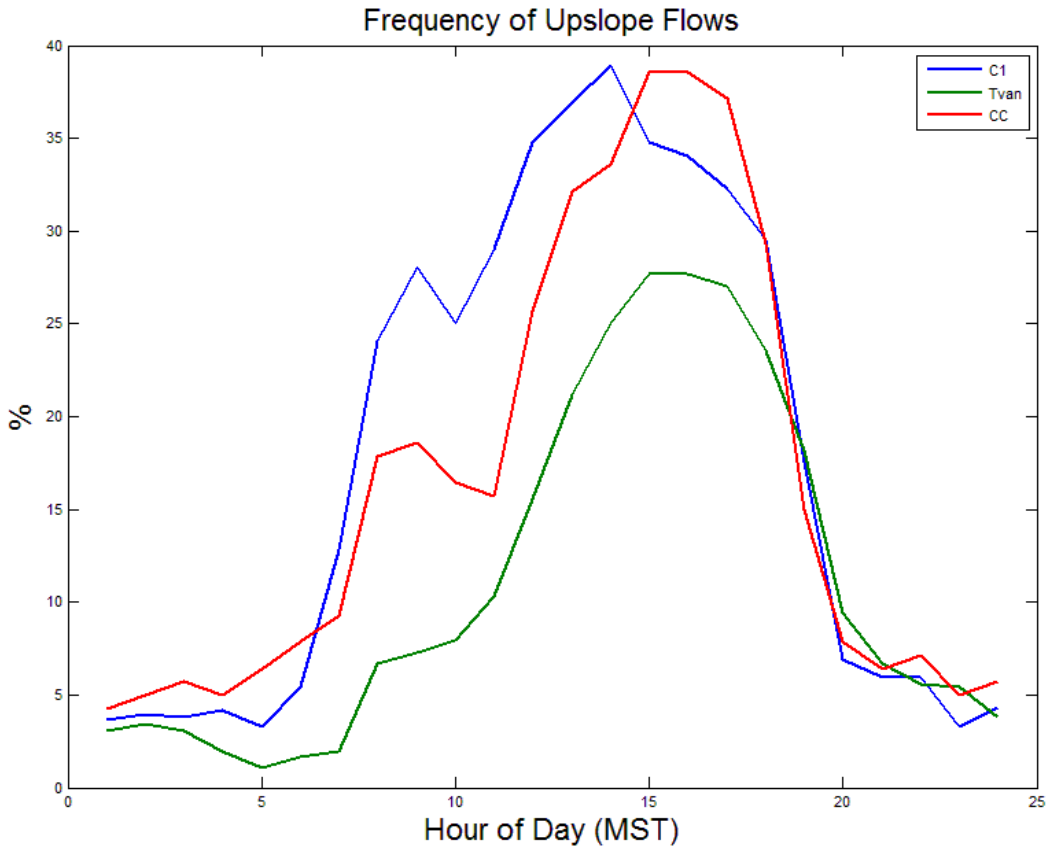

Figure 4.4. Shows the frequency of upslope flow at different times of day for the summer months (JJA). For C1 and Tvan data are from 2008-2009 and for CC data are from 7/29/09 to 7/8/10. It shows the percentage of each hourly block that the *WD* values fell between 50^{o} and 130^{o} at C1 and CC and 100^{o} and 180^{o} at Tvan.

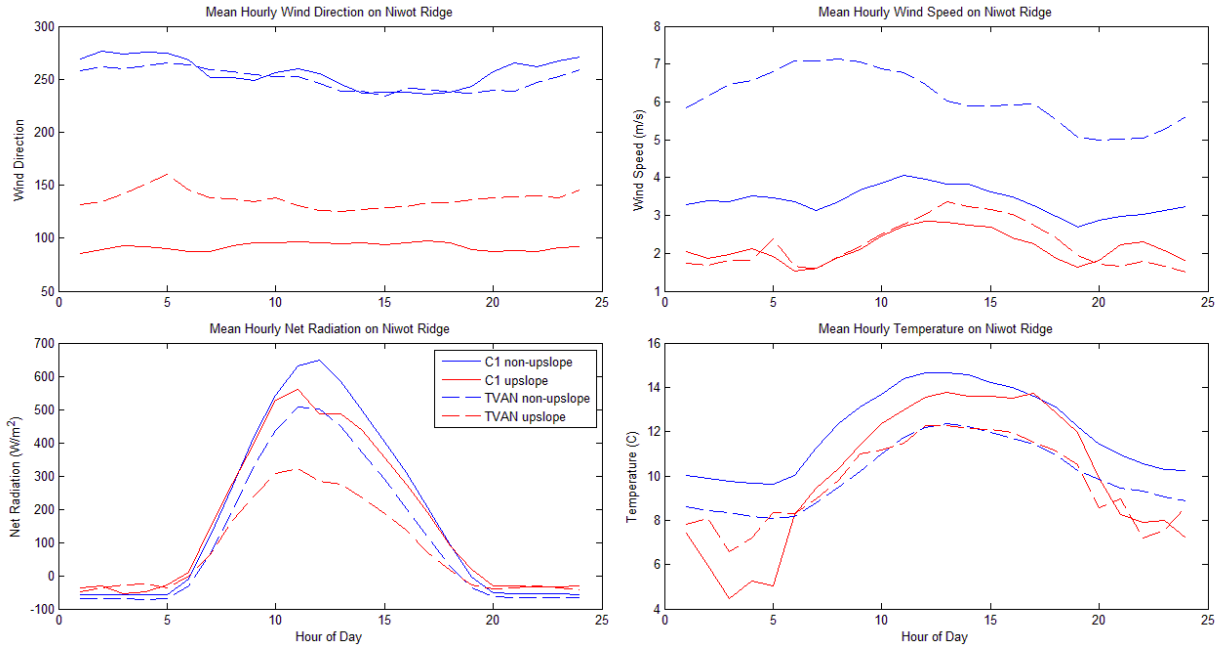

Figure 4.5. Mean hourly *WD*, *U*, R_n, and T_a at C1 and Tvan for summer months (JJA). These are split into two categories: upslope and non-upslope. The previously defined method for determining upslope winds was used. These plots are not means of full days but of partial days. For example, the variable means for hour 6 may come from a completely different set of days than the means for hour 7.

compared to non-upslope flows. This finding suggests that times where the subalpine forest had lower than normal T_a, compared normal T_a in the tundra, were more likely to exhibit upslope flow.

4.3.3 Initiation Method

The last method used to determine airmass composition was the *initiation method*. As described above, this method aligns all upslope flow events by their initiation time. This method gives the clearest picture of what happens as at the moment wind transitions from westerly to upslope (easterly/southeasterly) and therefore gives a very clear indication of the airmass characteristics.

The first round of this analysis averaged *WD*, T_a, T_d, and *h* (Figure 4.6). Wind direction (*WD*) at the moment of initiation of our upslope group showed a sharp decrease from southwesterly flow to upslope flow at both sites, while the two control groups (24 hours prior to and following each upslope wind event) steadily dropped to southerly flow throughout the day. It is unlikely that this southerly flow is truly southerly, with a more than likely probability that within the control groups there was a certain degree of easterly flow (not strong enough to be selected) causing the average of westerly (270^o) and easterly (90^o) components to meet somewhere in between.

Temperature (T_a), T_d, and *h* also changed with the passage of the upslope flow. Air temperature (T_a) showed a very clear dip from the control group at the time of initiation. Both T_d and *h* showed strong increases at the passage of upslope flow. These findings support the earlier finding that upslope flows bring more humid air. It also supports the finding that T_a within these

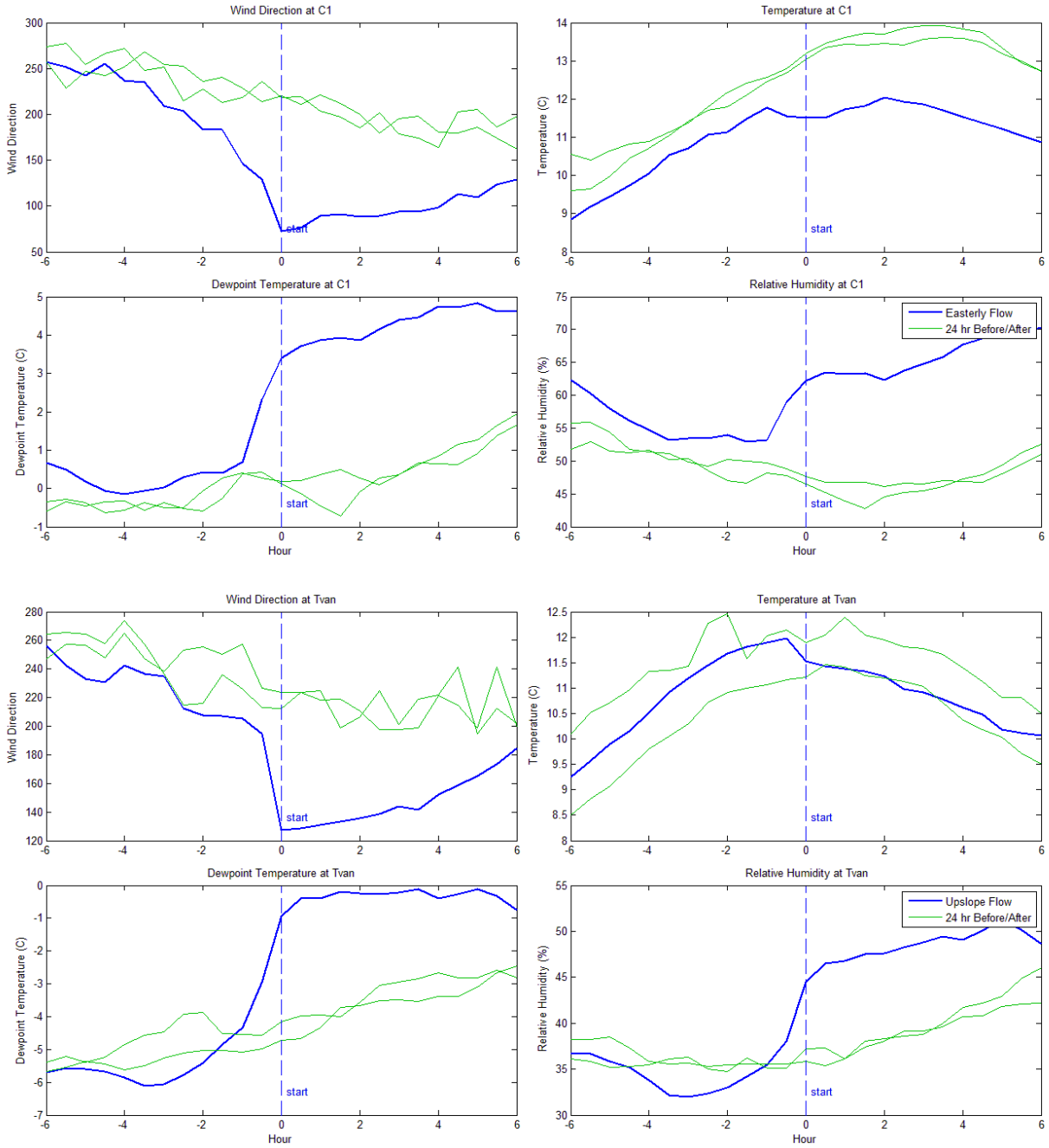

Figure 4.6. Mean *WD*, T_a, T_d, and *h* at C1 (top) and Tvan (bottom) on the six hours prior and following all upslope events that lasted a minimum of four hours. The dotted blue line shows the moment of initiation of upslope flow. The control groups are the means taken at the exact same hours on the days prior to and following each upslope event.

upslope airmasses is slightly cooler than westerly flow. From the first analysis, the *hourly means* method, it was unclear whether T_a drop was due to the airmass itself or dependent upon a possible increase in cloud cover. This finding suggests that these upslope airmasses are, on average, cooler. This makes sense within the current literature as the mechanism describing upslope flow is that cold air pools in valley bottoms are drawn upslope in response to warm, rising air over the mountains (Whiteman *et al.* 2004).

The next part of this analysis looked at the surface fluxes: H, λE, R_n, and CO_2 flux at C1 and Tvan (Figure 4.7). In general these means were noisier than the previous set and therefore are observed here as moving averages (three blocks – 1.5 hours). In addition, the control groups (24 hours before and after) have been combined here so as to reduce clutter. While the findings here are not as dramatic as the previous plot, there was a very distinct reduction of λE with the passage of upslope flow at both sites. This also supports the earlier findings of increased h (reducing the moisture gradient between the surface and the air and therefore reducing the λE). The other variables show slight deviations, such as very slight decreases in R_n and H at the hour of initiation, although none strong enough to suggest inherent differences between upslope days and westerly days. A slight reduction in CO_2 flux at C1 on days with upslope flows suggests increased plant productivity. The other noticeable feature in these plots is that the maximum variable values (minimum for CO_2 flux) were reached after initiation of upslope flow at C1 and before the initiation of upslope flow at Tvan. This is probably the result of the later initiation time for upslope flows in the tundra.

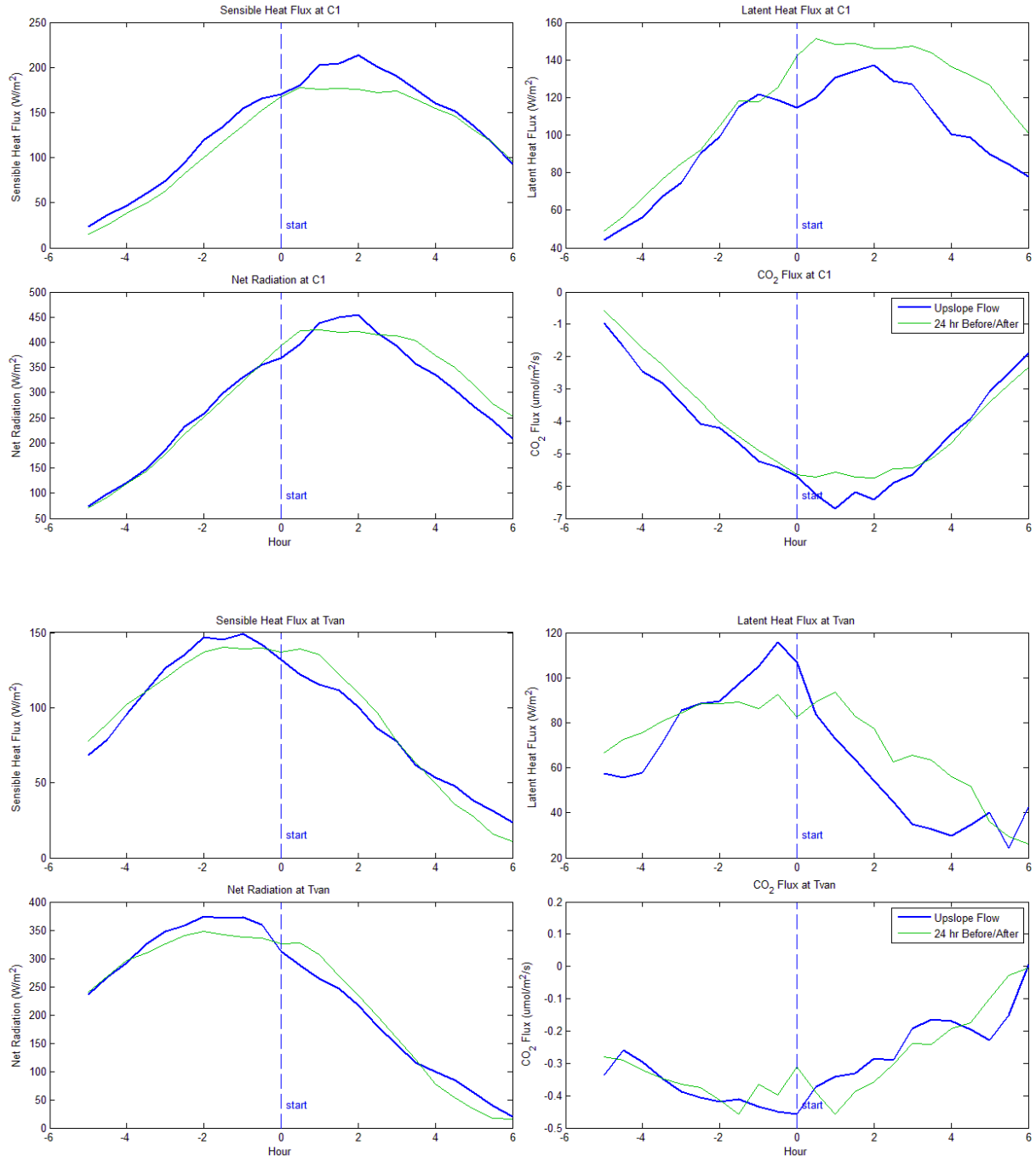

Figure 4.7. Moving average [three blocks] of H, λE, R_n, and H_2O flux hourly means at C1 and Tvan on the six hours prior and following all upslope events that lasted a minimum of four hours. The dotted blue line shows the moment of initiation of upslope flow. The control group is the hourly mean of variables from the exact same hours on the days prior to and following each upslope event.

4.3.4 Normalized Difference

The final analysis used to determine airmass composition was the *normalized difference* approach between the two main sites (Tvan and C1). In this approach the formula ($VAR_{Tvan} - VAR_{C1}$) / ($|VAR_{Tvan}| + |VAR_{C1}|$) was used as our normalized difference and plotted against wind difference ($WD_{Tvan} - WD_{C1}$). The main goal of this analysis was to determine if there were any broad differences in the data that existed between times of convergence, divergence, and times in which both tundra and subalpine forest experienced the same flow patterns. To interpret the results, the slope of the trend line must be taken into account. Positively sloped trend lines show that during periods of divergence (easterly flow at Tvan and westerly flow at C1) Tvan values are lower than C1 values. During convergence Tvan values are higher than, or at least closer to, C1 values.

The three most positive trend lines were *WD*, *U*, and the λE (Figure 4.8, Figure 4.9). Wind direction (*WD*) was highly positive because the x and y axis were both based on the same criteria. When we had divergence at Niwot Ridge (i.e. Tvan 90^o and C1 270^o) the normalized values were -0.5 and when we had convergence the normalized values were 0.5. Wind speed (*U*), however, is an independent variable that was not predetermined by the analysis. The positive slope shows that *U* is lower at whichever site is experiencing easterly flow. This holds with our previous analyses. Latent heat flux (λE) also follows a similar pattern, where it is reduced at sites experiencing easterly flow. This too fits results from the previous analyses.

Interestingly, the median values for the λE normalized difference for periods of divergence were much lower than the median values for periods in which wind direction at both sites are congruous or convergent. This suggests that when Tvan is experiencing easterly flow it

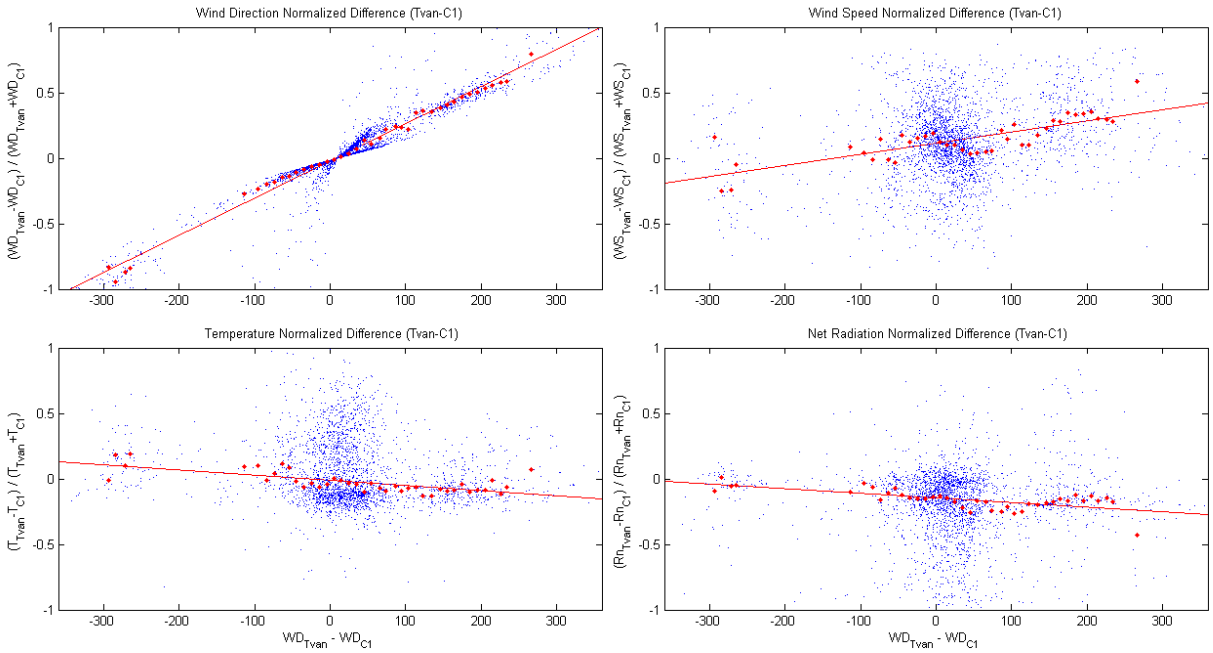

Figure 4.8. Normalized difference (($Var_{Tvan} - Var_{C1}$)/ (|Var_{Tvan}| + |Var_{C1}|)) vs. wind difference ($WD_{Tvan} - WD_{C1}$) between Tvan and C1 for *WD*, *U*, T_a (at 2 m agl), and R_n for all summer values from 2008 and 2009. The red dots show the median value of normalized difference points in each 10^o block from -360^o to 360^o. Blocks with fewer than 10 data points were excluded. A least-squares trend line is shown for these block medians.

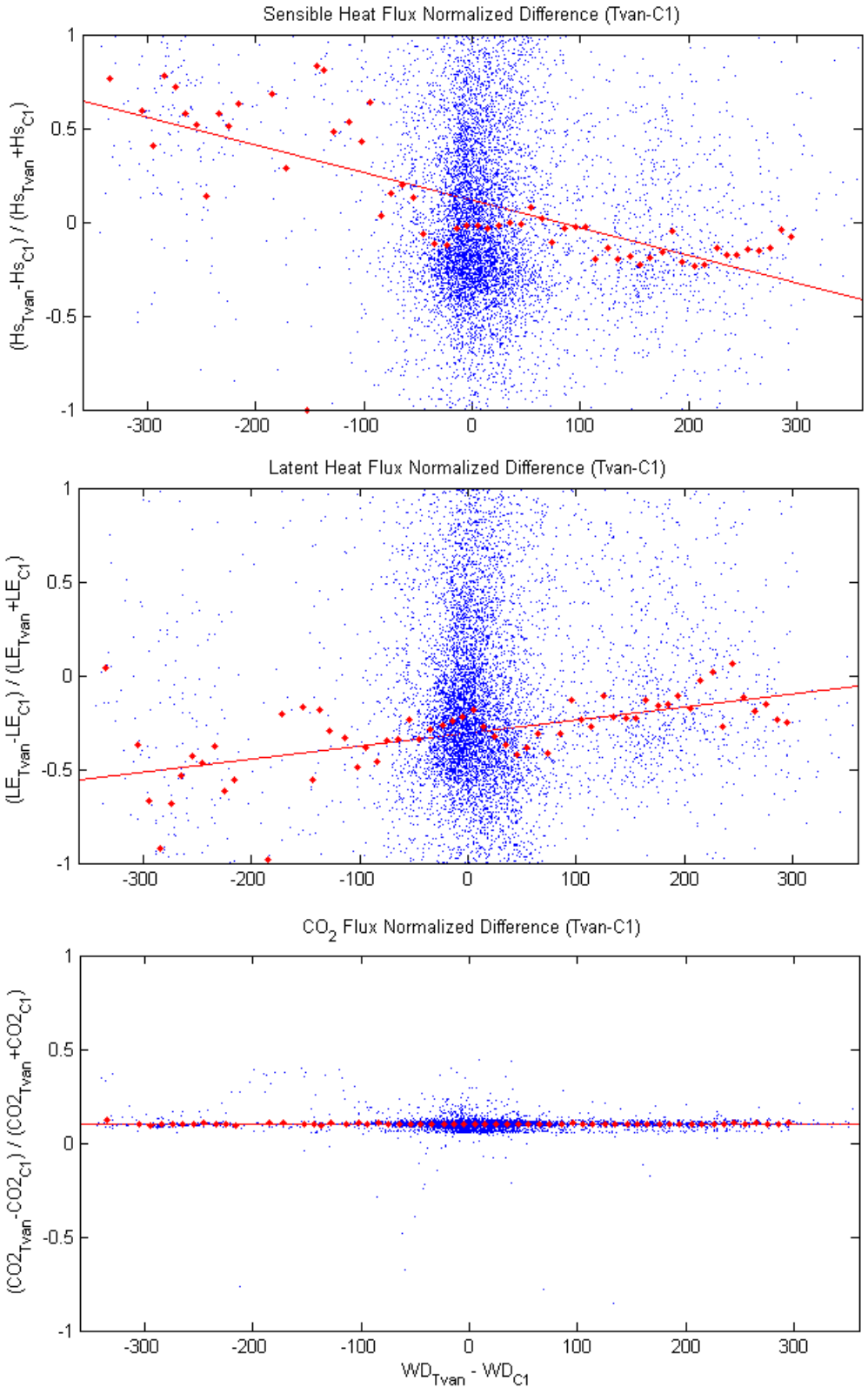

Figure 4.9. The same as Figure 4.8 except for *H*, λE, and CO_2 flux.

exhibits lower λE values. The conclusion from the previous analysis was that upslope (easterly) flow forced a reduction in λE. This was due to the subalpine forest origin of the airmass increasing the h of the air through higher evapotranspiration rates. A reduced water vapor gradient between soil and air effectively reduced λE. However, during divergence events winds at C1 were westerly, suggesting that the easterly flow at Tvan had not traveled over large tracts of forest before arriving at Tvan. Yet the airmass still reduced λE at Tvan. A possible explanation to such a phenomenon is that the westerly flow at C1 is a small scale local event and Tvan is receiving the larger easterly flow. Otherwise the small region of forest between Tvan and C1, which appears to be the origin of the easterly airmass at Tvan, may still provide a significant amount of humidity to the air.

In addition, difference in T_a, R_n, H, and the CO_2 flux at both sites during different WD events were observed in this fashion. Air temperature (T_a), R_n, and H all had negative slopes in the normalized difference plots (Figure 4.8, Figure 4.9). A negative slope shows that the observed variable is higher for a site experiencing easterly flow. This means that at times of convergence T_a was higher at C1 than Tvan and during times of divergence T_a was higher at Tvan than C1. This was an unexpected finding because our previous analysis showed that T_a drops slightly with the passage of upslope (easterly) flow (Figure 4.6).

A closer inspection reveals that 87.3% of all divergence events ($50^o<WD_{Tvan}<130^o$ and $230^o<WD_{C1}<310^o$) in the summer occur during non-daytime hours (1600 MST to 0800 MST). Given no correlation we would expect to see only 66% of divergence events occurring in non-day hours. This shows that divergence has a propensity to occur at night. Conversely there is an increased frequency of convergence events ($50^o<WD_{C1}<130^o$ and $230^o<WD_{Tvan}<310^o$) during

summer daytime hours (0800 MST to 1600 MST). These events occur 55.3% of the time during these hours even though these hours are only 33% of all hours.

This difference in timing helps explain the T_a difference. At night, the atmospheric boundary layer (ABL) becomes stable and well stratified. Katabatic flow brings cold air downslope, causing lower T_a at C1 than Tvan. In fact, 97.1% of the time T_a at C1 was at least 5^{o}C lower than Tvan it occurred in non-day hours (1600 MST to 0800 MST), thus supporting the idea that the T_a distribution of these divergence events is influenced by cold, gravity driven flows. It is also likely that these katabatic flows are the reason we see divergence. The surface flow at C1 is downslope (westerly), while the tundra, under circumstances where there is synoptic-scale wind from the east, could exhibit easterly flow.

Net radiation (R_n) also showed a weakly negative slope (Figure 4.9). This means that generally R_n values at C1 were higher than Tvan during convergence events and lower than Tvan during divergence events. As explained above, convergence favors summer days. Looking more closely at R_n we saw that on summer days R_n was almost always higher in the subalpine forest than the tundra. This was most likely due to the lower albedo of the forest causing greater retention of incoming shortwave radiation. This helps explain why we observed the negative sloping trend line.

The last and most negatively sloping normalized difference in this analysis was *H*. This shows that there was a larger *H* at C1 than Tvan during times of convergence and a much lower *H* at C1 during times of divergence. The cause of this pattern is probably similar to that of R_n and T_a. As stated above, nearly 90% of divergence occurred in non-daytime hours. Therefore for the majority of these events *H* was negative, with the ground absorbing heat from the air.

Under these circumstances the *H* of the subalpine forest was more negative than the tundra. This is not intuitive as it was just stated the T_a is lower in the subalpine forest at night, therefore we should expect a lower heat flux to the ground.

The last variable observed was CO_2 flux (Figure 4.9). In this analysis, similar to the previous analyses, there are no differences in CO_2 flux between tundra and subalpine forest during divergence or convergence, as seen by the lack of any slope to the trend line.

To avoid the influence of diurnal variation the same analysis was run for summer days (0800 MST to 1600 MST). We did not see changes in the patterns for *WD*, *U*, or λE, all of which still had lower values for the site experiencing easterly flow (Figure 4.10, Figure 4.11). Carbon dioxide flux also showed no sign of influence from *WD*. The patterns for T_a, R_n, and *H* changed when applied to this new set of data. Sensible heat flux (*H*) went from a strongly negative slope in the first part to no slope in this analysis. This shows that, on average, there was no measurable difference in *H* between Tvan and C1 during daytime convergence, divergence, or similarly-directed flow events. Net radiation (R_n) and T_a, however, showed switched signals (negative to positive slope) under daytime conditions. The first analysis which included day and night showed that T_a and R_n were higher for sites experiencing easterly flow. When selecting only for daytime hours the pattern switched, with sites experiencing easterly flow exhibiting reduced T_a and R_n. This fit more coherently with the previous findings. We did expect a small reduction in T_a with the transition from westerly to easterly flow, as was seen by the initiation method described above. In addition, we saw that occasionally upslope flow leads to cloud formation, which in turn may play a role in reducing R_n.

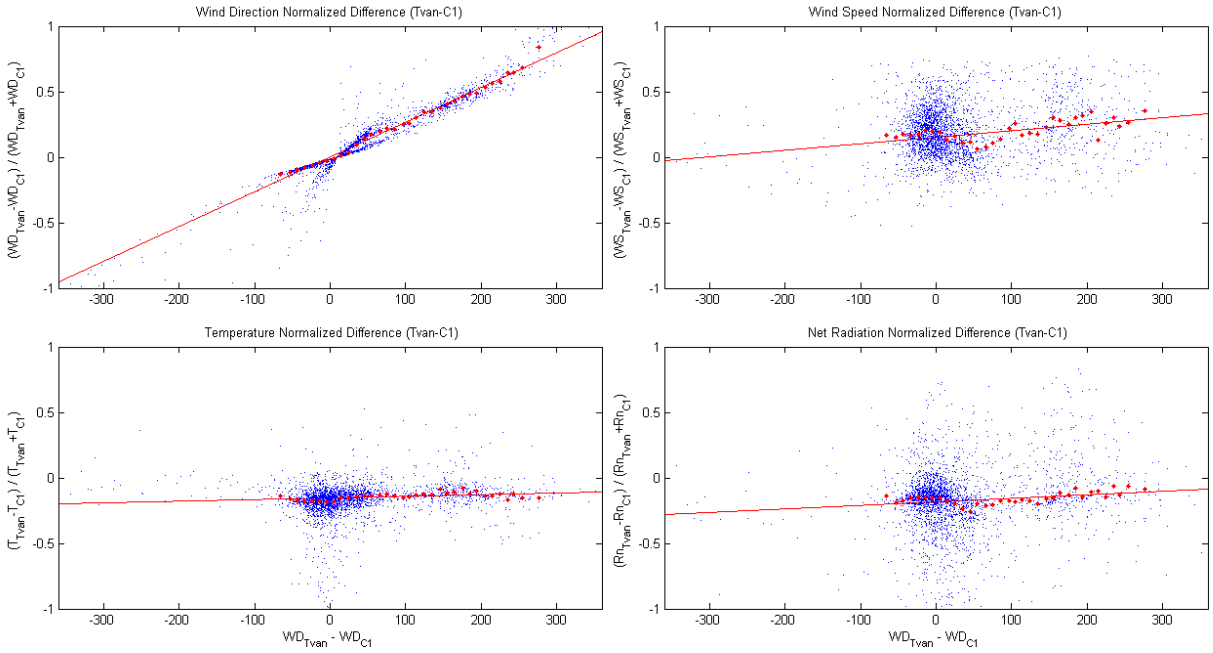

Figure 4.10. Same as Figure 4.8, except limited solely to summer (JJA) days (0800 MST to 1600 MST).

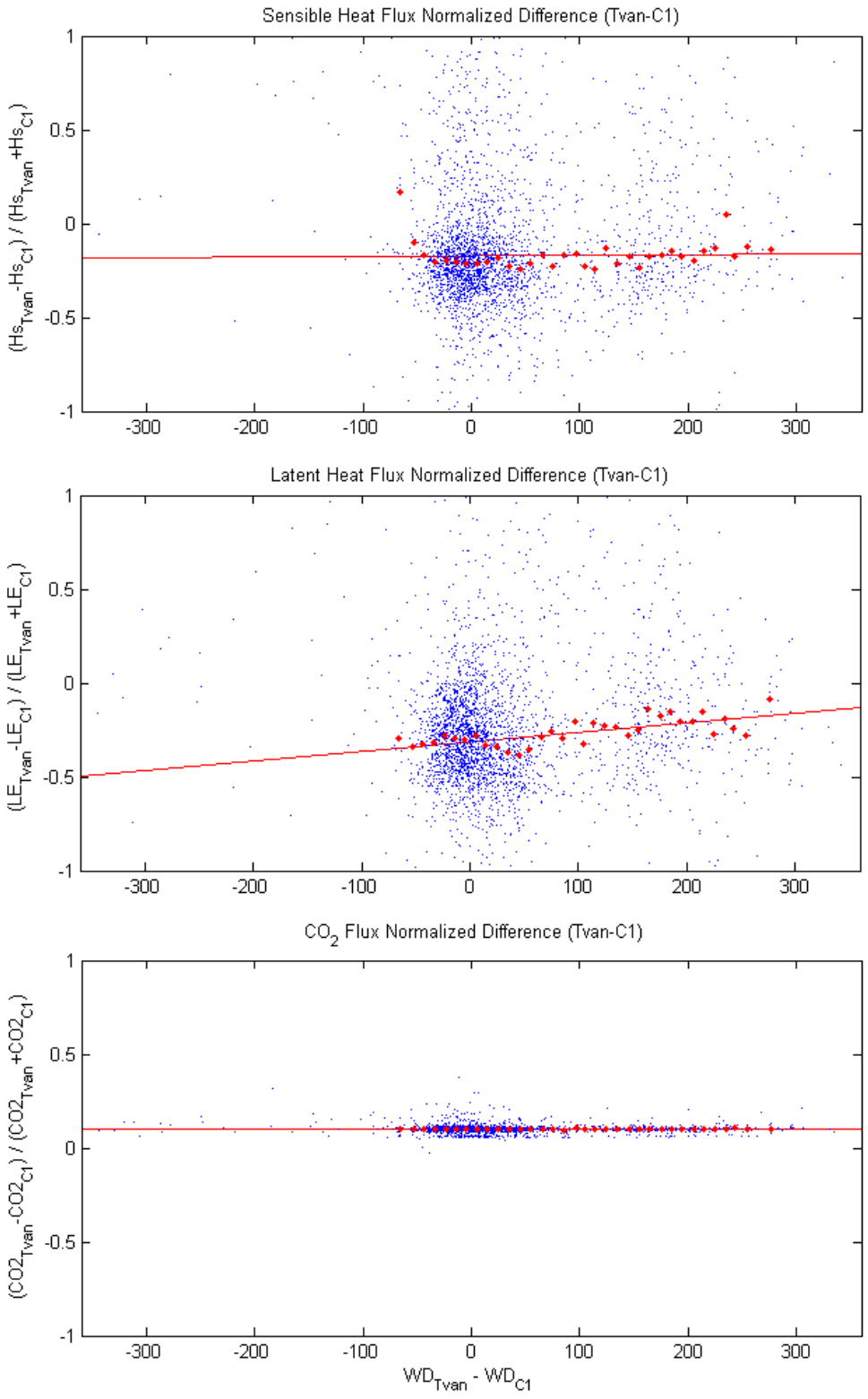

Figure 4.11. Same as Figure 4.9, except limited solely to summer (JJA) days (0800 MST to 1600 MST).

4.4. Conclusions

The main finding from these analyses was the increased *h* during daytime summer-season, upslope air flow. This makes sense given the underlying vegetation characteristics to the west (alpine tundra and bare rock) and to the east (subalpine forest) of the alpine treeline. We expected that evapotranspiration would cause an increase in *h* above these forested regions which have greater plant biomass. In addition, westerly flow reaching Niwot Ridge must pass the Continental Divide, making these airmasses more susceptible to orographic precipitation prior to arrival, thus decreasing the *h* and increasing T_a (due to additions from the latent heat of condensation). In addition to *h*, upslope flows have much lower *U* and slightly lower T_a.

This study shows that wind patterns may be a major contributor to the location of alpine treeline on Niwot Ridge. While it was not designed to be able to make a definitive claim that alpine treeline exists in its current location due to thermally-driven, upslope winds, this study did find that the unique signature of upslope flow appears to have characteristics more beneficial to plant growth. The transport of atmospheric moisture up from lower elevation regions will undoubtedly play a crucial role in plant physiological response. In addition, greater frequency of upslope winds may provide refuge from damaging, high speed winds which scour the alpine tundra. Therefore the atmospheric environment on Niwot Ridge, in which the subalpine forest at lower elevation experiences weak, upslope flow with high humidity and the tundra experiences strong, westerly flow with low humidity, does appear to influence on the location of alpine treeline.

Chapter 5

Conclusions

Two years of measurements, collecting meteorological data in the alpine tundra and subalpine forest, as well as a soil temperatures (T_{soil}) across Niwot Ridge, has enabled an in-depth study of the relationship between thermally-driven, upslope winds and alpine treeline. Soil temperature data, complemented by surface temperature (T_s) measurements derived from Landsat 5 thermal imagery, were used to address whether the differences in the thermal environment, caused by land cover differences (tundra vs. forest), were responsible for creating the unique signature of thermally-driven, upslope flow on Niwot Ridge. The relationship between thermally-driven flows and the alpine treeline was also addressed by observing differences in airmass composition between prevailing westerly flow and upslope flows, to determine whether the location of alpine treeline is influenced by the presence of upslope flow.

5.1 Atmospheric Environment

This study began by characterizing the atmospheric environment of Niwot Ridge. The characteristics of upslope flow events were analyzed to determine what type of upslope flows (thermal, synoptic-scale, or mechanical) existed on Niwot Ridge. The temporal and spatial distribution of these winds was determined so that the alpine treeline analyses could proceed with knowledge of the underlying mechanisms causing upslope winds.

It was found that synoptic-scale winds were rarely (less than 3.5% of the time) oriented at Niwot Ridge in an upslope trajectory (easterly/southeasterly), more often coming from the west.

Therefore the influence of these upslope-oriented synoptic-scale events was considered to be minimal. However, this finding does not rule out the importance of synoptic-scale flow on the existence of upslope winds, since many studies have claimed that synoptic-scale winds must be weak or non-existent for thermally-driven, upslope winds to occur (Baumann *et al.* 1993, Turnipseed *et al.* 2002). However, this study found that there was only a modest relationship between upslope flow and synoptic-scale (500 mb) wind speed (*U*), with only roughly 60% of all upslope events occurring in the 50% of times when synoptic-scale *U* was below the median value of 15.28ms^{-1}. This means upslope winds can often occur when synoptic-scale *U* is high.

This finding may be partly explained by the existence of upslope flow due to mechanical forcing by mountain gravity waves. These were determined to occur mainly during night and winter periods and were characterized by strong westerly winds in the alpine tundra and weak easterly (upslope) flow in the subalpine forest. Therefore these winds may have contributed to the higher than expected frequency of upslope flow during periods of strong synoptic-scale winds.

While these mechanically-driven, upslope flows may contribute to the number of upslope events that occur under strong synoptic-scale winds it was also observed that thermally-driven, upslope winds can occur under these conditions of strong synoptic-scale winds as well. Data collected from a tethersonde system revealed a strong shear layer 80 m agl (in the subalpine forest) on the morning of 8/10/10 separated thermally-driven, upslope flows from strong, synoptic-scale westerlies. Since the dynamics of this system did not support the theoretical constructs of mechanically-driven, upslope flow from rotor winds, and because the initiation of upslope flow occurred in the hour following sunrise it was concluded that these were indeed

thermally-driven, upslope flows. The results from this one day's soundings contradicted previous findings that thermally-driven upslope winds cannot exist under strong ambient winds.

Thermally-driven, upslope flows were typically observed during summer, daytime hours. These winds were observed roughly 15% and 30% of all summer, daytime hours in the tundra and subalpine forest, respectively. It was observed that there were distinct differences in the diurnal pattern of these upslope winds in these different environments. The two subalpine forest sites exhibited a transition to upslope flow during the morning hours following sunrise, showing a large increase in the frequency of upslope flow starting at 0600 MST (C1) and 0700 MST (CC), while the frequency of upslope flow did not increase for the tundra site (Tvan) until 1200 MST.

5.2 Differential Land Temperatures

Prior to this study it was assumed that all thermally-driven, upslope flows on Niwot Ridge were the result of anabatic flow. The findings from previous section required this assumption to be reconsidered. It was expected that transition to anabatic flow would directly follow sunrise due to surface heating; a pattern that was observed in the subalpine forest. However, the distinctly different temporal pattern of transition in the tundra (usually not preceding noon) led us to believe that another force was causing upslope flow in this region. It was hypothesized that the more exposed tundra surface would cause it to reach higher T_s and T_{soil} values (compared to forest) during the day which would lead to land cover-induced, upslope flow.

This problem was approached by obtaining T_s, derived from satellite imagery, and by placing 36 in-situ T_{soil} probes across the face of Niwot Ridge. These data were then analyzed with regard to their land cover type (tundra, krummholz, and forest) to determine the temporal patterns in the thermal environment of these different regions. It was found that the alpine tundra does exhibit higher T_s and T_{soil} than the subalpine forest, with the greatest differences occurring in the afternoon. Dividing the wind direction (*WD*), sensible heat flux (*H*), and surface pressure (p_o) into groups based on the degree to which T_{soil} of tundra and forest differed revealed that upslope winds were more common on afternoons that exhibit large T_{soil} contrast than days with low T_{soil} contrast. This finding supported the idea that land cover-induced flow was responsible for the afternoon upslope winds observed at the tundra site.

However the results of this analysis for *H* and p_o did not support this hypothesis. For land cover-induced flow to exist it was expected that higher T_{soil} in the tundra must cause relatively higher *H* and lower p_o in the tundra compared to the forest, as these are the factors which should theoretically induce local, upslope winds. However, the results showed that on days with higher T_{soil} contrast between the tundra and forest ($T_{tundra} >> T_{forest}$), the tundra had lower *H* and higher p_o relative to the subalpine forest.

While T_s and T_{soil} distributions did appear to influence the frequency of upslope flow in the alpine tundra it is clear from the meteorological variables that such temperature differences did not cause land cover-induced flow. A likely explanation for the high frequency of upslope flow under these conditions is that the high T_{soil} in the tundra was responsible for generating anabatic flow. In addition, it is likely that atmospheric conditions which also support high T_{soil} in the tundra also support upslope flow – high pressure systems, with weak synoptic-scale winds, and high insolation.

5.3 Airmass Compositions

The last part of this study was to determine the ecological significance of upslope flows on Niwot Ridge. The findings from Chapter 2 revealed that the subalpine forest experienced a greater frequency of upslope winds than the tundra. The main objective was to determine whether the airmass composition associated with upslope flows (compared to prevailing westerlies) influenced the location of alpine treeline.

Observing the atmospheric composition of these differing airmasses revealed a couple differences. First, it was observed that upslope flows have modestly lower air temperatures (T_a). This is most likely due to the fact that the mechanics of thermally-driven flows generally cause the movement of cold air into regions of warm air. Essentially cold air pools in the valley are being drawn up by these circulations. Another factor contributing to this difference in T_a is that westerly winds on Niwot Ridge must traverse the Continental Divide prior to arrival, making it likely that atmospheric moisture has precipitated and added latent heat to this air.

The second finding was that humidity (h) was higher in upslope airmasses compared to westerly airmasses. These high h values had the effect of reducing latent heat flux (λE) in both the subalpine forest and alpine tundra, by reducing the water gradient between the soil and atmosphere. High h and low λE are predicted to enhance forest growth by reducing vegetation stress in this dry environment. The transport of atmospheric moisture upslope is most likely an important source of precipitable water during convective storm events over this region, likely recirculating downwardly draining water back to the high elevation regions of the mountains. In

addition, low λE values, drawn out over long periods (i.e. growing seasons), may increase the ability of soil to retain its water.

One other major finding from this study was that upslope flows almost always exhibited lower U than westerly flows. It was found that synoptic-scale winds can travel in an elevated layer over weak upslope winds in the subalpine forest. Under such circumstances it appears that upslope winds may create a degree of buffering between damaging synoptic-scale winds and the surface vegetation. This result was also expected to enhance tree growth by reducing physiological stresses related to strong winds.

While this analysis cannot claim definitive evidence that the location of alpine treeline is influenced by upslope winds, it does reveal distinct differences in airmass composition between westerly and upslope flows. The characteristics of atmospheric variables, such as h and U, can influence plant physiology. In addition, these different airmasses have been shown to influence surface heat fluxes (e.g. λE). It was concluded that the distinct characteristics of upslope airmasses cause them to be inextricably linked to the local ecology of a region. It is believed that lower mountain regions which experience higher frequency of upslope flows should experience more favorable growing conditions and therefore should be more resilient during disturbance events.

5.4 Future Work

The findings from this study could lead to many new avenues of research. The finding that thermally-driven, upslope flows in the alpine tundra were typical to the afternoon (but not

the morning) was not fully explained. It was found that land cover-induced flow was not responsible, a finding contrary to modeling results. To determine whether anabatic forcings were responsible for afternoon upslope flows in the tundra a closer examination of the *H* in the tundra could be undertaken. Determining which parts of the sensible heat flux equation (e.g. gradient between T_s and T_a, eddy diffusivity of air, etc.) have the greatest contribution at different times of day may yield some understanding.

Probably the most important work to follow this study would be a more in-depth study of the interaction between large-scale and local weather processes. It is important to observe synoptic-scale weather patterns, not just as *WD* or *U*, but as whole systems which influence thermally-driven flows.

References

Barclay, A. M. & R. M. M. Crawford (1982) Winter Desiccation Stress and Resting Bud Viability in Relation to High Altitude Survival in Sorbus-Aucuparia L. *Flora,* 172**,** 21-34.

Barry, R.G. (1973) A climatological transect on the East slope of the front range, Colorado. *Arct. Alp. Res.*, 5, 89–110.

Barthlott, C., U. Corsmeier, C. Meissner, F. Braun & C. Kottmeier (2006) The influence of mesoscale circulation systems on triggering convective cells over complex terrain. *Atmospheric Research,* 81**,** 150-175.

Baumann, K., E. J. Williams, J. A. Olson, J. W. Harder & F. C. Fehsenfeld (1997) Meteorological characteristics and spatial extent of upslope events during the 1993 Tropospheric OH Photochemistry Experiment. *Journal of Geophysical Research-Atmospheres,* 102**,** 6199-6213.

Becker, F. & Z. L. Li (1990) Towards a Local Split Window Method Over Land Surfaces. *International Journal of Remote Sensing,* 11**,** 369-393.Blanken, P. D., M. W. Williams, S. P. Burns, R. K. Monson, J. Knowles, K. Chowanski & T. Ackerman (2009) A comparison of water and carbon dioxide exchange at a windy alpine tundra and subalpine forest site near Niwot Ridge, Colorado. *Biogeochemistry,* 95**,** 61-76.

Blanken, P. D., M. W. Williams, S. P. Burns, R. K. Monson, J. Knowles, K. Chowanski & T. Ackerman (2009) A comparison of water and carbon dioxide exchange at a windy alpine tundra and subalpine forest site near Niwot Ridge, Colorado. *Biogeochemistry,* 95**,** 61-76.

Brinkman,W. (1974) Strong Downslope Winds at Boulder Colorado. *Monthly Weather Review,* 102**,** 592-602.

Cairns, D. M. (2001) Patterns of winter desiccation in krummholz forms of Abies lasiocarpa at treeline sites in Glacier National Park, Montana, USA. *Geografiska Annaler Series a-Physical Geography,* 83A**,** 157-168.

Cellier, P., G. Richard & P. Robin (1996) Partition of sensible heat fluxes into base soil and the atmosphere. *Agricultural and Forest Meteorology,* 82**,** 245-265.

Chander, G. & B. Markham (2003) Revised Landsat-5 TM radiometric calibration procedures and postcalibration dynamic ranges. *Ieee Transactions on Geoscience and Remote Sensing,* 41**,** 2674-2677.

Chase, T. N., R. A. Pielke, T. G. F. Kittel, J. S. Baron & T. J. Stohlgren (1999) Potential impacts on Colorado Rocky Mountain weather due to land use changes on the adjacent Great Plains. *Journal of Geophysical Research-Atmospheres,* 104**,** 16673-16690.

Dash, P., F. M. Gottsche, F. S. Olesen & H. Fischer (2002) Land surface temperature and emissivity estimation from passive sensor data: theory and practice-current trends. *International Journal of Remote Sensing,* 23**,** 2563-2594.

Delucia, E. H. & G. P. Berlyn (1984) The Effect of Increasing Elevation on Leaf Cuticle Thickness and Cuticular Transpiration in Balsam Fir. *Canadian Journal of Botany-Revue Canadienne De Botanique,* 62**,** 2423-2431.

Doyle, J. D. & D. R. Durran (2002) The dynamics of mountain-wave-induced rotors. *Journal of the Atmospheric Sciences,* 59**,** 186-201.

Doyle, J. D., Q. F. Jiang, R. B. Smith & V. Grubisic (2011) Three-Dimensional Characteristics of Stratospheric Mountain Waves during T-REX. *Monthly Weather Review,* 139**,** 3-23.

Duane, W. J., N. C. Pepin, M. L. Losleben & D. R. Hardy (2008) General characteristics of temperature and humidity variability on Kilimanjaro, Tanzania. *Arctic Antarctic and Alpine Research,* 40**,** 323-334.Eigenmann, R., S. Metzger & T. Foken (2009) Generation of free convection due to changes of the local circulation system. *Atmospheric Chemistry and Physics,* 9**,** 8587-8600.

Eleftheriadis, K., I. Colbeck, C. Housiadas, M. Lazaridis, N. Mihalopoulos, C. Mitsakou, J. Smolik & V. Zdimal (2006) Size distribution, composition and origin of the submicron aerosol in the marine boundary layer during the eastern Mediterranean "SUB-AERO" experiment. *Atmospheric Environment,* 40**,** 6245-6260.

Franca, G. B. & A. P. Cracknell (1994) Retrieval of Land and Sea-Surface Temperature Using NOAA-11 AVHRR Data in North-Eastern Brazil. *International Journal of Remote Sensing,* 15**,** 1695-1712.

Fujibe, F., K. Saito, D. S. Wratt & S. G. Bradley (1999) A numerical study on the diurnal variation of low-level wind in the lee of a two-dimensional mountain. *Journal of the Meteorological Society of Japan,* 77**,** 827-843.

Garratt, J. R. (1992) Extreme Maximum Land Surface Temperatures. *Journal of Applied Meteorology,* 31**,** 1096-1105.

Gerbush, M. R., D. A. R. Kristovich & N. F. Laird (2008) Mesoscale boundary layer and heat flux variations over pack ice-covered Lake Erie. *Journal of Applied Meteorology and Climatology,* 47**,** 668-682.

Grace, J. (1977) *Plant Response to Wind*. London, UK and New York, NY: Academic Press.

Grubišić, V., and M. Xiao (2006) Climatology of westerly wind events in the lee of the Sierra Nevada, Poster. AMS 12th Mountain Meteorology Conference, Santa Fe, Amer. Meteor. Soc.

Henne, S., M. Furger & A. S. H. Prevot (2005) Climatology of mountain venting-induced elevated moisture layers in the lee of the Alps. *Journal of Applied Meteorology,* 44**,** 620-633.

Holtmeier, F. K. (1980) Influence of wind on tree physiognomy at the upper timberline in the Colorado Front Range. *New Zealand Forest Service Technical Papers,* 70, 247–261.

Holtmeier, F. K. & G. Broll (2010) Wind as an Ecological Agent at Treelines in North America, the Alps, and the European Subarctic. *Physical Geography,* 31**,** 203-233.

Hubbart, J., T. Link, C. Campbell & D. Cobos (2005) Evaluation of a low-cost temperature measurement system for environmental applications. *Hydrological Processes,* 19**,** 1517-1523.Kondo, J. & S. Ishida (1997) Sensible heat flux from the earth's surface under natural convective conditions. *Journal of the Atmospheric Sciences,* 54**,** 498-509.

Kalthoff, N., B. Adler, C. Barthlott, U. Corsmeier, S. Mobbs, S. Crewell, K. Traumner, C. Kottmeier, A. Wieser, V. Smith & P. Di Girolamo (2009) The impact of convergence zones on the initiation of deep convection: A case study from COPS. *Atmospheric Research,* 93**,** 680-694.

Kassomenos, P. A. & G. R. McGregor (2006) The interannual variability and trend of precipitable water over southern Greece. *Journal of Hydrometeorology,* 7**,** 271-284.

Kossmann, M., U. Corsmeier, S.F.J. De Wekker, F. Fiedler, R. Vögtlin, N. Kalthoff, H. Güsten, & B. Neininger (1999) Observations of handover processes between the atmospheric boundary layer and the free troposphere over mountainous terrain. *Contrib. Atmos. Phys*., 72, 329-350.

Kossmann, M. & F. Fiedler (2000) Diurnal momentum budget analysis of thermally induced slope winds. *Meteorology and Atmospheric Physics,* 75**,** 195-215.

Kottmeier, C., N. Kalthoff, C. Barthlott, U. Corsmeier, J. Van Baelen, A. Behrendt, R. Behrendt, A. Blyth, R. Coulter, S. Crewell, P. Di Girolamo, M. Dorninger, C. Flamant, T. Foken, M. Hagen, C. Hauck, H. Holler, H. Konow, M. Kunz, H. Mahlke, S. Mobbs, E. Richard, R. Steinacker, T. Weckwerth, A. Wieser & V. Wulfmeyer (2008) Mechanisms initiating deep convection over complex terrain during COPS. *Meteorologische Zeitschrift,* 17**,** 931-948.

Lee, S. H. & F. Kimura (2001) Comparative studies in the local circulations induced by land-use and by topography. *Boundary-Layer Meteorology,* 101**,** 157-182.

Li, F. Q., T. J. Jackson, W. P. Kustas, T. J. Schmugge, A. N. French, M. H. Cosh & R. Bindlish (2004) Deriving land surface temperature from Landsat 5 and 7 during SMEX02/SMACEX. *Remote Sensing of Environment,* 92**,** 521-534.

Lin, C. Y. & C. S. Chen (2002) A study of orographic effects on mountain-generated precipitation systems under weak synoptic forcing. *Meteorology and Atmospheric Physics,* 81**,** 1-25.

Loescher, H. W., T. Ocheltree, B. Tanner, E. Swiatek, B. Dano, J. Wong, G. Zimmerman, J. Campbell, C. Stock, L. Jacobsen, Y. Shiga, J. Kollas, J. Liburdy & B. E. Law (2005) Comparison of temperature and wind statistics in contrasting environments among different sonic anemometer-thermometers. *Agricultural and Forest Meteorology,* 133**,** 119-139.

Losleben, M., N. Pepin, S. Moore (2000) http://culter.colorado.edu/Climate/Mrsclimate/agu2000.pdf.

Lu, R. & R. P. Turco (1994) Air Pollutant Transport in a Coastal Environment. Part I: 2-Dimensional Simulations of Sea-Breeze and Mountain Effects. *Journal of the Atmospheric Sciences,* 51**,** 2285-2308.

Luhar, A. K. & K. N. Rayner (2009) Methods to Estimate Surface Fluxes of Momentum and Heat from Routine Weather Observations for Dispersion Applications under Stable Stratification. *Boundary-Layer Meteorology,* 132**,** 437-454.

Mahrer, Y. & R. A. Pielke (1977) Effects of Topography on Sea and Land Breezes in a 2-Dimensional Numerical-Model. *Monthly Weather Review,* 105**,** 1151-1162.

McElroy, J. L. & T. B. Smith (1991) Lidar Descriptions of Mixing-Layer Thickness Characteristics in a Complex Terrain Coastal Environment. *Journal of Applied Meteorology,* 30**,** 585-597.

Meissner, C., N. Kalthoff, M. Kunz & G. Adrian (2007) Initiation of shallow convection in the Black Forest mountains. *Atmospheric Research,* 86**,** 42-60.

Miehe, G. (1996) On the connexion of vegetation dynamics with climatic changes in High Asia. *Palaeogeography Palaeoclimatology Palaeoecology,* 120**,** 5-24.

Nyeki, S., K. Eleftheriadis, U. Baltensperger, I. Colbeck, M. Fiebig, A. Fix, C. Kiemle, M. Lazaridis & A. Petzold (2002) Airborne lidar and in-situ aerosol observations of an elevated layer, leeward of the European Alps and Apennines. *Geophysical Research Letters,* 29**,** 4.

Orville, H. D. (1964) On Mountain Upslope Winds. *Journal of the Atmospheric Sciences,* 21**,** 622-633. Font/format

Pan, N. X. & C. C. Li (2008) Deduction of the sensible heat flux from SODAR data. *Advances in Atmospheric Sciences,* 25**,** 253-266.

Pang, H. X., Y. Q. He, Z. L. Zhang, A. G. Lu & J. Gu (2004) The origin of summer monsoon rainfall at New Delhi by deuterium excess. *Hydrology and Earth System Sciences,* 8**,** 115-118.

Parrish, D. D., C. H. Hahn, D. W. Fahey, E. J. Williams, M. J. Bollinger, G. Hubler, M. P. Buhr, P. C. Murphy, M. Trainer, E. Y. Hsie, S. C. Liu & F. C. Fehsenfeld (1990) Systematic Variations in the Concentration of NO_x (NO Plus NO_2) at Niwot Ridge, Colorado. *Journal of Geophysical Research-Atmospheres,* 95**,** 1817-1836.

Pielke, R. A. & P. L. Vidale (1995) The boreal forest and the polar front. *Journal of Geophysical Research-Atmospheres,* 100**,** 25755-25758.

Prata, A. J., Caselles, V., Coll, C., Sobrino, J. A., and Ottle, C. (1995) Thermal remote sensing of land surface temperature from satellites: current status and future prospects. *Remote Sensing Reviews,* 12m 175-224.

Pu, R. L., P. Gong, R. Michishita & T. Sasagawa (2006) Assessment of multi-resolution and multi-sensor data for urban surface temperature retrieval. *Remote Sensing of Environment,* 104**,** 211-225.

Qin, Z., A. Karnieli & P. Berliner (2001) A mono-window algorithm for retrieving land surface temperature from Landsat TM data and its application to the Israel-Egypt border region. *International Journal of Remote Sensing,* 22**,** 3719-3746.

Sasaki, T., P. M. Wu, S. Mori, J. I. Hamada, Y. I. Tauhid, M. D. Yamanaka, T. Sribimawati, T. Yoshikane & F. Kimura (2004) Vertical moisture transport above the mixed layer around the mountains in western Sumatra. *Geophysical Research Letters,* 31**,** 4.

Seluchi, M. E., F. A. Norte, P. Satyamurty & S. C. Chou (2003) Analysis of three situations of the Foehn effect over the Andes (zonda wind) using the Eta-CPTEC regional model. *Weather and Forecasting,* 18**,** 481-501.

Smith, C. M. & E. D. Skyllingstad (2009) Investigation of Upstream Boundary Layer Influence on Mountain Wave Breaking and Lee Wave Rotors Using a Large-Eddy Simulation. *Journal of the Atmospheric Sciences,* 66**,** 3147-3164.

Teitelbaum, H., H. Le Treut, M. Moustaoui, G. C. Cabrera & G. Ibanez (2008) Deep convection east of the Andes Cordillera: A test case analysis of airmass origin. *Monthly Weather Review,* 136**,** 2201-2209.

Telewski, F. W. (1995) Wind-induced physiological and developmental responses in trees. In M. P. Coutts and J. Grace, eds., *Wind and Trees*. Cambridge, UK: Cambridge University Press, 237–263.

Toth, J. J. & R. H. Johnson (1985) Summer Surface Flow Characteristics Over Northeast Colorado. *Monthly Weather Review,* 113**,** 1458-1469.

Tranquillini, W. (1980) Winter desiccation as the cause of alpine timberline. *New Zealand Forest Service Technical Paper,* 70, 263–267.

Turnipseed, A. A., P. D. Blanken, D. E. Anderson & R. K. Monson (2002) Energy budget above a high-elevation subalpine forest in complex topography. *Agricultural and Forest Meteorology,* 110**,** 177-201.

Turnipseed, A. A., D. E. Anderson, P. D. Blanken, W. M. Baugh & R. K. Monson (2003) Airflows and turbulent flux measurements in mountainous terrain Part 1. Canopy and local effects. *Agricultural and Forest Meteorology,* 119**,** 1-21.

Turnipseed, A. A., D. E. Anderson, S. Burns, P. D. Blanken & R. K. Monson (2004) Airflows and turbulent flux measurements in mountainous terrain Part 2: Mesoscale effects. *Agricultural and Forest Meteorology,* 125**,** 187-205.

Veltkamp, P. R., K. J. Hansen, R. M. Barkley & R. E. Sievers. 1996. Principal component analysis of summertime organic aerosols at Niwot Ridge, Colorado. *Journal of Geophysical Research-Atmospheres,* 101, 19495-19504.

Whiteman, C. D. & J. C. Doran (1993) The Relationship Between Overlying Synoptic-Scale Flows and Winds Within a Valley. *Journal of Applied Meteorology,* 32**,** 1669-1682.

Whiteman, C. D., B. Pospichal, S. Eisenbach, P. Weihs, C. B. Clements, R. Steinacker, E. Mursch-Radlgruber & M. Dorninger (2004) Inversion breakup in small Rocky Mountain and alpine basins. *Journal of Applied Meteorology,* 43**,** 1069-1082.

Withington, C. L. & R. L. Sanford (2007) Decomposition rates of buried substrates increase with altitude in the forest-alpine tundra ecotone. *Soil Biology & Biochemistry,* 39**,** 68-75.

Wolyn, P. G. & T. B. McKee (1994) The Mountain Plains Circulation East of a 2-km-High North-South Barrier. *Monthly Weather Review,* 122**,** 1490-1508.

Worthington, R. M., A. Muschinski & B. B. Balsley (2001) Bias in mean vertical wind measured by VHF radars: Significance of radar location relative to mountains. *Journal of the Atmospheric Sciences,* 58**,** 707-723.